To my PARENTS*:*
who made this possible,
and opened me the way...

È proprio la possibilità di realizzare un sogno
che rende la vita interessante.

PAULO COELHO, *L'Alchimista*

Abstract

Background: The technology that supports human motion analysis has advanced significantly in the past two decades. *Gait Analysis* has become a well established paradigm for the diagnosis of the patho-mechanics related to musculoskeletal diseases, and for the development and evaluation of rehabilitative treatments. Recently, the aquatic environment has gained an important role within the rehabilitation world. A biomechanics characterization of normal and pathologic walking in water could be useful to contribute to a more appropriate prescription of walking in water as part of alternative water-based rehabilitation programs. However, the measurement of common biomechanical parameters during water locomotion is more complicated than in laboratory conditions, since most instruments are not suitable for operating in a water environment. Therefore, the development of new technologies is highly sought. In this context, a markerless motion capture system has been investigated and its accuracy in 3D lower limbs joint kinematics reconstruction has been tested.

Methods: Three healthy males and an ACL-injured subject who underwent surgical reconstruction of the ligament, were recruited. Six walking trials at a self-selected speed have been acquired with 6 subaqueous video cameras, in a swimming pool, with water at a shoulder level. Two setups have been experimented to investigate the critical aspects in the definition of camera's position. Lower limbs joint angles with the markerless technique have been extracted. Correlation was used to aid in selecting which of each subject's representative walking trials were to be included in the computation of the mean; thus the correlation coefficient was calculated

for each subject's kinematic parameter. Walking trials with a correlation coefficient less than 0.75 (75%) were excluded from the statistical analysis. The outcomes for each subject have been summarized representing the corresponding correlated trials mean and its standard deviation. The resulting subject-specific representative bands have been compared with Normative Out of Water Bands, to assess differences between walking on land and in water. Pathologic patterns have been compared to the obtained underwater bands as well, to examine walking modifications caused by the ACL injury in the same underwater condition.

Results: The two different setups tested in this study yield to comparable results. However, an appropriate definition of cameras configuration turns out to be crucial, since common drawbacks come up handling underwater data. Correlation and repeatability have been found in the angular values, especially for the stance phases. Common patterns have been registered among the healthy subjects, which can be proposed as indicative of a normal underwater walking. Each subject walks in water with a 20°greater knee flexion angle during the early contact phase and at the end of the whole gait cycle. Moreover, during the stance phase, they present a pronounced extension of hip joint, while a slightly higher knee and hip flexion have been observed during swing phase. Only the first two characteristics are representative of a pathologic locomotion in water as well. When compared with the controls one, pathologic trends are characterized by less knee flexion in the early phase of contact and at the end of the gait cycle.

Conclusions: The results demonstrate the feasibility of calculating meaningful joint kinematics from subjects walking underwater without any markers attached to the limb. Thus, a markerless approach seems to offer the promise of expanding the applicability of human motion capture in an aquatic environment. However, the markerless framework introduces in this thesis should be taken as just a basis and a starting point for developing a broader application of markerless motion capture, and additional evaluations of the system are still needed. Future developments should concentrate on enhancing the background subtraction step, as well as the model matching.

The recruitment of a larger number of subjects, both healthy and pathologic, either to establish more reliable Normal Underwater Bands, or to be able to assess more general differences in the strategy of walking among the two groups, should be considered as well.

Sommario

Background: La tecnologia che supporta l'analisi del movimento umano è progredita in modo significativo negli ultimi due decenni. L'analisi del cammino è diventata un paradigma ben consolidato per la diagnosi della patomeccanica connessa alle malattie muscolo-scheletriche, e per lo sviluppo e la valutazione di trattamenti riabilitativi. Recentemente, l'ambiente acquatico ha acquisito un ruolo importante all'interno del mondo della riabilitazione. Una caratterizzazione biomeccanica della camminata normale e patologica in acqua potrebbe essere utile per contribuire ad una prescrizione più appropriata di camminate in acqua come parte di programmi alternativi di riabilitazione. Tuttavia, la misurazione di tradizionali parametri biomeccanici durante la locomozione in acqua è più complicata che in condizioni di laboratorio, poiché la maggior parte degli strumenti non è adatta ad operare in un ambiente acquatico. Pertanto, lo sviluppo di nuove tecnologie è molto ricercato. In questo contesto, è stato studiato un sistema markerless di motion capture ed è stata valutata la sua precisione nella ricostruzione della cinematica articolare 3D degli arti inferiori.

Metodi: Per questo studio, sono stati reclutati tre uomini sani e un soggetto infortunato al legamento crociato anteriore, che ne ha subito la ricostruzione chirurgica. Con 6 telecamere subacquee sono state acquisite 6 camminate a velocità naturale in una piscina, con acqua a livello delle spalle. Sono stati sperimentati due setup per indagare gli aspetti critici nella definizione della posizione delle telecamere. Sono stati estratti gli angoli articolari degli arti inferiori con una tecnica markerless. Si è utilizzata

la correlazione come indicatore per la selezione dei trials rappresentativi della camminata da includere nel calcolo della media; di conseguenza, il coefficiente di correlazione è stato calcolato per ogni parametro cinematico di ciascun soggetto. I trials con un coefficiente di correlazione inferiore a 0.75 (75%) sono stati esclusi dall'analisi statistica. I risultati per ciascun soggetto sono stati riassunti rappresentando la media e la deviazione standard dei corrispondenti trials correlati. Le fasce soggetto-specifiche risultanti sono state confrontate con le fasce standard di normalità fuori dall'acqua, per valutare differenze tra il camminare a secco e in acqua. Allo stesso modo, i patterns patologici sono stati confrontati con le fasce ottenute in acqua dai controlli, per esaminare modificazioni nel cammino a parità di condizione, dovute quindi all' infortunio del legamento crociato.

Risultati: I due diversi setups provati in questo studio portano a risultati comparabili. Ad ogni modo, un'appropriata definizione della posizione delle telecamere si rivela determinante, dato che inconvenienti comuni sono emersi elaborando i dati sott'acqua. Correlazione e ripetibilità sono state trovate nei valori angolari, soprattutto nella fase di stance. Si sono registrati andamenti comuni tra i soggetti sani, che possono essere proposti come indicativi di una generica camminata normale in acqua. Ogni soggetto, infatti, cammina in acqua con un angolo di flessione del ginocchio maggiore di 20°durante la fase iniziale di contatto e alla fine dell'intero ciclo del passo. Inoltre, durante la fase di stance, presentano tutti un'estensione pronunciata dell'articolazione dell'anca, mentre è stata osservata una flessione solo leggermente superiore sia per l'anca che per il ginocchio durante la fase di swing. Solamente le prime due caratteristiche si possono considerare rappresentative anche di una camminata patologica. Se confrontati con quelli dei controlli, gli andamenti patologici sono caratterizzati da una minor flessione del ginocchio nella fase iniziale di contatto e alla fine del ciclo del passo.

Conclusioni: I risultati dimostrano che è possibile calcolare in modo affidabile la cinematica articolare di soggetti che camminano in acqua senza alcun marcatore attaccato all'arto. Perciò, un approccio markerless

sembra offrire l'opportunità di espandere l'applicazione del motion capture in ambiente acquatico. Tuttavia, la struttura markerless introdotta in questa tesi va considerata solo come una base e un punto di partenza per lo sviluppo di un'applicazione più amplia di markerless motion capture, e sono ancora necessarie ulteriori valutazioni del sistema.
Sviluppi futuri potrebbero concentrarsi sul miglioramento della fase di sottrazione dello sfondo, così come in quella del matching del modello. Anche il reclutamento di un numero maggiore di soggetti, sani e patologici, sia per stabilire fasce di normalità in acqua, che per poter valutare differenze più generali nella strategia di cammino tra i due gruppi, andrebbe considerato.

Contents

List of Figures

List of Tables

Introduction

The present thesis has been realized in the Bioengineering of Movement Laboratory of the University of Padova (Department of Information Engineering), in collaboration with the Faculty of Exercise and Sport Science of the University of Bologna.

A markerless motion capture system for an underwater application has been investigated and tested.

The systematic measurement, description and assessment of those quantities which characterized human locomotion is known as *gait analysis*. It generally involves the investigation of different aspects of movement, such as kinematics, which is the description of the motion of body segments, kinetics, that represents the analysis of the forces that generate the motion, motor control and muscle activation. The technology most commonly employed in clinical gait analysis requires a laboratory equipped with infra-red cameras and makes use of reflective markers placed on the skin. This approach is traditionally used for the analysis of the patho-mechanics related to musculoskeletal diseases, and, recently, it has also been employed in the development and evaluation of traditional rehabilitative treatments and preventive interventions for musculoskeletal disease.

Nowadays, the aquatic environment is gaining an even important role within the rehabilitation world, thanks to water physical properties. A variety of physical activities different from swimming can be proposed in water to take advantages of its unique characteristics. Walking may be one of the most common motor tasks in water-based exercise programs and it may be considered a major underwater rehabilitative tool. Nevertheless, at present, few empirical data have been collected in order to quantitatively assess its

effectiveness [9].
A biomechanics characterization of normal and pathologic walking in water could be useful to contribute to a more appropriate prescription of walking in water as part of training and alternative water-based rehabilitation programs. However, the measurement of common biomechanical parameters during water locomotion is more complicated than in laboratory conditions, since most instruments are not suitable for operating in a water environment. Therefore, new technologies, which allow to evaluate and quantify the progression of an aquatic therapy, may be extremely useful, and give an important incentive to the development of even better rehabilitative programmes.

The aim of this work is to test the applicability of a markerless approach for an underwater gait analysis. So far, three healthy males and an ACL-injured subject who underwent surgical reconstruction of the ligament, were recruited. Six walking trials at a self-selected normal speed in a swimming pool, with water at a shoulder level, have been acquired with 6 subaqueous video cameras. Lower limbs joint angles with the markerless technique were then evaluated.

The present thesis is organized as follow: the first chapter outlines the current state of the art of human body analysis. After an introduction on optical marker-based systems, the fundamental principles, together with the main features and steps, of markerless motion capture are accurately described. The second chapter is dedicated to aquatic therapy: an introduction to water properties is followed by a comparison between biomechanical characteristics of normal walking strategy and alterations due to ACL injury as reported in literature. A description of the experimental setups and the explanation of the markerless data processing steps can be found in the third chapter. Results are then presented and, finally, conclusions and future developments are outlined.

Chapter 1

Human Motion Analysis

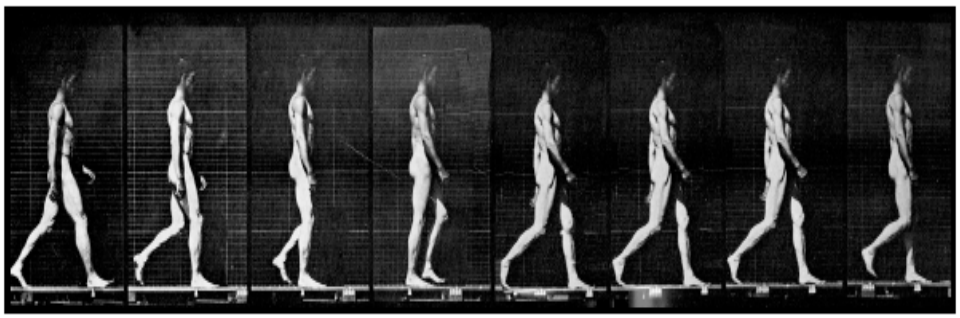

Figure 1.1: Eadward Muybridge, *The human figure in motion* (1907) [58].

1.1 What is Motion Capture?

A common and widespread definition of Motion Capture is the one given by Menache [85] in his book: "Motion Capture is the process of recording a live motion event and translating it into usable mathematical terms by tracking a number of key points in space over time and combining them to obtain a single 3D representation of the performance.". According to this description, motion capture consists on a mathematical representation of the movement of a subject. It makes possible to translate a live movement or performance into a digital model to be used for further studies and specific applications.

Motion capture started as a photogrammetric analysis tool in biomechanics research in the 1970s and 1980s, and nowadays, the interest in the topic is growing exponentially. The main reason of this development can be found in the large number of potential applications that arise from its technologies [18], [102]. In Table 1.1 are listed some of the current uses of motion capture.

Application Areas	
General Domain	Specific Domain
Virtual Reality	Interactive virtual worlds
	Character animation
	Teleconferencing
	Virtual film/TV production
	Computer Games
Smart surveillance systems	Indoor and outdoor scenes
	Gait recognition
Motion Analysis	Clinical studies
	Assisted sport training
	Choreography of dance/theatre
	Content based indexing of TV footage
Advanced user interfaces	Social Interfaces
	Sign Language interpretation
	Choreography of dance/theatre
	Gesture driven application interface
Model-Based Encoding	Clinical studies
	Assisted sport training
	Choreography of dance/theatre
	Content based indexing of TV footage

Table 1.1: Potential Applications of Motion Capture Technologies [18].

One of the established use of motion capture technologies is in clinical and sports analysis. Clinical studies take advantages from the reconstruction of the movement for a better understanding of locomotion difficulties in patients and for prosthesis design. In sports activities motion capture

systems are useful to record the athletes in order to achieve improvements in their performance [18].
In the aspects related to security, both police and army are interested in the capability of automatically monitor human activities in different contexts.
Another notable field of application for these technologies is virtual reality, which allows users to interact with digital content in real time. This can be useful for training simulations, visual perception tests, or computer-generated virtual character animation, largely used, for example, for the rendering of TV special effects and computer video games. Motion capture has begun to be used extensively to produce moves which attempt to simulate and approximate live-cinema, with nearly photorealistic digital character models, while video games often use motion capture to animate athletes, martial artists, and other in-game characters [48].

Prior to discuss the established motion capture technologies commonly used to reach all these targets, a brief history of human movement analysis is introduced in the next section.

1.2 Brief History

The science of motion analysis dates back to ancient Greeks, and its history is marked by the name of some of the most important scientists ever, like Aristotele (384-322 BC), Leonardo da Vinci (1452-1519), Galileo Galiei (1564-1643), Giovanni Borelli (1608-1679), Newton (1652-1727), Euler (1707-1783), Young (1773-1829) [7], [24]. Each of them gave their contribution to its development in terms of biomechanics studies.

However, it has been the invention of photography in the 19th century that led to the birth of what is now known as motion capture. In the late 1800s, Ètienne-Jules Marey (1830-1904) and Eadweard Muybridge (1830-1904) were the first to study human and animal motion by shooting multiple photographs of moving subjects over a short period of time [18].
Marey's invention of chronophotography made possible to record several phases of movement on one photographic surface (Fig: 1.2) and his studies strongly influenced Muybridge's work, who in 1878 succeeded in photographing a horse in fast motion [96]. The photos collected in that

occasion form the notable series *The Horse in Motion* (Fig: 1.3).

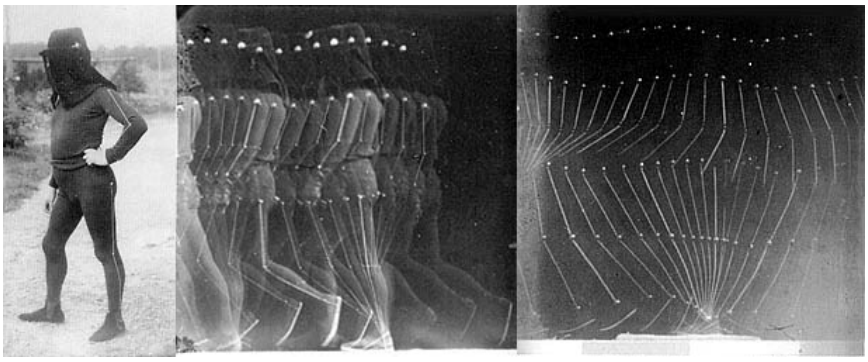

Figure 1.2: Marey's studies on human locomotion [57].

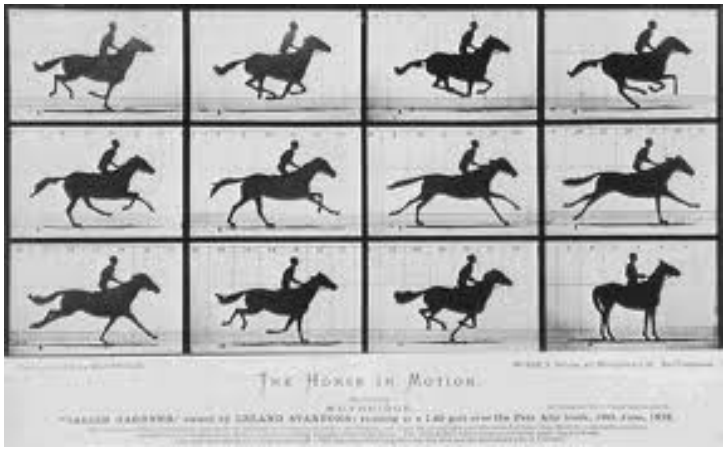

Figure 1.3: Eadward Muybridge, *The Horse in Motion* (1878) [96].

In the following years, Muybridge continued his analysis about the way in which both animals and humans moved taking photographs of people and animals performing a variety of tasks. His experiments have been collected and became famous under the names *Animal Locomotion* and *The human figure in motion* (Fig:1.4) [97]. For all his valuable studies in animation, Muybridge is considered the father of motion pictures.

A significant development of motion analysis science took place starting from the 1950s, when this kind of studies gained more importance as a means to find treatments for World War II veterans [93].

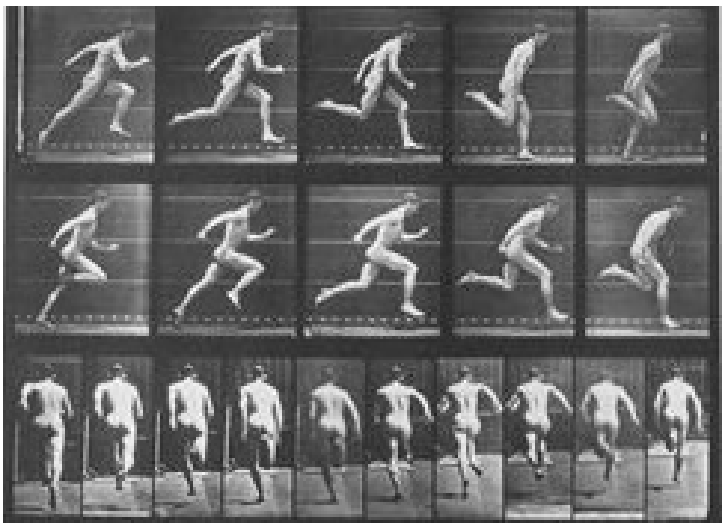

Figure 1.4: Eadward Muybridge, *The human figure in motion* (1907) [97].

In 1973, Johansson, in his *Moving Light Display experiments* [63], used small reflective markers attached to the joints of human subjects to record their motion. His purpose was to be able to identify known movements just starting from the markers trajectories. This is just an example among the numerous works of those years which set the basis of the main techniques currently used in the analysis of human motion [18].

The following section presents a short description of the most common ones.

1.3 Current Motion Capture Technologies

There are different ways of capturing motion. Existing motion capture technologies can be firstly divided into two main branches according to the leading principle: the optical and non optical ones. Non optical strategy includes electromechanical and electromagnetic devices, while the optical part consists of marked-based systems and the recent markerless approach (Fig: 1.5) [102].

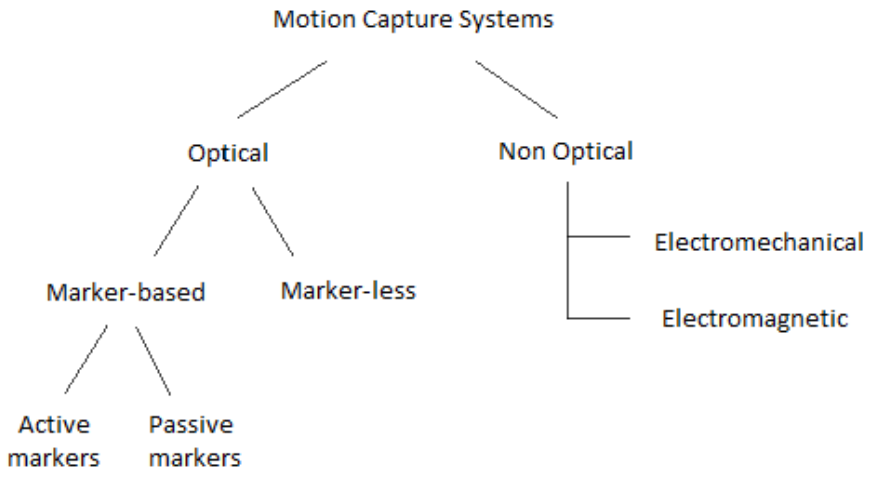

Figure 1.5: Taxonomy of Motion Capture Technologies.

1.3.1 Non Optical Systems

Electromechanical systems are generally made up of potentiometers and sliding rods fixed at specific point in the body. The movement of a subject is detected thanks to small changes in the potentiometers. As a direct result of their weight and encumbrance, they limit the range of motion that can be performed. Simple activities like walking, for example, cannot be analyzed with them [18].

On the other hand, electromagnetic devices involve the use of sensors able to register changes in an electromagnetic field. The required suits are lighter and more comfortable if compared with the electromechanical equipment. This gives the possibility to improve the range of motion that is possible to capture, but the need of wires attached to each sensor is still a strong limitation [18].

1.3.2 Optical Systems: Stereophotogrammetry and Marker-Based Techniques

Optical systems utilize data captured from video cameras in order to assess the 3D position of a subject. They are nowadays largely the most

popular in movement analysis, thanks to several advantages of the video images over the other techniques, especially in terms of quality of results [41]. Next paragraphs will focus only on marker-based methods, which can be classified according to a passive or active use of markers, since markerless approach will be the object of part 1.5.

Passive markers

Passive optical systems are the most widespread, especially for clinical applications. Data acquisition is implemented using retroreflective markers attached to the subject's skin according to various protocols. The scene is illuminated with infra-red light produced by an array of emitting diodes, mounted around the lens of each digital camera recording the scene (Fig: 1.6)[41]. The reflective material which coated the surface of the markers reflects the light back. In this way, markers appear much brighter than the background, making their detection simpler. Moreover, the camera's threshold can be adjusted so only the bright reflective markers will be sampled, ignoring skin and fabric [84].
Multiple cameras are needed, since the position of markers in space is calculated triangulating their position in space on at least two camera planes [32]. A rigid wand and a 3 axes grid, with markers attached at known positions, are usually used respectively to calibrate the cameras (intrinsic calibration) and to obtain their positions in the global frame reference (extrinsic calibration).

Figure 1.6: Array of infrared-emitting diodes mounted around a digital camera of a motion capture optical system with passive markers (BTS S.r.l motion capture system).

Optical marker-based systems for motion capture succeed in overcoming the other technologies mainly because they do not cause encumbrance on the subject: they do not require any powering and are less sensed by the subjects. However, the introduction of markers in human motion analysis gives rise to a drawback: when a marker is hidden to the cameras by a body part, the motion capture looses track of it. This chance represents one limitation concerning marker-based technologies, which can be partially overcome with the use of multiple cameras [32].

Despite its popularity, this approach has some important limitations that should be considered [41]. Even if the encumbrance on the subject is limited when compared with other systems, the presence of markers attached to the skin still influences the subject's movement. In addition, marker placement is time-consuming, non completely repeatable, as shown in [31], and the presence of soft tissue between the bones and the markers causes a relative motion which introduces a relevant artifact in the measurements, technically called "soft tissue artifact" [30]. Finally, a controlled environment is also required to acquire high-quality data [93].

Numerous solutions have been proposed in literature to overcome these constrains, but the purpose of a reliable evaluation of human movement has not yet been achieved satisfactorily. For this reason, an increasing interest in finding valid alternatives to this methodology is emerging, and a new area of research in Markerless Motion Capture is under continuous development.

Active markers

Active markers are LEDs which, differently from passive ones, emit light themselves. This represents an advantage because less power is needed, since light travels half the space than in the passive markers case before reaching the camera. They are usually activated sequentially, so the system can detect automatically each marker by virtue of the pulse timing, making marker tracking more easy [32]. Despite these positive considerations on active markers, the use of the passive ones is still widely preferred, mainly due to the fact that the wiring necessary to power the markers limits even more the subject's possibilities of motion [23].

1.4 Measuring Human Movement for Biomechanical Applications

In general, human movement analysis refers to studies on lower limb or whole-body human motion, with applications to posture studies, human identification, and detection of abnormal gait. As stated at the beginning of this chapter, it was first introduced in the biomechanical field, where it has become a well established paradigm for the diagnosis of the pathomechanics related to musculoskeletal diseases, the development and evaluation of rehabilitative treatments and preventive interventions for musculoskeletal diseases. Over the centuries, its development has been mostly motivated by the need for new information on the characteristics of normal and pathological movements, and consequently, by the need for new approaches for the treatment and prevention of diseases that are influenced by small changes in the movement patterns.

Therefore, one of the major application of motion capture in medicine can be considered the systematic study of human walking, known as *gait analysis*. It generally involves the investigation of different aspects of movement, such as kinematics, which is the description of the motion of body segments, kinetics, that represents the analysis of the forces that generate the motion, motor control and muscle activation.

Kinematics evaluation of human locomotion is dependent on the methods used to acquire the movement. At present, as explained in the previous section, the most common methods for accurate capture of three-dimensional human movement require a laboratory environment and the attachment of markers, fixtures or sensors to body segments. The constraints of the laboratory environment as well as the markers placed on the subjects can mask subtle but important changes occuring to the patterns of locomotion. The accurate capture of normal and pathological human movement without the artifacts associated with standard marker-based motion capture techniques such as soft tissue artifacts, spurious reflections and marker swapping is a requirement for modern biomechanical and clinical applications, where excellent accuracy and robustness are necessary. In fact, it has been demonstrated that also minor changes in the biomechanics of

locomotion are clinically relevant, since they can strongly influenced the outcome of treatment or progression of musculoskeletal pathology. For example, studies show how the gait cycle changes as a result of anterior cruciate ligament (ACL) deficiency [4], and how single gait variables can be predictive of a serious of pathologies of the musculoskeletal system. In these cases, the need for improving our understanding of normal and pathological human movement is the leading principle towards the introduction of new methods to acquire human movement.

A next critical advancement in human motion capture is the development of a non-invasive and markerless system. A technique for human body kinematics estimation that does not require markers or fixtures placed on the body would greatly expand its applicability. Gait analysis itself, has been recognized as clinically useful. However, eliminating the need for markers placement would reduce patient preparatory time and enable simple, time-efficient, and potentially more meaningful assessments of human movement in research and clinical practise.
To date, a markerless approach offers an attractive solution to the problems associated with marker based systems. However, the use of markerless techniques to capture human movement for biomechanical and clinical applications is still limited by the low accuracy of the current methods.
The next section will provide an overview on markerless motion capture approach.

1.5 Markerless Motion Capture

1.5.1 State of the Art

Markerless Motion Capture originated from the fields of computer vision and machine learning, instead of coming from a clinical perspective. Over the past two decades, the registration of human body motion and the reconstruction of its structure and movement using just sequences of images has gained in interest among the scientific communities, thanks to the wide spectrum of application they may have. In computer vision, new algorithms to detect, track and recover articulated motion are constantly researched.

A great variety of vision-based systems have been proposed for tracking human motion. These systems vary in the number of cameras used (camera configuration), algorithm scheme, representation of acquired data, use of different models and the application to specific body regions and whole body. Many examples of tracking and estimating human motion using models of different kinds have been proposed [114], [39], [15], [52], [66], [67], [27], [116], [115], [29].

In this brief review, the discussion of methods for human tracking for surveillance purposes, which aim at associating humans present in a video frame with those in the previous frames, as well as for action recognition, whose objective instead is to recognize the identity of individuals and understand behaviors and activities they perform, is neglected.
More attention is given to methods for 3D human pose estimation, and, in particular, to methods which employ multiple camera views. Pose estimation is defined as the process of identifying how a human body and/or individual limbs are configured in a given scene [91], and the use of a human model is a central aspect. This is the main reason why pose estimation methods are typically classified into three categories, according on how they make use of human models: model-free methods attempt to reproduce body features without a prior knowledge; a model can be used as a reference to constrain and guide the interpretation of measured data (indirect use of a model), or it can be a representation of the observed subject, continuously and updated by the data, that provides any desired information, including the pose at any time (direct use of a model).

An example of model-free algorithm is the "*probabilistic assembly of parts*", in which likely locations of body parts are first detected and then assembled to achieve the configuration which best matches the observations. Among model-free approaches, a classic one involves a stick-figure representation of the subject obtained from the images using medial axis transformation [12] or distance transformation. Isomaps [33] and Laplacian Eigenmaps [36], [34] have also been proposed to transform a 3D representation into a pose-invariant graph for extracting kinematics.

Indirect models make use of a-priori knowledge, which can vary from height of the subject to body part shape, relative size and configuration,

including dynamic information. Labeling and localization of different body parts are usually accomplished, on 2D images or on 3D visual hull data (for details on visual hull see section 1.5.3), looking for structures similar to the model. Tracking can be performed using an extended Kalman filter [87], or through 3D-to-3D non-rigid surface matching [113].

Anyway, the majority of approaches are model-based: an a priori model with relevant anatomic and kinematic information is tracked or matched to 2D images or 3D representations [52]. Its use introduces important advantages, such as the possibility of handling occlusion and the ease by which various kinematics constraints may be incorporated into the system, thus limiting the search space and the number of possible poses. Human models employed by direct use techniques are usually very detailed. Different model types, such as stick-figure, cylinders, super-quadrics [52], and CAD model, are often adopted. A typical model definition, with joints, the sticks (bones) connecting them and a surface representation, is described in section 1.5.4.

Different approaches can be used to relate the image-data acquired to this pose-data representation; the most common one is known as "*analysis-by-synthesis*" and is based on a matching process, either on the camera planes (reprojecting the model on them and finding correspondences with cues like edges, silhouettes, blobs, texture) or directly in 3D space, for example generating a 3D representation like a visual hull.
The matching problem is generally formulated as an optimization function, solved through numeric iterative procedures. Gradient-descent methods or Kalman filter were commonly used until few years ago, when research started to move towards more sophisticated stochastic approaches, like the simulated annealing [34], [37] or the particle filter tracker [14]. However, the computational cost required to solve a human pose problem typically characterized by an high-dimension state space makes the application of these methods rather complicate. For that reason, a combination of stochastic and deterministic approaches is often preferred. The annealed particle filter [39] and the stochastic meta descent [68] techniques have been proposed and tested.

The existing methods have been classified into different categories in

several surveys published in recent years and concerned with computer vision [1], [48], [91], [121]. Moeslund et al. [91] reviewed more than 130 human motion capture papers published between 1980 and 2000 and categorized motion capture approaches by the stages necessary to solve the general problem instead of by techniques used. Moeslund proposed a classification into 4 stages: initialization, tracking, pose estimation, and recognition. The majority of research on human motion capture in the field of computer vision and machine learning has concentrated on tracking, estimation and recognition of human motion for surveillance purposes, and to date, the developed methods have been mostly assessed through the use of qualitative tests and visual inspections. The comparison of performances presented by different groups is often not easy and feasible because no standard error measures exist and results are reported in a variety of ways which prevent direct comparison. Common datasets have been recently made available, such as the HumanEva [111], which aim at providing synchronized video sequences and marker-based motion capture data, along with a set of error measures and support software for manipulating the data and evaluating the results.

Markerless motion capture, as introduced in the previous section, offers great potential also for biomechanical applications, but here it has not been so extensively developed and tested as well as in other fields. To date, the detailed analysis of 3D joint kinematics through a markerless system is still lacking. Thus, evaluating this approach within a framework focused on addressing biomechanical applications may be of great interest. Moreover, quantitative measurements of the movement are fundamental for valuable 3D gait studies.

In the following sections, the main concepts and the basis of the markerless motion capture technique will be introduced.

1.5.2 Background Subtraction

Almost all markerless video based approaches requires an initial step for identifying the objects of interest from the video sequence. This process is technically called *segmentation* and it is a critical task in many computer

vision applications. A typical method used is background subtraction, which identifies moving objects from the portion of a video frame that differs significantly from a background model [28]. Many background models have been introduced to deal with different problems [65], and many challenges have to be taken into account in developing a good background subtraction algorithm [28].

A controlled environment, where walls and floor of the area are covered by panels painted in a plain color not present in the subject, i.e. blue or green [62], would be preferable to perform this step in the simplest way. In such a case, the portions of the videos which match the preselected color are easily recognized as background. However, most applications involve relatively less controlled environment, such as clinical gait laboratories, where multiple instruments are used that remains in view of the cameras. Thus, a more general approach is necessary, where a reference background image, without the presence of the subjects, is taken and compared to each frame of the video sequence.

When color video cameras are employed, as commonly proposed in literature, the first step of the comparison consists in subtracting from each channel (Red, Green, Blue) of the considered frame the corresponding channels of the background image [25]. If the sum of the values of the three channels for one pixel in the image thus generated is below a fixed threshold (the sum is almost zero, due to the presence of noise), that pixel will be labeled as "background". This is usually not enough to achieve a satisfying foreground-background separation due to the presence of the soft shadows cast by the subject. To avoid considering these shadows as part of the subject itself, a second comparison is performed in the RGB space (Fig.1.7): the vectors for each pixel in the two images are computed, and if the angle between them is small enough (below a certain threshold) the pixel is still labeled as background.

The result is a binary segmentation of the image, which highlights regions of non-stationary objects. A typical problem is that in a wide range of situations, the background itself is subject to changes during the sequence, with the consequence that the adoption of a single static reference background image may become inadequate. That's the reason why

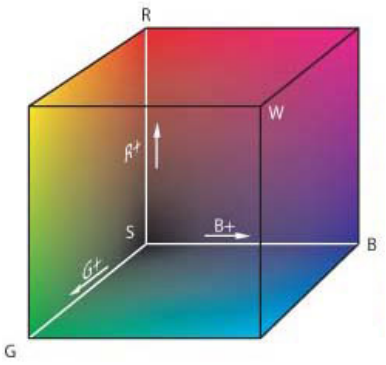

Figure 1.7: RGB space

more sophisticated stochastic approaches, developed in the computer vision field, are needed. They generally create a model of the background, based on the past history of the video sequence and which must be constantly reestimated [65]. Many adaptive background-modelling methods have been proposed to deal with different problems and applications [45], [53], [107]. A standard method of adaptive backgrounding is averaging the images over time, creating a background approximation which is similar to the current static scene except where motion occurs [114]. Another common approach entails the definition of eigenbackgrounds [103], obtained from dimensional reduction of the series of frames in the video sequence through principal component analysis: the assumption is that the PCA-reduced space will represent only the static parts of the scene.

A successful solution has been introduced by Grimson et al. [114], and later it has been slightly modified and improved by Kaewtrakulpong and Bowden [65]. The basic idea stands on model the RGB values of each specific pixel as a mixture of Gaussians, rather than explicitly modeling the values of all the pixels as one particular type of distribution. Based on the persistence and the variance of each of the Gaussians of the mixture, it is possible to determine which Gaussians may correspond to background colors. Pixel values that do not fit the background distributions are considered foreground until there is a Gaussian that includes them with sufficient, consistent evidence supporting it. The algorithm implemented for the data

processing in this study follows this approach.

However, regardless the actual technique employed for background/foreground segmentation, only the information relative to the shape of the subject is retained from the images. Each frame image is binarized assigning, for example, the value 0 (black) to all the background pixels and the value 1 (white) to all the foreground pixels. Often morphological operations, such as dilation and erosion (*binary closure*) are performed in order to get rid of spurious pixels or holes in the foreground patch. The images thus obtained are called *silhouettes* (Fig 1.8).

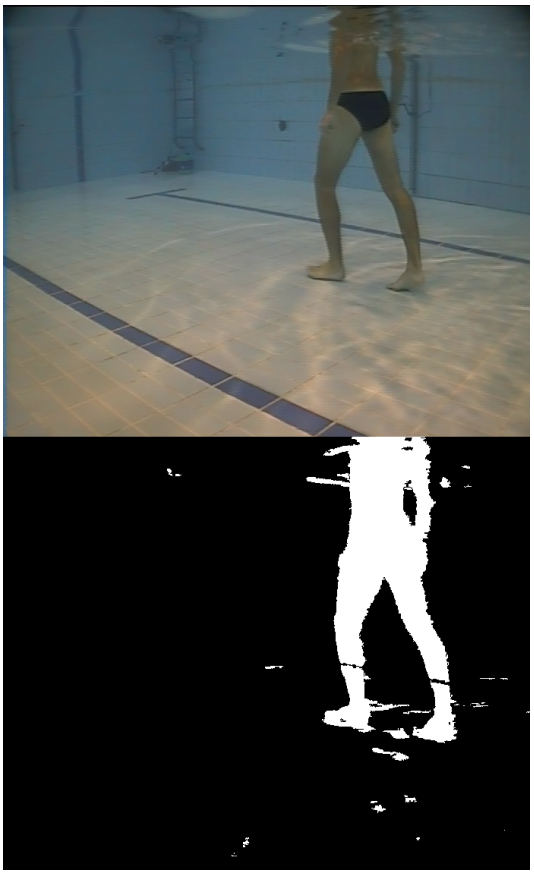

Figure 1.8: Example of original video frame (top) and the binary silhouette image (bottom) resulting from the background subtraction.

1.5.3 Visual Hull Creation

Silhouettes from all the different, synchronized views resulting from the background subtraction, are used to compute a visual hull [73], which is commonly defined as a locally convex over-approximation of the actual volume occupied by the object. The 3D representation of the motion of the subject across the motion capture volume consists of one visual hull for each instant of time acquired by the camera system. Knowing the position and the orientation of each camera, a generalized cone can be back-projected into space, and from the intersection of all these cones, a 3D volume is obtained (Fig. 1.9).

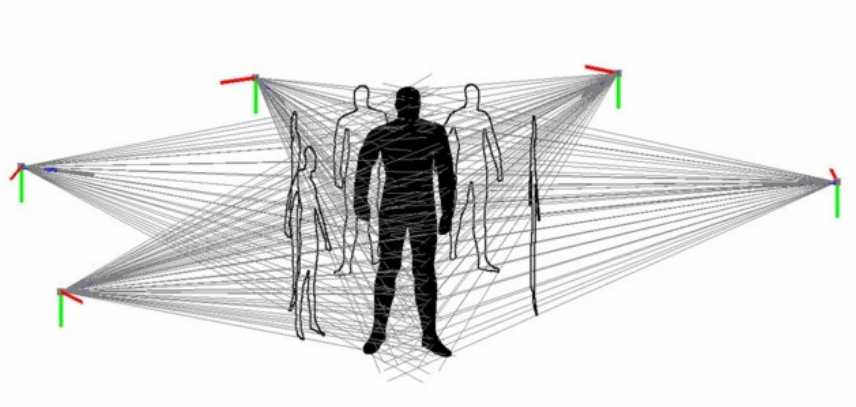

Figure 1.9: Visual Hull Generation from silhouettes

The simplest way to reconstruct the visual hull of a person is by partitioning the calibrated volume in small cubic samples, called voxels, and checking all the vertices against the input silhouettes: only the voxels whose projections on the camera planes belong to the silhouette are considered as belonging to the visual hull. The resolution of the visual hulls depends on the size of the voxels. When the projection of a voxel on a camera plane has smaller size than a pixel, a quantization error is more likely to occur.

However, one of the main problems affecting the visual hull approach is the presence of phantom volumes, artifacts which appear when an area of the working volume is occluded from the view of all cameras. For example, it can be registered when the body limbs of the subject occupy

an undesired position in a specific moment during the acquisition (Fig. 1.10). Furthermore, the number of cameras has been proved to be a critical parameter in order to deal with this problem [95].

Figure 1.10: Example of visual hull. Phantom volumes are present, i.e. between arms.

1.5.4 Model Definition

The model represents the a priori knowledge available about the subject's morphology (3D shape) and kinematics.
With the only exception of non model-based approach that doesn't rely on feature tracking, a model is definitely necessary to be matched with the experimental data, in order to discriminate for different body segments and recognize them, smooth errors in the visual hull reconstruction and measure joints parameters. It should be considered that the points cloud generated by the visual hull reconstruction has not itself information about which points belong to which segment. Moreover there is not a correspondence between the points generated in one frame and the ones generated in the previous or the next ones. Therefore, without a model, no tracking of single point is possible.

Morphology

The 3D shape information is expressed as a triangle mesh (Fig. 1.11), preferably obtained using a laser scanner. A general triangle mesh is described by an ordered list of 3D points, called vertices of the mesh, and by a list of the triangles which describe how the vertices are connected. Each vertex is uniquely identified by its position in the list, and defined by its three coordinates in a reference coordinate system, while each triangle is described by the identifiers of its three vertices in counter-clockwise order (when viewed from outside).

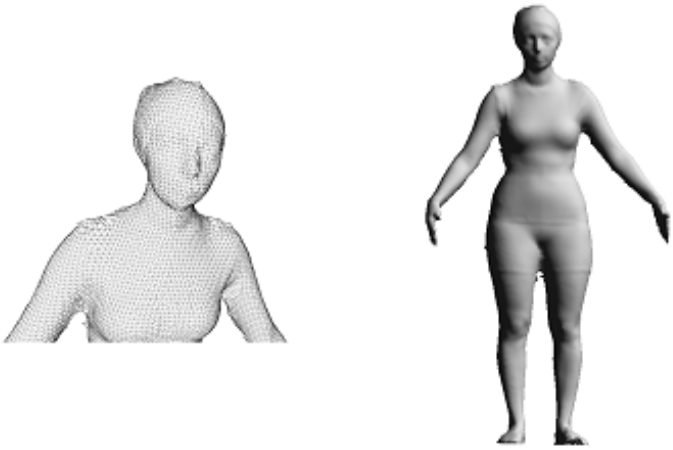

Figure 1.11: Model mesh: detail of the triangles (left) and whole subject's mesh (right).

Kinematics

The kinematic information is represented by an articulated model of the human body. The model for general full-body analysis consists of 15 rigid segments (Fig: 1.12), corresponding to the principal clusters of rigidly-linked bones (head, torso, pelvis, arms, forearms, hands, thighs, shanks, and feet), linked through joints with 6 degrees of freedom (3 translations and 3 rotations). However, different models can be defined, depending on the particular needs or problems. Each segment has a "parent" segment (except

for the root), to which it is connected through its "parent joint"; segments can have multiple "child segments", to which they are connected through "child joints". A local technical coordinate system is embedded in each segment: its origin is coincident with the parent joint and, for the segments that only have one child, the longitudinal (Z) axis is the line connecting child and parent joint. The root segment is initialized with the same orientation as the global coordinate frame, while segments without children inherit the Z orientation from their parent (Fig: 1.12). X and Y axes are defined starting from the global frame of reference so that orthogonality is respected for every segment. The pose of the model is completely determined by the position and orientation of each body segment's coordinate frame relative to its parent's, so that the body segments form a kinematic chain. Rotations are expressed using exponential maps formulation [19] to allow an easier calculation of point's position derivatives with respect to rotational parameters, which are needed in the matching process described in section 1.5.5.

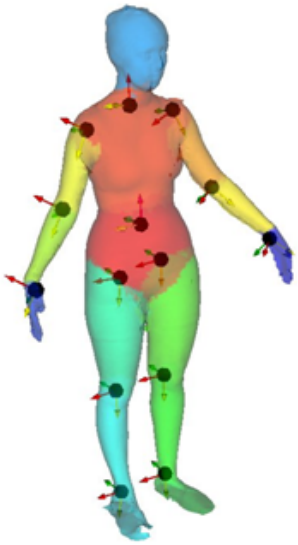

Figure 1.12: Segmented model of the subject: each color represents a body segment. Joint center's position (red circles) and segment's embedded frames of reference are shown.

Joint constrains are also part of the a priori information that can be exploited, as they prevent the model from reaching anatomically incorrect configurations.

Automatic Model Generation

The anatomic model can be obtained using a 3D laser scanner, which gives an accurate acquisition of subject's outer surface.
On the other hand, to define the kinematic model is necessary to state which joints are considered and how they are modeled. In this case, the most crucial task to be accomplished is the identification of joint centers.

Recently, an algorithm has been developed to automatically generate a subject-specific model from simple 3D surface representations of the subjects [35] and to directly embed kinematic information in the subject-specific mesh, obtaining joint centers' positions and segmentation of the mesh into the different body parts.
This algorithm can be used with any human shape, since it has been built on a database of laser scans of people in the same reference pose. Principal Component Analysis (PCA) has been applied to reduce the dimensionality of the space. In this way, human body shapes can be expressed as linear combination of principal components. For most applications, the first ten principal components are usually considered enough to achieve an acceptable level of detail. Examples of body shapes' variations as a function of principal components are shown in Fig.1.13.
A reference mesh (the center of the space of human shapes) has been segmented, assigning a body part to each of its vertices, so that registering it with any other mesh will provide the segmentation of the latter. The registration process iterates the following four steps, summarized in Fig. 1.14:

1. find the transformation to be applied to each segment of the reference mesh to match the pose of the subject's mesh, using a pose registration algorithm such as the one described in section 1.5.5;

2. segment the subject's mesh, assigning each vertex to the same segment

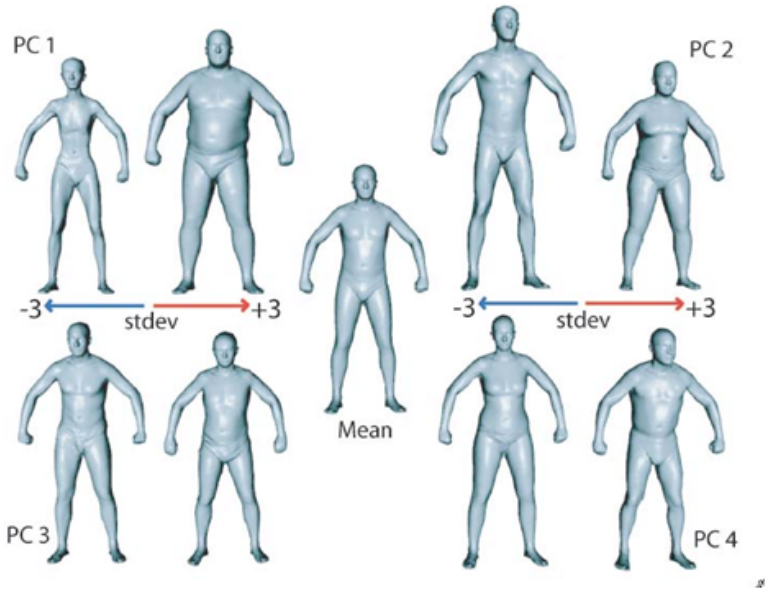

Figure 1.13: Effects of principal components' variation on human body shape space.

as the closest vertex on the transformed mesh obtained in the previous step;

3. apply the inverse of the transformation found in the first step to all the segments of the subject's mesh: in this way, the subject's mesh is registered in the reference pose;

4. morph the reference mesh into this new subject's mesh: this is achieved finding the human shape space parameters which describe the mesh most "similar" to the subject's mesh, where the similarity is mathematically defined as the sum of squared distances from the vertices of the mesh to the corresponding closest vertices on the target mesh.

At every iteration, the reference mesh has a different shape; usually, four or five iterations are needed for the algorithm convergence, which occurs when no differences are still present among the reference mesh and the subject's one.

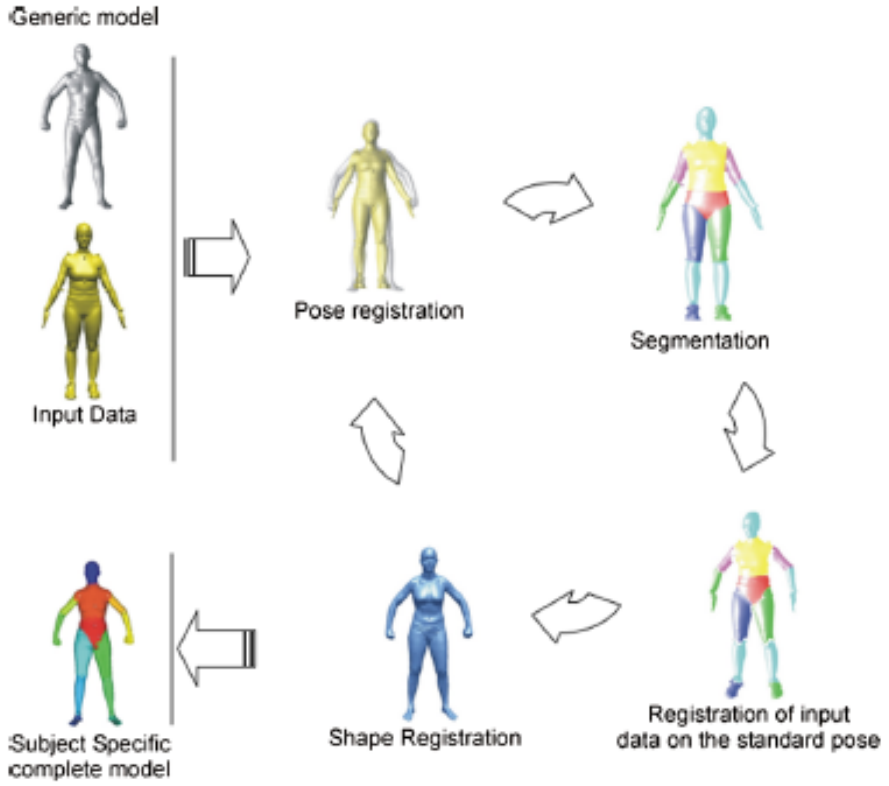

Figure 1.14: Automatic Model Generation pipeline.

The kinematic component of the model, that is each joint center location, is then given as a linear combination of the positions of seven vertices on the morphed reference mesh. The number of necessary vertices, their identifiers and the regression coefficients were determined from a training set of 9 subject meshes, in which the joint centers had been previously identified through virtual palpation, after they had been registered in the reference pose and shape as described in Corazza et. al [35]. For most of the joints the error has been shown to be similar to the markers placement error due to inaccurate identification of the bony landmarks on the subject's skin when marker-based motion capture is performed [31].

Once all the joint centers were identified, the pose shape registration algorithm formerly described was used to bring both the data mesh and

the joint centers in the reference pose of the space of human shapes.
In order to make the process of model generation fully automatic, the joint centers locations were linked to some reliable features on the mesh. In this way, every time a pose shape registration was performed on some data mesh, the joint centers location information would be automatically provided.

It has been proved that the presented automatic procedure can work accurately also when using visual hull data as input instead of a laser scan, which requires expensive dedicated hardware and is not always available [35]. In such a case, the subject can be requested to stand at the center of the measurement volume in orthostatic posture while few frames are acquired. A visual hull of the subject in the static configuration can be used to generate a model, which usually looks "fatter" than the actual subject, since the visual hull is an over-approximation of the represented object. Even if the model thus generated is generally less accurate than using a laser scanner, it can serve properly if the number of cameras used is big enough (≥ 8, possibly at least 16) [34].

The introduction of a completely automatic generation of the model enable to eliminate the most time-consuming task in model-based markerless motion capture. This is a crucial aspect since it makes easier the use of markerless motion capture for clinical and other applications in which there is an intensive acquisition process of different subjects.

1.5.5 Model Matching

As introduced in section 1.5.1, in order to identify the motion of the subject throughout a sequence, an algorithm is needed to recover his instantaneous pose frame by frame, exploiting all the available information. This is achieved finding the particular configuration of the model which better explains the data, represented by the visual hulls, while being anatomically correct since it respects the bounds imposed on the kinematic chain. This configuration can be found matching the points of the visual hull to the points of the model mesh, using the Articulated Iterative Closest Point (ICP) algorithm. The opposite matching (model to data) is also possible, but the two approaches differ in the handling of corrupted data. In the

first case, the algorithm is less robust to "phantom volumes" in the visual hull, caused by concavities or self-occlusion; in the second, missing parts in the visual hull (especially missing limbs), due for example to errors in the background subtraction, lead to the model reaching completely wrong configurations.

Articulated ICP

The *Articulated ICP* [94] is a modification of the standard ICP [11]. ICP-like algorithms perform the point matching between two sets of points (e.g. set V of points belonging to the visual hull, and set M of points belonging to the model) iterating the two following steps:

1. for each point belonging to V, find the corresponding closest one in M (or viceversa), according to some metric, which in our case is the Euclidean distance;

2. find and apply the relative transformation between the two sets (usually a rigid body transformation), which minimizes the total distance between corresponding points.

In the second step, the transformation consists in a change of the model configuration. The configuration of an articulated model with n body segments is function of $6 \cdot n$, which can be represented by a vector β. Six parameters represent the degrees of freedom associated to the position and orientation of the root segment relative to the global coordinate system:

$$\beta_0 = [\omega_{1,0}, \omega_{2,0}, \omega_{3,0}, t_{1,0}, t_{2,0}, t_{3,0}]^T.$$

Parameters $t_{1,0}, t_{2,0}, t_{3,0}$ are the components of the translation vector $T_0 \in R^3$ that defines the position of the origin of the root segment's embedded frame of reference. Parameters $\omega_{1,0}, \omega_{2,0}, \omega_{3,0}$ are the components of the rotation vector $\omega_0 \in R^3$, that is a concise representation of the rotation R_0 of the root segment's frame of reference.
Similarly, for all other body parts, the six parameters represent their position and orientation, each relative to their own parent's coordinate system.

The position of a vertex on the model mesh is therefore a function of a subset of these roto-translation parameters: only the segment the vertex belongs to, and all the segments which link it to the root of the kinematic chain, need to be taken into consideration for that vertex.
In mathematical formulae, this problem can be expressed as follows: given a set VH of N points belonging to the visual hull, $VH_i, i = 1...N$, a set of points M belonging to the model, which are function of a vector of parameters β, and an injective function $C{:}VH \rightarrow M$ so that, for fixed $\beta, M_i(\beta) = C(VH_i)$ is the point on the model that is closest (Euclidean distance) to point VH_i, we need to find

$$argmin_\beta \sum_{i=1}^{N} \|VH_i - M_i(\beta)\|^2 \tag{1.1}$$

This comes out to be a typical nonlinear least-squared problem. The Levenberg-Marquardt approach [50] can be employed in order to solve it. It is an iterative procedure which interpolates between the Gauss-Newton algorithm and the method of gradient descent, depending on a viscosity (damping) factor which changes at each iteration according to the linearity of the problem. A detailed description can be found in [46].
In order to prevent the model from reaching anatomically incorrect configurations, an adopted solution is to add to the cost function 1.1 of the least squares problem a soft bound in the form of a polynomial function, which discourages the minimization algorithm from moving to unlikely configurations close to the edges of the "anatomically correct" range.
Moreover, a clipping routine, which at the end of each ICP iteration checks if the bounds are respected, can be included, so that in case they are not, that model configuration is replaced with the acceptable solution that best approximates it.

The articulated-ICP approach to shape matching is based on correspondence between couples of closest points on two meshes: the algorithm therefore acts "locally", not considering all the possible combinations of corresponding points on the two meshes. This reduces significantly the computational costs, at the expense of an increased

sensitivity to the initialization of the pose of the model.
Similarly, the choice of an iterative algorithm such as Levenberg-Marquardt instead of MonteCarlo techniques, which are more robust, but extremely computationally expensive, is motivated by the need to keep processing times at an acceptable level.

Chapter 2

Aquatic Rehabilitation

Figure 2.1: Aquatic Therapy [56].

Recently, the aquatic environment has gained an important role within the rehabilitation world. An extensive research base supporting aquatic therapy has shown its great rehabilitative potential, mainly due to water physical properties. Aquatic immersion causes physiological changes related to the fundamental principles of hydrodynamics, that allow water to be used with therapeutic efficacy for a great variety of common rehabilitative issues and problems.

2.1 Physical Properties of Water and Benefits of Aquatic Rehabilitation

The main physical properties of water that affect aquatic therapy are buoyancy and viscosity [106].

As a person is gradually immersed, water is displaced, creating the force of buoyancy, which reduces the effect of gravity on the body, progressively unloading immersed joints. This is explained by Archimedes' principle, which states that a body partially or completely immersed in a fluid experienced an upward thrust equal to the weight of the fluid that was displaced. Buoyancy is defined as the upward thrust acting in the opposite direction of gravity. The capacity of decreasing the effective weight of an individual in proportion to the degree of immersion is of primary therapeutic utility. Axial loading on the spine and weigh-bearing joints, especially the hip, knee and ankle is reduced with increasing depths of immersion. By monitoring the depths at which functional movements and exercises are performed, the effect of gravity can be reintroduced and, consequently, gradual strengthening is promoted [108], [123]. Thanks to this property, water provides a low-stress physical environment ideal when full weight-bearing activities are premature, but at the same time mobilization is likely to be avoided. Buoyancy can also be exploited to assist joints for working through greater range of motion, promoting the recovery of both active and passive natural range of motion. The advantages of early restoration of joint mobility are well documented [61], [55].

Viscosity refers to the magnitude of internal friction specific of a fluid during motion. A person moving relative to water is subjected to a resistance due to the fluid. This resistive effect is called drag force. The degree of effort necessary to overcome it, is determined by the size of the moving body, or limb, plus the speed or velocity of the movement. Viscous resistance increases as more force is exerted against it, and the faster the movement, the greater the drag and the greater resistance to movement. Water is more viscous than air, so it is particularly useful to promote muscle strengthening. Since the resistance to movement in water equals the force exerted, matching the patient's effort, it also reduces the probability of reinjury.

Another important property of water is hydrostatic pressure. Pascal's law states that at any given depth, the pressure from the liquid is exerted equally on all surfaces of the immersed object. As the density and depth of the liquid increase, so does the volume of liquid overhead and, therefore, the hydrostatic pressure. As such, hydrostatic pressure may be used in rehabilitation to reduce effusion or to allow patients to exercise an injured extremity without increased the effusion. Hydrostatic pressure is the force that aids resolution of edema in an injured body part and it is also responsible for the cardiovascular changes seen with immersion.

Thanks to these properties and their positive effects, water provides many benefits and alternatives to the traditional land-based physical therapy program. The main advantages can be summarized in: decreased weight bearing, increased range of motion and strength, early restoration of joint mobility, decreased pain, increased balance training and reduced edema.

2.2 Biomechanical characteristics of adults walking on land and in water

A wide variety of physical activities different from swimming can be proposed in water to exploit its unique characteristics. Walking may be one of the most common motor tasks in water-based exercise programs because it can be practise by any age-group and with most medical conditions. Moreover, it does not require any specific skills, unlike swimming for example. Walking in water is considered a major rehabilitation therapy for patients with orthopedic disorders. As already explained in section 2.1, from a mechanical point of view, two main reasons can be found for this: the lower apparent body weight due to the buoyant force (the larger the submersed part of the human body, the lower the apparent body weight), and the increased resistance to movement due to the drag force exerted by water on the human body (the larger the frontal area and faster the movement of the body, the larger the resistance to movement, see section 2.1). Consequently, it appears easier to support the body in water than on land, movements are typically performed slowly in water with longer time

to control them, and the impact forces on the musculoskeletal system are diminished.

Even though walking on water has been an effective way of practising such activities as both training and rehabilitation, there are few empirical data about their effectiveness. Historically, research on water locomotion has focused on cardiorespiratory responses and perceived exertion levels [22], [42], [78]. More recently, a growing part of research is moving the attention on biomechanical parameters during water locomotion. For examples, numerous studies have been conducted to quantify muscle activity [82], [9], [8], [80], [81], [79], [78], [88], [90], and to understand stride characteristics [78], kinematics [9], [8], [88], [90], and kinetics [9], [8], [88] during locomotion.

It should be noticed that measurement of common biomechanical parameters during water locomotion is more complicated than in laboratory conditions since most instruments are not suitable for operating in a water environment. A clear example is the quantification of muscle activity through electromyography (EMG) techniques underwater. It is challenging due to the difficulty in preventing water from interfering with the recording of the electrical signal of a muscle and because of safety concerns regarding the immersion of electrical components in water. Overcoming this challenge is worthwhile because knowledge of muscle activity is crucial for a comprehension of neuromuscular responses to water locomotion. Similarly, a biomechanics characterization of walking in water could be useful for a better understanding of the mechanical loads on the human body, on how human behave and adapt to such a different environment, and consequently, to contribute to a more appropriate prescription of walking in water as part of training and rehabilitation programs.

Despite the increasing interest, still few studies have been conducted to describe some aspects of walking in water [55], [80], [89], [88], and so far only one provided a full description of the gait characteristics of a complete gait cycle [9]. This work has been realized by Barela Ana M.F. and his group, who first qualitatively and quantitatively characterized normal adults walking biomechanics in shallow water and on land. The same analysis was also repeated with elderly individuals.

Ten healthy adults walked at self-selected comfortable speeds in two different

environment conditions: first ten repetitions were made on a walkway in the laboratory (on land condition), and then they repeated it for ten times on a walkway in the swimming pool (water condition), with water at the Xiphoid process level. Kinematics, ground reaction forces (GRF), and electromyographic data were investigated in order to compare walking in both conditions. The experimental setup was designed to performed a bi-dimensional gait analysis of one stride. The participants movement on the sagittal plane (the main plane of movement) was recorded at 60 Hz with digital cameras, while, regardless the water environment, passive reflective markers were placed on the participants right side of five bony landmarks. The reconstruction of the real coordinates was performed using the direct linear transformation (DLT) procedure on land, and using a localized two-dimensional DLT procedure in water to account for refraction in the underwater video. The surface electromyographic activity from eight muscles on the body's right side has been registered, while the vertical and the anterior-posterior components of the ground reaction force has been recorded using force plates. From the kinematics data, the following variables were obtained: stride length, duration, speed, support phase duration, ankle, knee, and hip joints range of motion (ROM), and 2-D foot, shank, thigh, and trunk segments ROM during each stride. From the GRF vertical component, the reduction of apparent body weight from land to water, the magnitudes of the two peaks and the valley, and the impact force, were considered.

With respect to joint angles, it has been observed that "the ankle was more plantar flexed in water during the support phase (the first 60% of the stride cycle approximately) and at the end of the swing phase (the remaining 40% of the stride cycle approximately) than on land. The knee joint in water presented a reduced flexion during about the first 15% of the stride cycle (known as the weight acceptance phase during walking) compared to on land, and as a result, the knee was more extended in water than on land during the support phase. The hip joint in the water condition was similar to the condition on land with the exception of a flexion peak at the swing phase that was observed during walking in water" [9] (Fig: 2.2). Regarding the joint ROM, participants presented the same ROM for all the three joints

on land and in water.

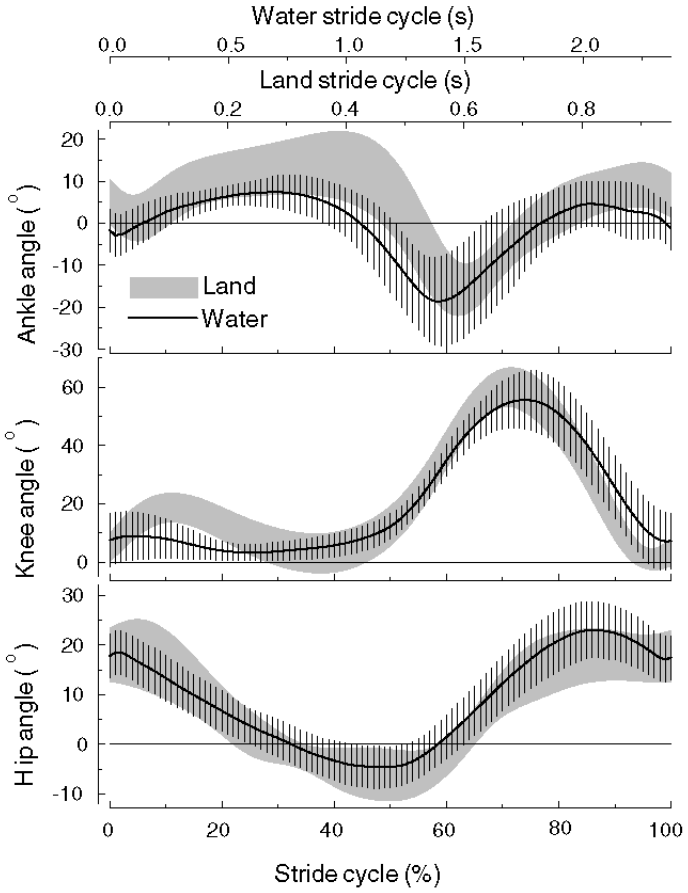

Figure 2.2: Mean stride cycle of ankle, knee, and hip joint angles for the participants walking on land (grey area) and in water (line). Positive values mean ankle dorsiflexion, knee and hip flexion, negative values mean ankle plantar flexion, knee and hip extension (N=10) [9]

.

According to the results of this study, walking in shallow water is shown to be different from walking on land, and the observed differences have been attributed to either the water drag force during movement, or the lower apparent body weight in water, as well as the lower comfortable walking speed selected by the subjects in water. Some of the differences have been

connected also to the different speeds the subjects walked at, since it is proved that when walking on land the speed is responsible for changes in walking characteristics. Therefore, differences between the two conditions have been found and reported, and it has been pointed out that these differences are not only affected by the different environment conditions, but also by the different walking speeds. The same authors, in a later work [8] suggested that future research should aim at estimating joint moments during walking in water for a better understanding of the mechanical load and the neuromuscular demand in water. Moreover, they conclude that "It is also necessary to investigate subjects with locomotor impairments who perform rehabilitation in the shallow water environment to understand how they move in water and how exactly they may profit from this environment" [8].

Starting from this statement and aiming at following this open research path, this study has chosen to focus its attention on the biomechanics characteristics of ACL-injured subjects, as explained in the next paragraphs.

2.3 Alteration in 3D joint kinematics after ACL injury during walking

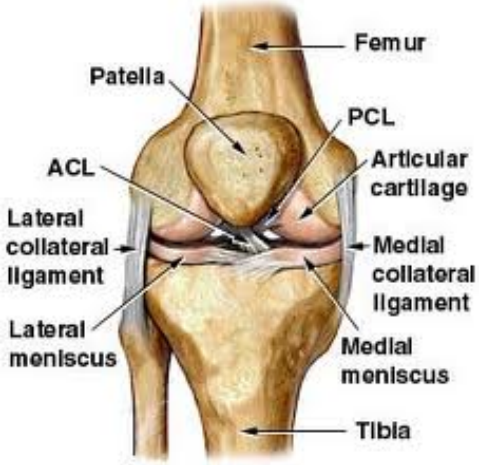

Figure 2.3: Anterior Cruciate Ligament Anatomy [59] .

The ACL is a fundamental structure in controlling knee joint stability and movement, and its rupture is one of the most common sports-related injuries. It is one of a pair of ligaments in the center of the knee joint that form a cross, and this is where the name "cruciate" comes from (Fig. 2.3). Loss of the ACL disrupts the delicate balance of knee structures. ACL injury and its effects on knee stability and movement have been investigated extensively. The ACL has been shown to be the primary restrain to the anterior tibial translation relative to the femur, providing about 86 % of the restraining force [21]. Loss of the ACL causes excessive anterior displacement of the tibia relative to the femur in the range of 30°knee flexion to full extension [54].

As stated by Chaudhari et al. [26], ACL injuries alter not only joint stability, but also load-bearing pattern between contact joint surfaces, resulting in abnormal loadings on the cartilage during functional activities. Consequences of this change in biomechanical environmental could be an high risk of cartilage degeneration and premature osteoarthritis development [3], which have been clinically observed in ACL deficient knees (ACL-D). Noyes et al.[99] reports a risk of knee osteoarthritis for untreated ACL-deficient knees of about 44% after 11 years, while for Nebelung [98] over the 50% of cases have led to a total knee arthroplasty before age 63.

ACL reconstructive surgery is typically recommended to restore the knee joint stability and function after ACL injury. However, its effectiveness in preventing cartilage degeneration and osteoarthritis development remains controversial. Studies indicate that current reconstructive surgeries may not effectively reduce the risk of early cartilage degeneration and osteoarthritis development in ACL-reconstructed (ACL-R) knees [75], [38], [6].
Researchers have suggested this could be a consequence of the knee joint kinematics that have not been fully restored by the reconstructive surgery and the rehabilitation that follows [100], [17]. It has been hypothesized that injury and subsequent repair of the anterior cruciate ligament leads also to significant alterations in lower extremity joint kinetics, kinematics, and energetic patterns during gait. These gait patterns may arise as a result of muscle adaptations and neuromuscular reprogramming, possibly in response to pain or instability, to stabilize the knee and to prevent re-injury during

gait [10], [40], [122].

Zhang [124] investigated six degrees-of-freedom (DOF) kinematic changes in ACL-D knees during locomotion and the possible compensatory mechanism involved. The study showed differences in six DOF knee kinematics between ACL-D and healthy knees, which indicated possible adaptations adopted by chronic ACL-D patients to avoid unstable knee positions due to the loss of the ACL or to avoid stretching a partially torn ACL. Compared with healthy subjects, ACL-D patients walked with increased tibial external rotation throughout most of the stride, increased tibial abduction at the heel contact and the tibia was translated anteriorly during swing phase. Considering the oblique orientation of the ACL, tibial internal and external rotation relative to the femur load and unloads the ACL, respectively (Fig: 2.4).

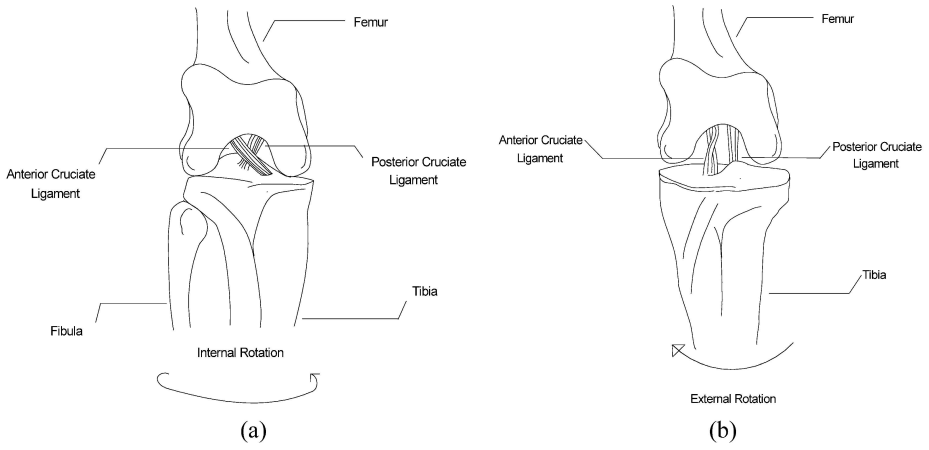

Figure 2.4: (a) The ACL is twisted and stretched when the tibia is internally rotated relative to the femur, due to its oblique orientation inside the knee. (b) The ACL is unwound and becomes slack and unload with the tibia externally rotated relative to the femur. Similarly, the ACL may be loaded and unloaded by tibial adduction and abduction, respectively. [124]

The increased tibial external rotation associated with ACL-D knees indicated the patients' tendency to avoid unstable knee positions due to the loss of the passive constrain associated with complete rupture of the ACL, or

to avoid loading the injured ACL if it was partially torn. Similarly, the more abducted knee around heel contact associated with ACL-deficiency indicates another possible compensatory mechanism adopted by the patients: an abducted knee would unload the ACL because the opposite adduction moment would load the ACL due to the oblique orientation of the ligament in the frontal plane [77].

As already said, one of the most important function of the ACL is restrain the tibial anterior displacement relative to the femur [77], [21]. A loss of the ACL eliminates such restraint, and the posterior pulling generated by the hamstrings and other soft tissue is not strong enough to pull the tibia back fully. Therefore, the tibia of the ACL-D patients displaces more anteriorly relative to the femur, as compared with that of normal controls. This is consistent with a previous study on three-dimensional kinematics of ACL deficient knees in which Marans et al. reported significantly increased tibial anterior translation in ACL-D knees [76].

In order to identify the risk factors that contribute to the biomechanical environment change after ACL injury, it is critical to understand the three-dimensional joint kinematics not only between healthy and ACL-D knees, but also to compare ACL-D and ACL-R knees during daily activities. Ground walking is the most common and frequently performed ambulatory activity. Quite a few studies have been performed to evaluate joint kinematics of ACL-D/ACL-R knees during walking [2], [49], [51], [60], [69], [70], [20], [5]. Most of them focused on joint movement in the sagittal plane, even if movements on the other planes are considered clinically significant [95]. Reduced anterior translation and tibial external rotation before heel strike were observed in ACL-D knees by Andriacchi and Dyrby [5], while more internal tibial rotation during the initial swing phase in ACL-D knees compared to ACL-R knees was reported by Georgoulis et al. [49].
So far, little has been reported about kinematic alterations of frontal plane movement in ACL-D knees or about secondary movement in ACL-R knees during walking. Gao et al. [47] dealed with this topic, with interesting results. Spatiotemporal parameters and three-dimensional knee joint rotations and translations were measured in ACL-D, ACL-R, and ACL-intact (ACL-I) knees during level walking. Kinematic differences were

observed in 3-D rotations between the three groups (Fig. 2.5). In the sagittal plane, the ACL-D knees were significantly less extended than the ACL-I knees during a large portion of midstance (30-44% of gait cycle). A consistent offset between the curves of the ACL-D and ACL-I knees in both the frontal and transverse plane was observed. Greater varus and internal tibial rotation were identified in the ACL-D knees, in agreement with what affirmed by Georgoulis [49] and Andriacchi [5]. Although being small in magnitude, these secondary kinematic alterations were consistent throughout the whole gait cycle, and, what's more, such trends were not eliminated in the ACL-R knees. Overall, the kinematics profiles of the ACL-R knees were closer to the ACL-D knees than to the ACL-I knees. This finding indicated that the reconstructive surgery had not restored the joint kinematics of the ACL-D knees to a normal level. This could potentially explain the outcomes observed in clinic that early cartilage degeneration and progressive development of knee osteoarthritis were not effectively prevented even after ACL reconstruction [6], [38].

The influence of the ligament reconstruction on gait mechanics has been investigated also by Ferber et al. [43]. 10 chronic anterior cruciate ligament deficient subjects have been tested prior to and 3 months following reconstructive surgery, together with 10 uninjured controls. The results from this investigation support the thesis that ACL surgical repair significantly alters lower extremity gait patterns. Several gait characteristics observed three months following surgery come out to be considerably different compared to pre-surgical values. The ACL reconstructed subjects produced an appreciably greater knee extensor moment during early stance if compared to controls and pre-surgical values, and a significantly reduced knee flexor moment for the remainder of stance. They exhibited also a greater hip extensor moment, perhaps to reduce anterior tibial translation. Therefore, the re-establishment of pre-injury gait patterns is considered feasible, but it is shown to take longer than 3 month to occur. Time since injury is suggested to play an important role in the adaptation of gait mechanics and must be considered when evaluating post-surgical ACL subjects.

The disagreement in the results can be explained if considering that

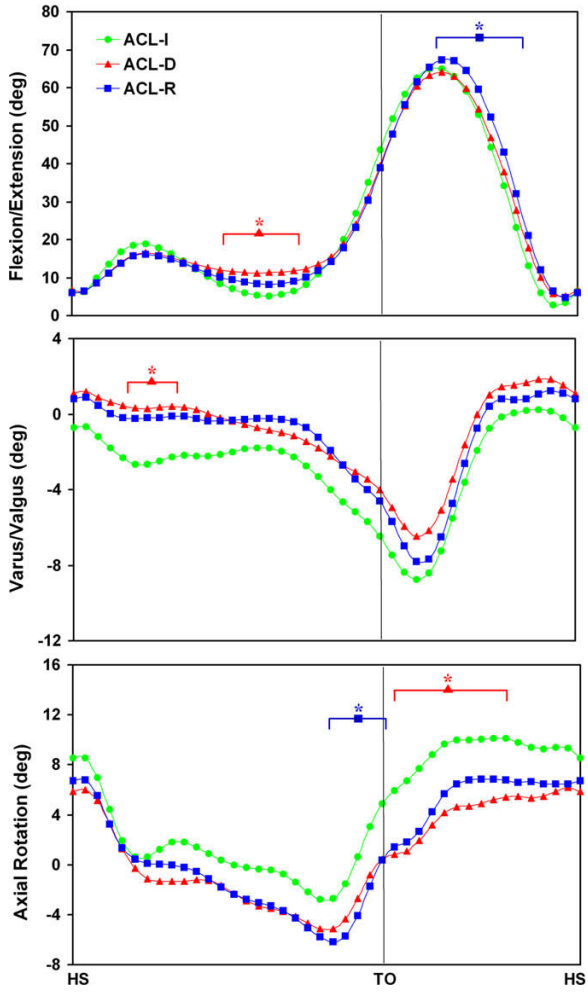

Figure 2.5: The 3-D joint rotations during walking of ACL-I, ACL-D and ACL-R knees. Ensemble curves of each subject group were normalized from heel strike to heel strike in a gait cycle. Segments with significant statistical differences ($P < 0.05$) between the patients and the control groups were marked with asterisks. Flexion, varus, and external tibial rotation were illustrated as positive in the graphs [47].

different patients may adapt to ACL injury in quite different ways. In some cases a surgical reconstruction of the ACL may reduce the need for the adaptations or correct potential excessive compensations, while in others may not have the desired effects.

A better understanding of the adaptations following ACL injury may help to develop more effective rehabilitation treatment for the injury, selectively and differentially strengthen individual muscles crossing the knee joint more appropriately to protect the ACL, and evaluate outcome of ACL reconstructions more objectively. Identification of biomechanical environment alterations that occur during daily activities in ACL-D and ACL-R knees could help to better understand clinical outcomes, as well as provide guidance for improvement in surgical technique and rehabilitative regimens for ACL injury treatment.

2.4 Rehabilitation after Anterior Cruciate Ligament Reconstruction

Water-based rehabilitation has been shown to have a wide range of applicability. Some examples of common rehabilitative conditions which may benefit mostly from aquatic therapy are: athletic injuries [106], degenerative disc disease, spinal cord injuries, post-stroke treatments [64], fibromyalgia, osteoarthritis/rheumatoid arthritis [112], [120] and chronic pain disorders.

Among athletic injuries, shoulder and knee rehabilitation and training are the most documented for respectively upper and lower extremities [118], [16], [119], [44], [92]. Since in this work, all the recruited subjects suffered a complete Anterior Cruciate Ligament (ACL) rupture and underwent a surgical reconstruction, in this section more attention is dedicated to the rehabilitation of patients with ACL lesion.

Rehabilitation after anterior cruciate ligament reconstruction is crucial in guaranteeing a beneficial outcome following surgery [101]. It has evolved over the past few decades thanks to the advances in surgical approaches, such as graft placement and graft fixation, the use of arthroscopically assisted procedures and new knowledge of stress-strain patterns in the ACL during various exercises [110]. Since the first half of the 1990s, the widespread twelve-month protocols requiring immobilization and non-weight bearing have started to give way to accelerated rehabilitative programmes based

on immediate weight bearing, no immobilization and aiming at a return to activity in 6 months. The primary goals of accelerated rehabilitation following ACL reconstruction are to recover joint range of motion, strength, quadriceps femoris muscle force-generating capability, and ambulatory skills [110], [119]. Postoperative joint effusion and the persistence of pain, however, may delay the achievement of these aims. Therefore, early phases of rehabilitation must minimize the deleterious effects of surgery without overstressing the injured part.

Although traditional rehabilitation after ACL reconstruction has taken place on land, published studies into the physical properties and biomechanical effects of water on the knee provide support for the use of hydrotherapy in knee rehabilitation [13], [104], [105], [106], [117].
Aquatic exercises have been recommended especially in the initial phase of rehabilitation to allow early mobilisation and to improve neuromuscular function [104].
In water, buoyancy greatly reduces the impact force, so the knee joint plays no role in the absorption of forces. This is an important aid to accomplish early full weight-bearing in water to enable gait re-education.
Moreover, exercises in water have been shown to be effective for improving strength and passive range of motion, and even if they may not have the same effects of exercise on land in regaining maximum muscle performance [119], aquatic rehabilitation may minimize the amount of joint effusion [119], leading to a significant reduction of pain.

To date, accelerated land-based and in water rehabilitation programmes for patients with ACL reconstruction have been proposed, as well as a combination of them. Future studies should continue to improve the effectiveness of combined protocols. New techniques which allow to evaluate and quantify the progression of the therapy may be extremely useful and give an important incentive to the development of even better rehabilitative programmes.

Chapter 3

Under-Water Markerless Gait Analysis

3.1 Subjects

Group	ACL-deficient	Normal	Total
Number of subjects	1	3	4
Male (No.)	1	3	4
Female (No.)	0	0	0
Age (year [mean±SD])	47	27.3±5.5	32.2±10.8
Height (cm [mean±SD])	180	177±11	177±9
Weight (kg [mean±SD])	85	67.5±15.2	71.9±15.2
BMI (kg/m^2 [mean±SD])	26.2	21.3±2.6	23.8±3.3
Post-injury (year)	3.4	-	-

Table 3.1: Subjects data.

Three healthy males with no past history of orthopedic and neurological disorders, and no recent injury or surgery that could affect their walking patterns, were recruited, in order to test the applicability of a markerless approach for an underwater gait analysis. Their mean age, height and mass (± 1 standard deviation) were 27.3±5.5 years, 1.77±0.11 m, and 67.5±15.2 kg respectively (Tab. 3.1), while single subject data are specified in Table 3.2.

Control Subjects	1	2	3
Age (year)	31	21	30
Height (cm)	165	186	180
Weight (kg)	50	76.5	76
BMI	18.4	22.1	23.5

Table 3.2: Control subjects single data.

A male ACL-injured subject has been investigated in this study. The patient was 47 years old and the complete ACL rupture occurred 3 years before the experiment (Tab. 3.1). He underwent surgical reconstruction of the ligament and the rehabilitative program was based on instrumental and functional physiotherapy, muscle strength training and proprioceptive exercises. No aquatic rehabilitation was included.
All subjects gave their informed consent before participating in the experiment.

3.2 Experimental Setup

Recruited subjects performed 6 walking trials at a self-selected normal speed in a swimming pool, with water at a shoulder level (water condition, UW). At least an average of 3 complete gait cycles for both left and right leg were extracted for each subject.
Video-based underwater markerless analysis requires subaqueous video cameras to record the walking patterns. The latter should be synchronized and spatially calibrated in order to perform a three-dimensional reconstruction of the subject. Video acquisition of the sole background was also performed.
The appropriate positioning of the set of cameras is one of the most challenging aspects for the adoption of the markerless technique in a swimming pool environment. Two different setups were tested to better investigate and assess the critical aspects in the definition of cameras' position. The equipment employed for this study, common for both setups, will be described in the following paragraphs, along with a brief mention of

the synchronization technique and the calibration procedure adopted.

3.2.1 Equipment

Six underwater colour analog cameras (TS-6021PSC, Tracer Technology Co. Ltd) has been used in the experiment presented in this thesis (Fig: 3.1).

Figure 3.1: Colour analog camera by Tracer Technology Co. Ltd.

Each camera was connected to a FireWire (IEEE 1934a)-equipped notebook through an Analog to Digital Video Converter (Canopus ADVC55; output DV video, PAL interlaced, 25 frames/second). A total of 5 notebooks were involved: one of them was equipped with a PCMCIA IEEE 1394a card, which enable it to be connected to two cameras. Although in theory two cameras could be connected to the same FireWire controller, provided that multiple input ports are available, this solution has proved to be experimentally unreliable. All notebooks were linked to a hub through Ethernet cables. The swimming pool where cameras were placed was 25 meters long and 16 meters wide. Depth varied from 1.20 to 1.70 meters, but acquisitions only regarded the most shallow half.

3.2.2 Synchronization

A custom-made software that could allow to acquire data simultaneously from different A/D converters has been adopted in order to synchronize the acquisition from all cameras.
It has been developed in C++ language and it is based on the Microsoft *DirectShow* engine, which is an extensible, filter-based framework that can

render or record media files. In particular, software code for accessing DV video streams from FireWire inputs, and writing them to hard disk, was based on the DVapp Sample application (*http://msdn.microsoft.com/en − us/library/ms783409(v=VS.85).aspx*), included in the Windows Software Development Kit (SDK). Handling of multiple video devices, which is a feature needed when more than one converter are connected to the same PC through additional FireWire cards, was implemented following the design provided by the open source *videoInput* library by Theodore Watson (*http* : *//www.muonics.net/school/spring*05/*videoInput/*).
Nevertheless, no direct control is possible on the operation of A/D video converters, which are independent one from the other. Therefore, due to the temporal discreteness of input video signals, delays of up to one frame have sometimes been found on the videos, and in such cases corrected through the identification of the same event in all the video sequences (i.e. heel contact).

3.2.3 Calibration

Calibration of the subaqueous cameras is a crucial step for the three-dimensional reconstruction of the subject. It involves the estimation of two different sets of parameters: the intrinsic ones, which are the parameters of the optical model that explains how the 3D scene is projected to the 2D image frame, and the extrinsic parameters, which are associated to the position and orientation of the cameras in the space.
Calibration techniques commonly proposed in literature are based on direct linear transformation (DLT) [71]. Intrinsic and extrinsic parameters are estimated at the same time from the projection image of a calibration grid of known size. Similarity equations are written for every control point, and then combined into a system that is solved by standard methods.
In this study, a two steps calibration algorithm has been adopted instead [125], performed using the *Camera Calibration Toolbox for Matlab* by Jean-Yves Bouguet (http://*www.vision.caltech.edu/bouguetj/calib_doc/*).
The optical model that has been assumed is the "*pin-hole*" camera, and the intrinsic (or internal) parameters are:

- focal length f: the distance from the center of projection (*focal point*)

to the image plane;

- principal point c: the projection on the image plane of the focal point;
- skew coefficient α: the angle between the pixels axes; usually pixels are assumed to be square, so that this parameter is often set to zero;
- distortion coefficients $\beta, \gamma, \xi, \zeta$: represent the radial and tangential distortion with which the nonlinearities due to the difference of the camera from the pin-hole model are modeled.

For ideal pin-hole cameras, the relationship between a 3D point $P = [x\ y\ z]^T$ expressed in the camera frame of reference, and the corresponding point's projection on the image plane $p = [u\ v]^T$ is:

$$p = \frac{1}{z} \begin{bmatrix} f_x & \alpha & c_x \\ 0 & f_y & c_y \end{bmatrix} P \tag{3.1}$$

where $\mathbf{f}$=$[f_x, f_y]$ is the focal length expressed in pixel size, respectively horizontal and vertical, $\mathbf{c}$=$[c_x, c_y]$ is the position on the image plane of the central point, α described the skewness of the two image axes, but is often considered unnecessary and set to 0.
Defining $r^2 = (x^2+y^2)/z^2$, lens distortion can be included as a multiplicative factor (representing the radial distortion) and an additive factor (tangential distortion), so the projection equation becomes:

$$p = \frac{(1+\beta r^2+\gamma r^4)}{z} \begin{bmatrix} f_x & \alpha & c_x \\ 0 & f_y & c_y \end{bmatrix} P + \frac{1}{z} \begin{bmatrix} 2\xi xy + \zeta(r^2 + 2x^2) \\ \xi(r^2 + 2y^2) + 2\zeta xy \end{bmatrix} \tag{3.2}$$

Initial estimate of focal length and central point parameters is given by the closed form solution of the pin-hole camera equations. From these, an initial estimation of distortion parameters is calculated, then all parameters are optimized minimizing the global distance between feature points measured on the images, and the projection, through the complete model, of the 3D points that generate them. A non-linear least square minimization algorithm (Levenberg-Marquardt) is employed.

In this work, intrinsic parameters are calculated from a series of images of a wooden panel with checkerboard-pattern drawn on it (13 x 9 black and white squares, side 42 millimeters), acquired from different angulations in space (Fig: 3.2). This allows their evaluation on a greater number of points (all corners, in all images), distributed on the whole image.

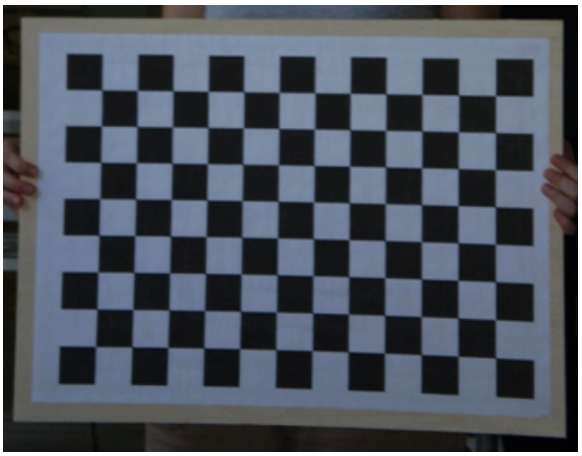

Figure 3.2: Checkerboard panel employed for intrinsic calibration.

The presence of water, however, renders this operation more complicated, because of the distortion due to refraction of the light beams [72]. Since calibration of intrinsic parameters has been performed out of water, they need to be corrected for use in the underwater environment. The change in refractive index from air (n_a) to water (n_w) must be taken into account. Following the work of Lavest et al. [74], the focal length has to be multiplied by $n_a/n_w = n = 1.333$; radial distortion coefficients consequently become

$$\rho_{1,w} = \rho_1/n, \rho_{2,w} = \rho_2/n^2$$

Extrinsic (or external) parameters are instead obtained capturing a calibration grid (Fig: 3.3) of known geometry (sized 2.07 x 1.07 x 1.40 meters). 24 control points were identified on it, and their position relative to an embedded system of reference were known.

Figure 3.3: Grid employed for extrinsic calibration of the cameras.

Once the intrinsic parameters are available, the position (a 3x1 translation vector T) and orientation (a 3x3 rotation matrix R) of the calibration grid relative to each camera (which represent the desired extrinsic parameters) can be computed from the projections of the predefined set of control points. The transformation from the coordinate system embedded in the camera to the global coordinate system associated to the object and a DLT technique are usually exploited. A point P of coordinated $[X_G, Y_G, Z_G]$ in the global coordinate system will have coordinates

$$\begin{bmatrix} X \\ Y \\ Z \end{bmatrix} = R \begin{bmatrix} X_G \\ Y_G \\ Z_G \end{bmatrix} + T \tag{3.3}$$

in the camera frame of reference. More numerous sets are usually advantageous to increase the estimation robustness.

3.2.4 Setup 1

Most acquisitions have been made with this setup. The position and orientation of the cameras as reconstructed by calibration is shown in Fig. 3.4, while an example of an image frame from each video sequence is illustrated in Fig. 3.5.

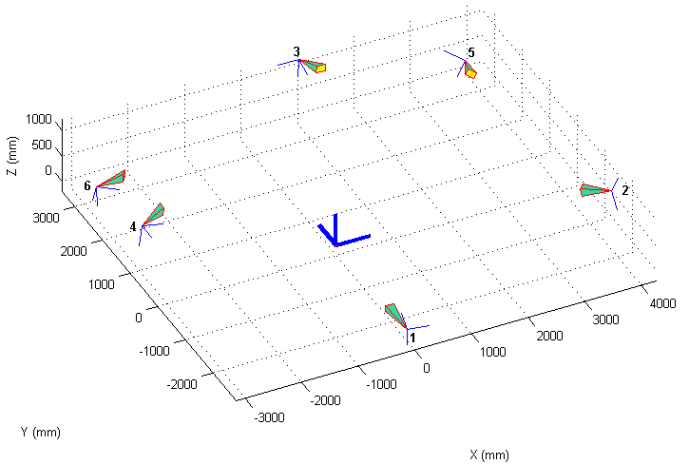

Figure 3.4: Setup 1: Camera's position as resulting from extrinsic calibration.

Calibration accuracy has been evaluated both in terms of calibration error and reconstruction error for the 24 control points. Calibration error is determined for each camera as the mean squared distance between measured control points' positions and projections of the corresponding 3D control points. Reconstruction error is the mean squared distance between known coordinates of 3D control points, and the corresponding points reconstructed from measured 2D projections. Both results are reported

Figure 3.5: Setup 1: Frame from each synchronized view of the gait analysis trial acquisition.

respectively in Table 3.3 and 3.4.

Calibration Error						
camera ID	1	2	3	4	5	6
calibration error (pixel)	1.8429	1.8824	1.6807	2.1395	2.2900	1.6327

Table 3.3: Setup 1: Calibration error (average over the 24 calibration points in each camera).

Reconstruction Error				
coordinate	X	Y	Z	3D
reconstruction error (mm)	6.8134	6.4722	3.7025	8.8017

Table 3.4: Setup 1: Average reconstruction error on the 24 calibration points.

3.2.5 Setup 2

This setup represents an attempt to enhance some critical aspects observed during the processing phase of data acquired with the previous setup. The position and orientation of the cameras in this case, as reconstructed by calibration, is shown in Fig. 3.6. Calibration and reconstruction errors are reported respectively in Table 3.5 and 3.6.

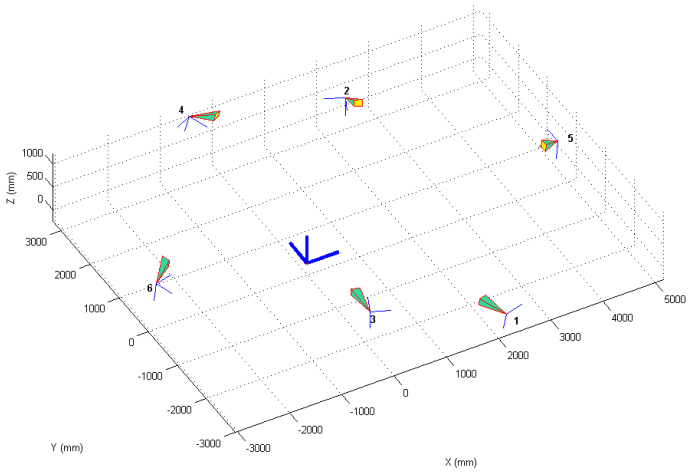

Figure 3.6: Setup 2: Camera's position as resulting from extrinsic calibration.

Calibration Error						
camera ID	1	2	3	4	5	6
calibration error (pixel)	1.2230	1.8616	1.8589	2.1048	1.7668	1.8106

Table 3.5: Setup 2: Calibration error (average over the 24 calibration points in each camera).

An example of an image frame from each video sequence is shown in Fig. 3.7.

Reconstruction Error				
coordinate	X	Y	Z	3D
reconstruction error (mm)	4.0122	6.3600	3.6847	7.6526

Table 3.6: Setup 2: Average reconstruction error on the 24 calibration points.

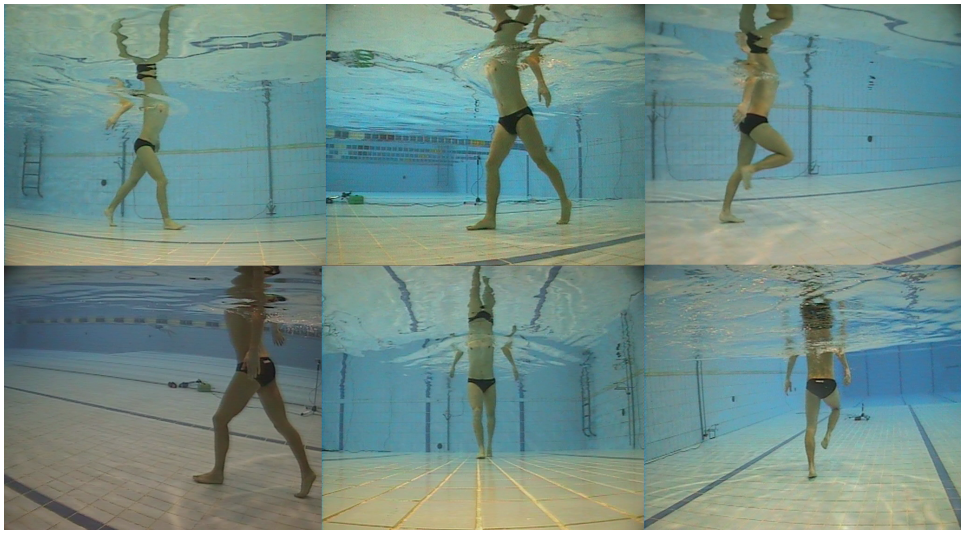

Figure 3.7: Setup 2: Frame from each synchronized view of the gait analysis trial acquisition.

3.2.6 Dry setup

A laboratory equipped with a 9-cameras BTS s.r.l motion capture system was also available. It has been exploited for a full-body static acquisition of the subjects in a reference pose, since from underwater video is not achievable due to head lack. Grayscale images have been acquired at 50Hz with a resolution of 640x480 pixels. Calibration was performed following manufacture's recommendations (Thor2 calibration system, BTS_SMARTD, *http://www.btsbioengineering.com/BTSBioengineering/Kinematics*):
a rigid wand, with three markers mounted on it, is swept through the volume of interest, in a dynamic acquisition, for simultaneous calibration of intrinsic parameters, and relative position of the video-cameras (Fig. 3.8

left). A three axes calibration grid was then placed on the ground and acquired for determination of the global frame of reference (Fig. 3.8 right).

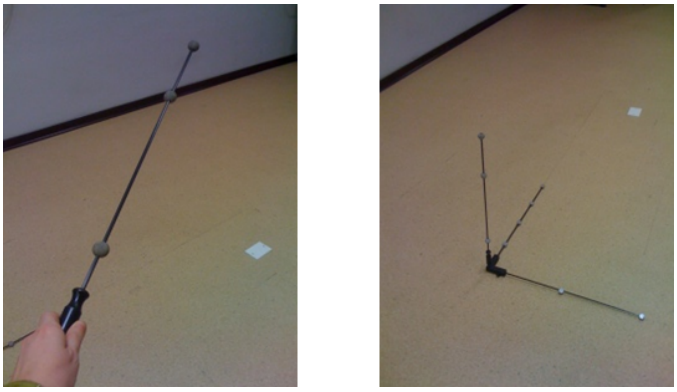

Figure 3.8: Rigid wand with three markers, employed for intrinsic calibration of the cameras (left) and calibration grid with 9 markers, for extrinsic calibration (right).

3.3 Data Processing

3.3.1 Out of Water data

Out of water data are represented by the static acquisitions of the subjects in the reference pose with the dry setup previously described (paragraph 3.2.6). These are necessary to generate the visual hulls input of the algorithm described in section 1.5.4 for the creation of each subject specific model.

Background subtraction and visual hull creation

Generally, foreground/background segmentation of gray scale images is more difficult than for color data, since the chromatic component is often more discriminative than sole luminance. However, in this case, the foreground has been extracted by simple subtraction of a reference background image from each frame of the video sequence. Pixels of the

resulting image that present values greater than a fixed threshold (usually set in the 4-6 range) are considered foreground. A Matlab function has been exploited to perform this operation. A visual hull has been created from the silhouettes thus obtained as indicated in section 1.5.3. An example of the silhouettes extracted from the nine cameras' views, together with the corresponding visual hull are shown in Fig. 3.9.

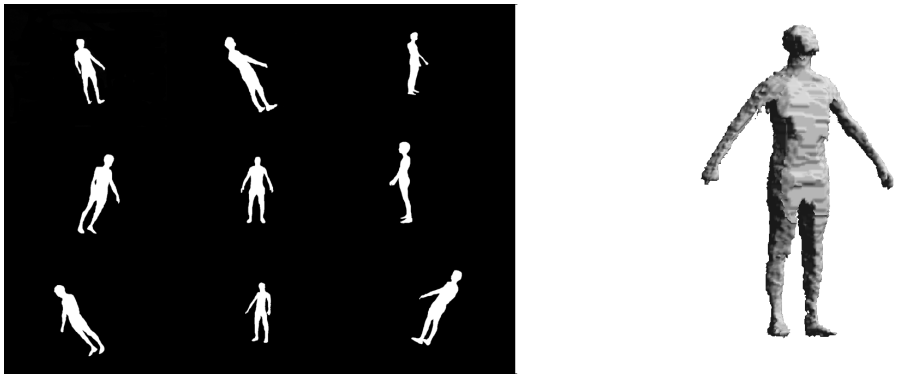

Figure 3.9: Static acquisition of the subject: silhouettes from all the cameras (left) and corresponding visual hull (right).

Model definition and initialization

A subject-specific model has been generated automatically employing the procedure explained in section 1.5.4. The full-body dry visual hull of each subject, obtained as explained above, has been taken as starting point. The kinematic relationship between the segments is shown in Fig. 3.10. The pelvis is chosen as root of the kinematic chain.
A transformation has been applied to the segments' frames of reference so that they could assume a little more anatomical meaning, helpful in the later interpretation of joint angles. Since the longitudinal axes connecting child and parent joint has no anatomical correspondence, a 90° rotation around X axis reports it into the medio-lateral direction, while Y axis assumes a vertical positive orientation. A model with the orientation of the initial markerless technical frames for the right leg is illustrated on the left in Fig.

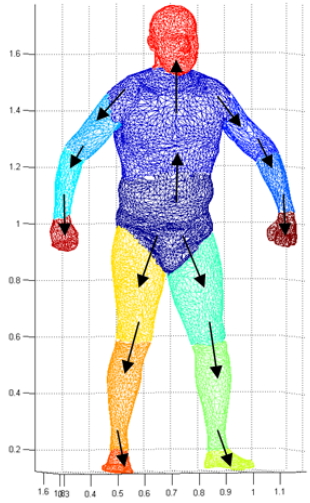

Figure 3.10: Scheme of the model kinematic chain: each arrow point from "parent" to "child" segment.

3.11, while on the right the same model with the frames of reference after the modification is displayed.

Model initialization has also to be considered. The model's orientation could be different from the swimming pool's global frame of reference and they must be aligned for a successful matching process. Another important adjustment is the barycenter's position. Since the subjects walked with the head out of water, the reconstructed underwater visual hulls (see section 3.3.2) have no head. This represents a problem for the matching algorithm, which always tries to fit the head with the points in the visual hull that belong to the body. A future enhancement could be to eliminate the head from the model chain, even if a model initialization will still remain an unavoidable step.

3.3.2 Under-Water data

In the present section, all the processing steps that have been followed to extract kinematics data from the video acquired with the two underwater setup presented in paragraphs 3.2.4 and 3.2.5 are explained.

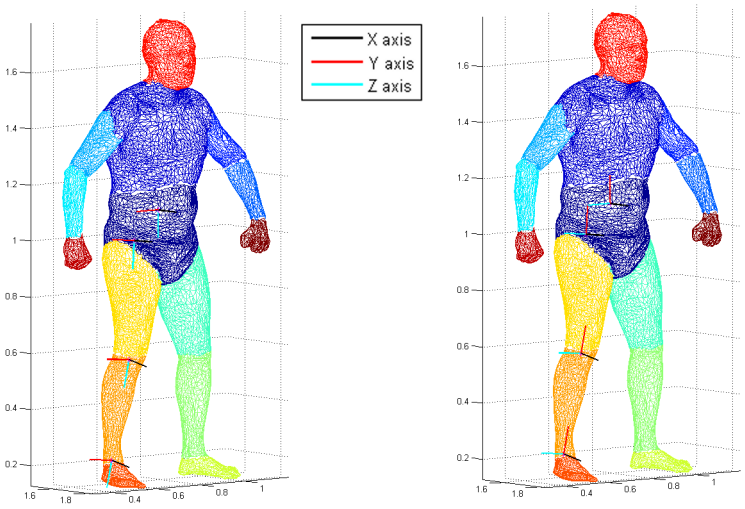

Figure 3.11: Model with markerless technical frames of reference of the right leg (left) and the same model with the rotated reference frames for joint angle calculation.

Deinterlacing

DV videos obtained from A/D video converters are interlaced. This means that each frame consists of two consecutive sub-fields, one containing all even lines, another with the odd lines. The fields are captured in succession at a rate twice that of the nominal frame rate. For instance, a PAL video has a nominal acquisition rate of 25 frames per second, while a half image (a single field) is captured every 50 seconds.

Analog television employed this technique because it allowed for less transmission bandwidth and matched the properties of CRT screens. Only traditional CRT-based TV sets are capable of displaying interlaced signal, which requires a screen that can natively show the individual fields in a sequential order. Most modern monitors, such as LCD, DLP and plasma, are not able to work in interlaced mode, because they are fixed-resolution and only support progressive scanning. Moreover, since the interlaced signal contains two fields of a video frame shot at two different times, images thus

recorded cannot be directly employed for 3D reconstruction. Therefore, the two frames need to be combined to a single progressive frame.

Deinterlacing refers to this process of creating a progressive video, where each frame corresponds to a different time instant, from an interlaced video. The most advanced deinterlacing techniques consist basically in a spatial and temporal interpolation of pixel values in the images (bob-deinterlacing), so that the resulting video has double frame rate. Implementation has been realized with *S*mart-Bob filter for VirtualDub developed by Donald Graft (http://*neuron*2.*net*/*bob.html*). *VirtualDub* is a video processing utility for Microsoft Windows, written by Avery Lee and available as free software (*www.virtualdub.org*). In order to apply the bob-deinterlacing filter to videos, they need to be input to VirtualDub as double rate, half vertical resolution videos. This is achieved on-the-fly through the use of the Avisynth frameserver (*www.avisynth.org*). The result of this operation on one of the acquired frames is shown in Fig. 3.12.

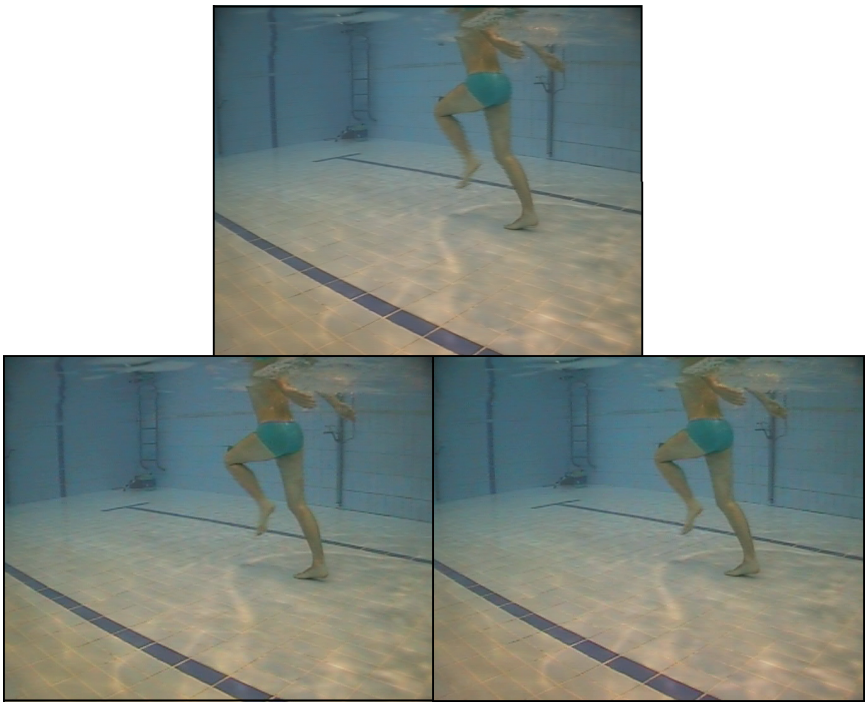

Figure 3.12: Example of original frame from a DV video (top), and the corresponding frames obtained through interpolation (bottom).

Background subtraction

The background of underwater videos is not static, mainly due to water unavoidable movement, which causes a continuous variation of the scene. Therefore, the use of a single background image as reference for the subtraction comes out to be inappropriate. The creation of a background model from a video sequence of the empty swimming pool is necessary to characterize the variations in pixel intensity values belonging to the moving background. The Gaussian-mixture model approach, described in section 1.5.2, has been adopted. The implementation provided by the Intel OpenCV open source C++ library (*http : //opencv.willowgarage.com/wiki/*) has been taken as a starting point. The algorithm has been slightly modified to account for the water environment.

However, reflexes remain the main problem within underwater images. They appear so similar to the actual subject in the original videos, that it is not possible to discriminate between the two on the sole base of pixels color content. An example of this kind of artifact is reported in Fig. 3.13.

Silhouettes extraction from underwater videos recording walking patterns suffers also for specific drawbacks connected to the application itself. The subject shadow on the pool pavement, for instance, moves with the subject and, at the beginning of the video sequence, is often recognized as a foreground element, with the result shown in Fig. 3.14(left). This, in some cases, makes necessary to impose more strict parameters, which leads to a loss in feet details with the consequent higher uncertainty in their reconstruction (Fig. 3.14 right).

Presence of other subjects or external moving objects inside the cameras' views during the acquisition is highly undesirable and must be avoid, to not be extracted as a foreground elements together with the actual subject. Particular features of the swimming pool has to be considered as well, such as, for example, color lines on the pool pavement, which can be identified as background even if the subject in a specific frame covered them (see the three horizontal lines that cross the subject lower limbs in the silhouette of Fig. 3.14 left).

Improving this first initial step is challenging but highly desirable, since it

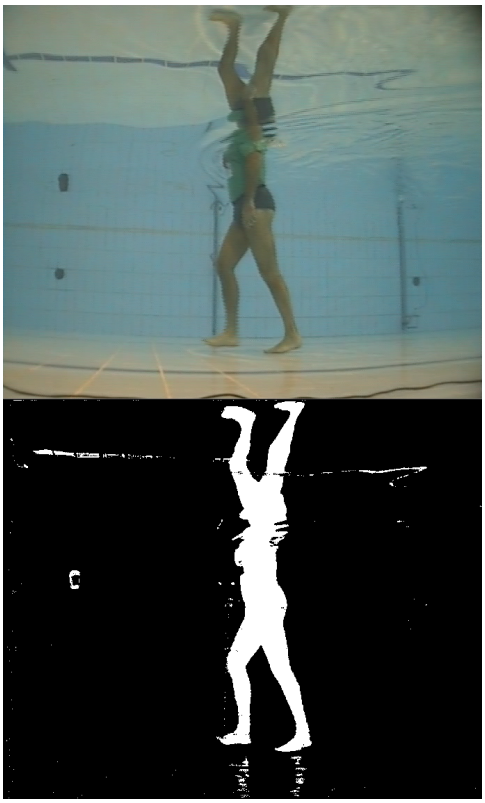

Figure 3.13: Background subtraction: example of reflexes.

is critical for the accuracy achievable in the following processing phases.

Visual hull creation

Visual hulls are created from silhouettes as indicated in section 1.5.3. The volume of interest is partitioned into voxels of size 0.01 m; then, each of the voxels' vertices is projected on the silhouettes, exploiting the calibration functions of the OpenCV library, that are analogous to those provided by the Calibration Toolbox for Matlab. The 3D meshes thus obtained are saved in PLY format, also known as Polygon File Format or Stanford Triangle Format. An example is shown in Fig. 3.15.

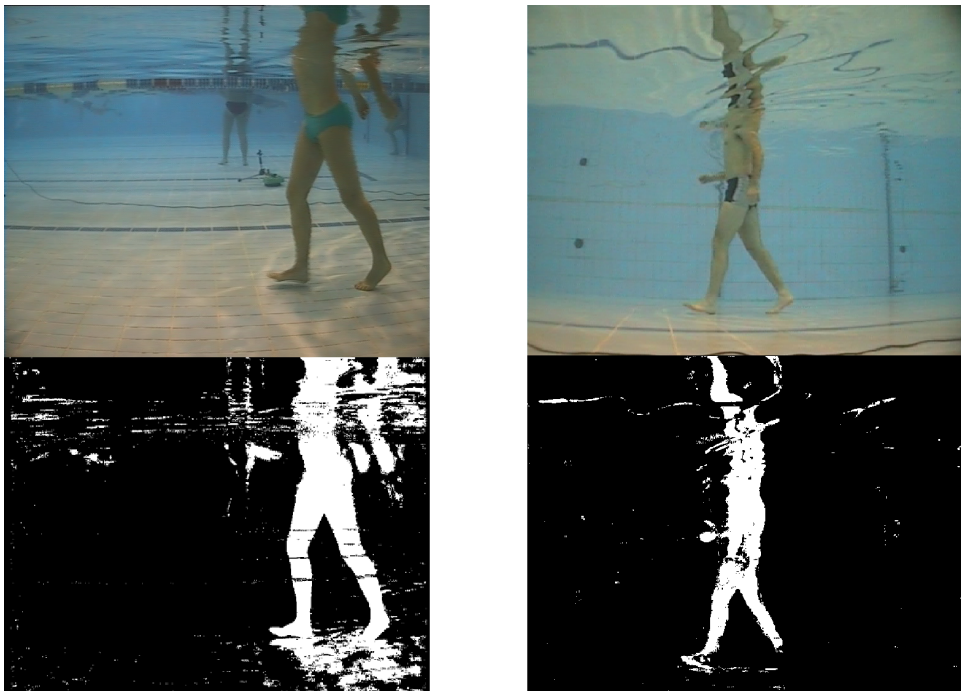

Figure 3.14: Background subtraction: example of subject's shadow extraction (left) and loss of feet details (right).

Figure 3.15: Visual hull reconstructed from a frame of an acquired gait trial.

Model Matching

The sequence of visual hulls is tracked employing the articulated-ICP algorithm described in section 1.5.5, with a data-to-model approach. An example of a matching result, with the comparison between the model and the visual hull at the corresponding frame beside, is shown in Fig. 3.16. The position and orientation in space of each body segment's embedded frame of reference are obtained for the whole sequence.

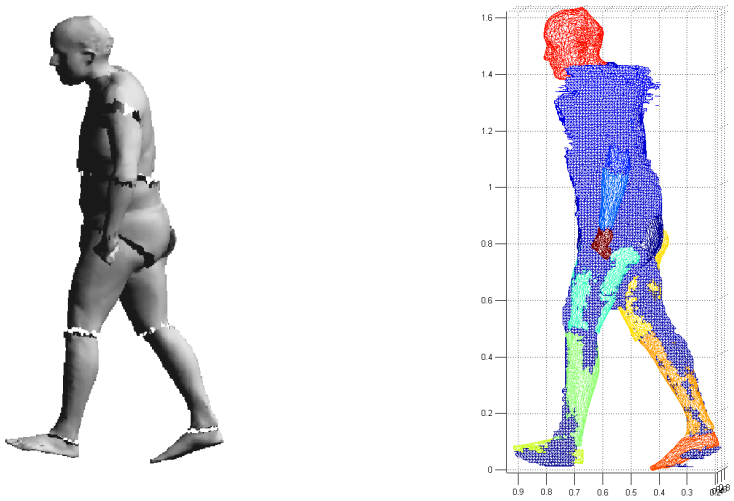

Figure 3.16: Example of matching result (left) and a comparison between the model and visual hull at the corresponding frame (right).

Joint angles calculation

Joints angles evaluated with a markerless system are inevitably different from those assessed using a marker-based technique. This is one of the main difficulty in comparing the two approaches and it is due to the basic discrepancy in the definition of the segments' frames of reference. Several studies have been realized to quantitatively compare the two technologies [25], [86]. In this work, a purely markerless joint angles definition has been given and its feasibility tested. Only flexion/extension (flex/ext) angles

have been taking into account. Frames of reference of pelvis, femur, tibia and foot, oriented as shown on the right in Fig. 3.11, have been considered (Fig. 3.17 left). Hip, knee and ankle joint angles have been calculated as the rotation around Z axis (medio-lateral axis) of the parent segment which causes the X axis of the child segment's frame of reference to overlap to the same forward direction axis of the parent segment. Thus, hip flex/ext angle is obtained from relative rotation of femur frame of reference on pelvi coordinate system, knee flex/ext angle from tibia and femur relative rotation around Z-femur axis, while ankle flex/ext angle from the relative rotation of foot and tibia reference's frame. Positive and negative signs are defined according to clinical conventions. A clarification can be found in Fig. 3.17 (right).

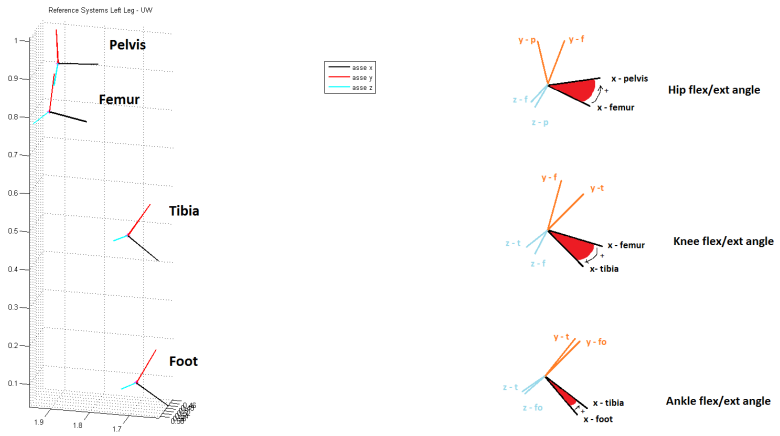

Figure 3.17: Left leg's frames of reference (left) and clarification of flex/ext joint angles calculation.

Statistical Analysis

A Matlab code has been developed to compute the correlation among all stances and gait cycles available from the 6 acquired trials of each subject. Mean and standard deviation have been evaluated considering just those which show a correlation coefficient with almost another one greater than

0.75 [109], [83]. For each subject, representative bands of the correlated results for both stances and gait cycles are thus obtained. An example taken from control subject 1 is proposed. In Fig. 3.18 and 3.19, all correlated trials used to assess subject joint ankles mean and standard deviation are shown, while on Fig. 3.20 and Fig. 3.21 the resulting bands are displayed.

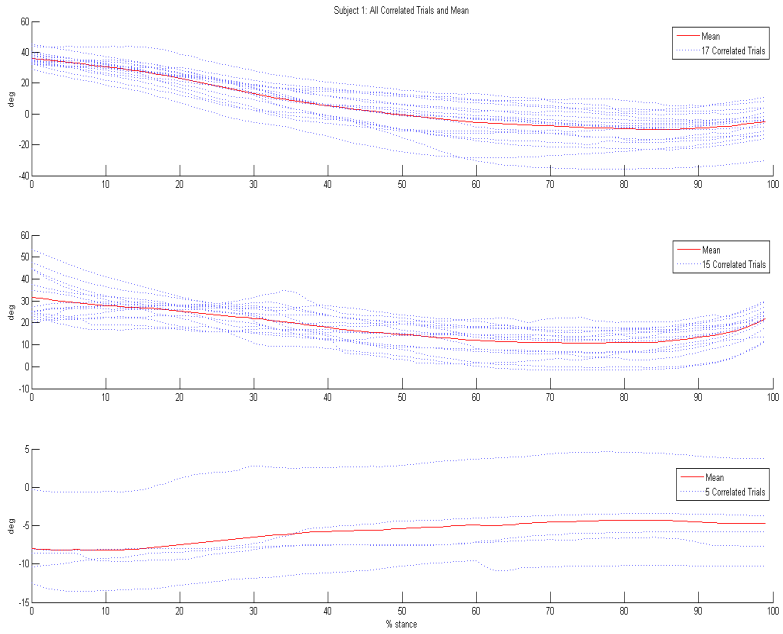

Figure 3.18: Subject 1: all correlated trials used to compute the mean patterns (reported in red).

The same strategy has been adopted considering all the control subjects together: correlation has been assessed combining all the already correlated trails of each control subject. Inter-subjects mean and standard deviation has been calculated and from them Control UW Markerless Bands have been obtained. These are indicative of how healthy people can walk underwater. To understand differences among dry and underwater conditions of walking, these UW Control Bands, with their strong limitation of accounting just for three subjects, have been then compared with Normative Out of Water (OW) Bands taken from Sawacha et. al [109].

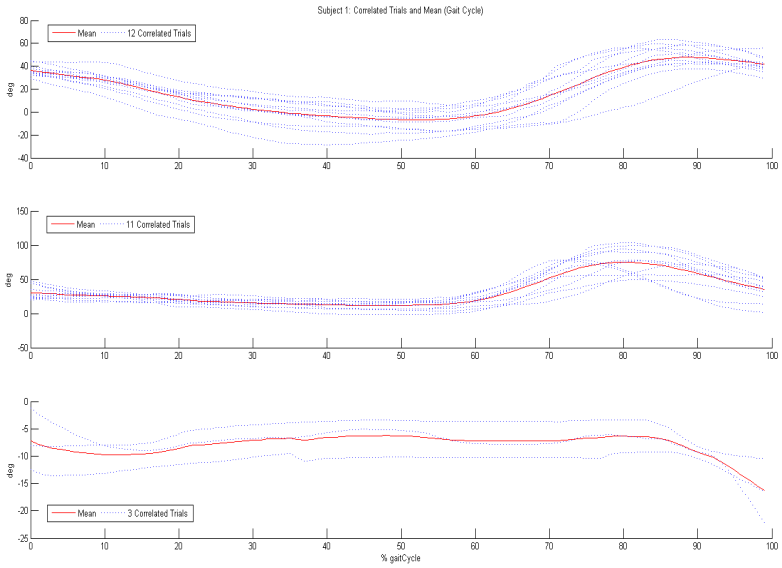

Figure 3.19: Subject 1: all correlated gait cycles used to compute the mean patterns (reported in red).

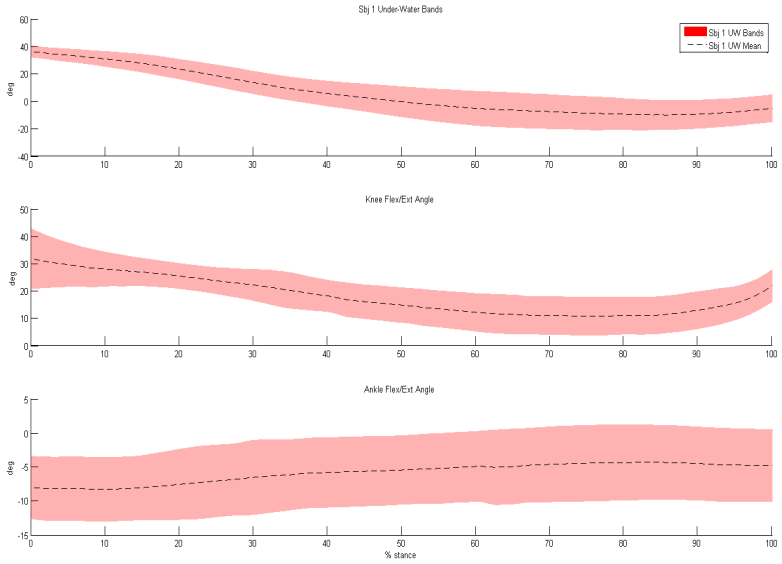

Figure 3.20: Underwater bands from control subject 1.

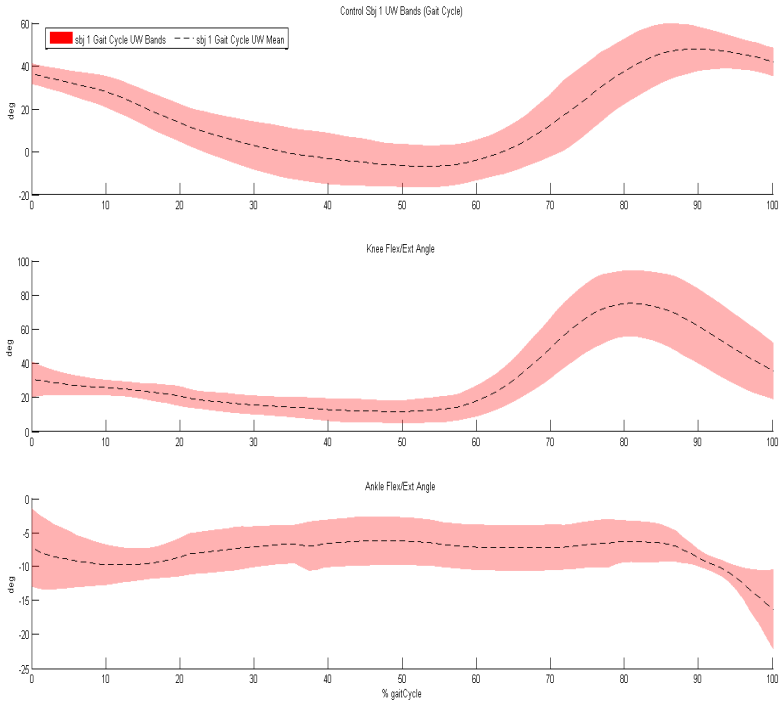

Figure 3.21: Gait Cycle underwater bands from control subject 1.

Chapter 4

Results

4.1 Control Subjects

4.1.1 Subject 1

This subject has been acquired with Setup 1 (see section 3.2.4). Stance phases and gait cycles (gc) analyzed for each recorded trials are reported on Table 4.1. Stances between which the gait cycles are considered, are indicated in parentheses.

Trails	Left	Right
	Stance and Gait Cycles	
1.	I,II,gc(I-II)	II,gc(I-II)
2.	I,gc(I-II)	I
3.	I,II,gc(I-II),gc(II-III)	I,II,gc(I-II)
4.	I	gc(I-II)
5.	I,II,gc(I-II),gc(II-III)	I,II,gc(I-II)
6.	I,II,gc(I-II),gc(II-III)	I,gc(I-II)

Table 4.1: Processed stance phase and gait cycles for each trial.

Findings regarding stance and gait cycle analysis are presented in the following distinct sections.

Stance Results

Left and right leg are examined separately, since it has been possible to extract a considerable number of both stance and gait cycle for each. Left correlated trials are first represented in Fig. 4.1, followed by the corresponding correlation values reported in Tab. 4.2, 4.3 and 4.4 for hip, knee and ankle joint respectively (for each trials the considered stance is specified below brackets). The same is then presented for the right leg (Fig. 4.2 and Tab. 4.5, 4.6, 4.7).

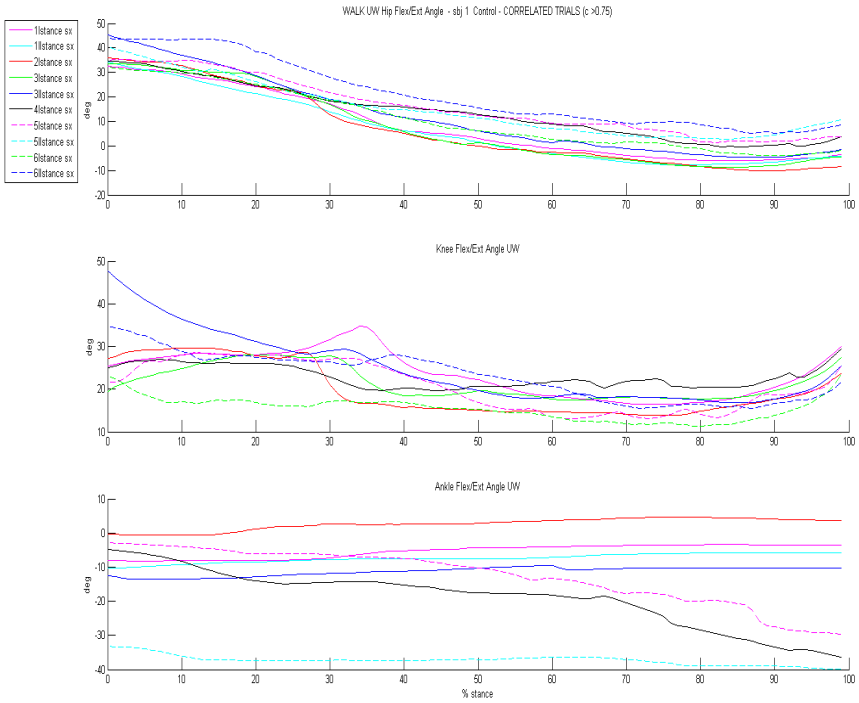

Figure 4.1: Subject 1: Left Correlated Trials.

Gait Cycle Results

Whole gait cycles have been examined as well. Correlated trials are shown in Fig. 4.3 and 4.4, while correlation coefficients are specified in Tab. 4.8, 4.9 and 4.10 for the left limb, Tab. 4.11, 4.12 and 4.13 for the right one.

Left Hip Correlation										
Trials										
1. (Ist)	1	0,997	0,995	0,997	0,994	0,981	0,991	0,984	0,995	0,994
1. (IIst)	0,997	1	0,993	0,993	0,997	0,980	0,984	0,993	0,989	0,988
2. (Ist)	0,995	0,993	1	0,994	0,995	0,981	0,992	0,981	0,992	0,995
3. (Ist)	0,997	0,993	0,994	1	0,990	0,973	0,988	0,981	0,992	0,995
3. (IIst)	0,995	0,997	0,995	0,990	1	0,990	0,989	0,991	0,991	0,990
4. (Ist)	0,981	0,980	0,981	0,973	0,986	1	0,991	0,971	0,985	0,979
5. (Ist)	0,991	0,985	0,992	0,988	0,989	0,991	1	0,970	0,996	0,994
5. (IIst)	0,984	0,993	0,981	0,981	0,991	0,971	0,970	1	0,971	0,974
6. (Ist)	0,995	0,989	0,992	0,992	0,991	0,985	0,996	0,971	1	0,995
6. (IIst)	0,994	0,988	0,995	0,995	0,990	0,979	0,994	0,974	0,995	1

Table 4.2: Subject 1: Left Hip Correlation Coefficients.

Left Knee Correlation										
Trials										
1. (Ist)	1	0,702	0,653	0,805	0,703	0,471	0,936	0,546	0,787	0,765
1. (IIst)	0,702	1	0,877	0,665	0,946	0,817	0,751	0,611	0,886	0,802
2. (Ist)	0,653	0,877	1	0,826	0,871	0,893	0,813	0,461	0,671	0,704
3. (Ist)	0,805	0,665	0,826	1	0,639	0,753	0,871	0,510	0,609	0,547
3. (IIst)	0,703	0,946	0,871	0,639	1	0,722	0,785	0,384	0,787	0,881
4. (Ist)	0,471	0,817	0,893	0,753	0,722	1	0,616	0,566	0,623	0,472
5. (Ist)	0,936	0,751	0,813	0,871	0,785	0,616	1	0,483	0,736	0,786
5. (IIst)	0,546	0,611	0,461	0,510	0,384	0,566	0,483	1	0,699	0,234
6. (Ist)	0,787	0,887	0,671	0,609	0,787	0,623	0,736	0,699	1	0,799
6. (IIst)	0,765	0,802	0,704	0,547	0,881	0,472	0,786	0,234	0,799	1

Table 4.3: Subject 1: Left Knee Correlation Coefficients.

Left Ankle Correlation										
Trials										
1. (Ist)	1	0,903	0,919	0,576	0,951	0,808	0,831	0,582	0,175	0,154
1. (IIst)	0,903	1	0,948	0,603	0,857	0,924	0,895	0,820	0,096	0,493
2. (Ist)	0,919	0,948	1	0,607	0,934	0,806	0,779	0,671	0,030	0,330
3. (Ist)	0,576	0,603	0,607	1	0,651	0,547	0,532	0,552	0,414	0,515
3. (IIst)	0,951	0,856	0,934	0,651	1	0,751	0,749	0,568	0,040	0,191
4. (Ist)	0,808	0,924	0,806	0,547	0,751	1	0,968	0,866	0,106	0,576
5. (Ist)	0,831	0,895	0,779	0,532	0,749	0,968	1	0,744	0,045	0,450
5. (IIst)	0,582	0,820	0,671	0,552	0,568	0,866	0,744	1	0,499	0,826
6. (Ist)	0,175	0,096	0,030	0,414	0,040	0,106	0,045	0,499	1	0,827
6. (IIst)	0,154	0,493	0,330	0,516	0,191	0,576	0,450	0,826	0,827	1

Table 4.4: Subject 1: Left Ankle Correlation Coefficients.

Right Hip Correlation							
Trials							
1. (IIst)	1	0,922	0,972	0,961	0,984	0,993	0,933
2. (Ist)	0,921	1	0,982	0,983	0,933	0,901	0,986
3. (Ist)	0,972	0,982	1	0,998	0,979	0,960	0,990
3. (IIst)	0,961	0,983	0,998	1	0,975	0,951	0,995
5. (Ist)	0,984	0,933	0,979	0,975	1	0,990	0,959
5. (IIst)	0,993	0,901	0,960	0,951	0,990	1	0,924
6. (Ist)	0,933	0,986	0,989	0,995	0,959	0,924	1

Table 4.5: Subject 1: Right Hip Correlation Coefficients.

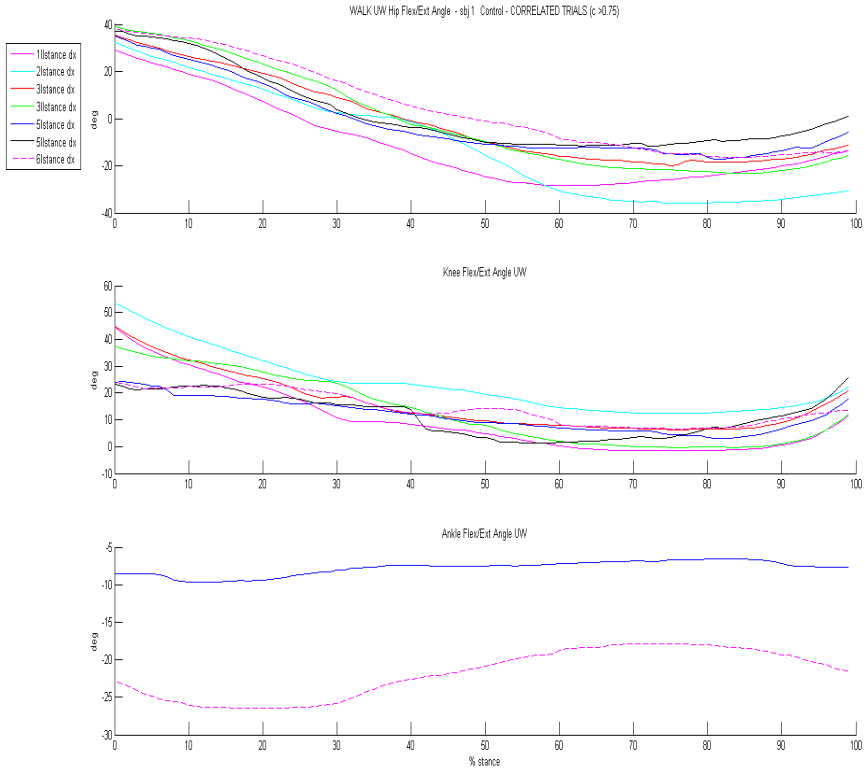

Figure 4.2: Subject 1: Right Correlated Trials.

Right Knee Correlation							
Trials							
1. (IIst)	1	0,996	0,991	0,957	0,954	0,826	0,907
2. (Ist)	0,996	1	0,982	0,953	0,948	0,797	0,894
3. (Ist)	0,991	0,982	1	0,943	0,958	0,862	0,893
3. (IIst)	0,957	0,953	0,943	1	0,968	0,841	0,965
5. (Ist)	0,954	0,948	0,958	0,968	1	0,864	0,940
5. (IIst)	0,826	0,797	0,862	0,841	0,864	1	0,814
6. (Ist)	0,907	0,894	0,893	0,965	0,940	0,814	1

Table 4.6: Subject 1: Right Knee Correlation Coefficients.

Right Ankle Correlation							
Trials							
1. (IIst)	1	0,389	0,123	0,229	0,334	0,438	0,286
2. (Ist)	0,389	1	0,384	0,261	0,823	0,099	0,876
3. (Ist)	0,123	0,384	1	0,398	0,495	0,557	0,537
3. (IIst)	0,229	0,261	0,398	1	0,070	0,453	0,284
5. (Ist)	0,333	0,893	0,495	0,070	1	0,091	0,913
5. (IIst)	0,437	0,099	0,557	0,453	0,091	1	0,335
6. (Ist)	0,286	0,876	0,537	0,285	0,913	0,335	1

Table 4.7: Subject 1: Right Ankle Correlation Coefficients.

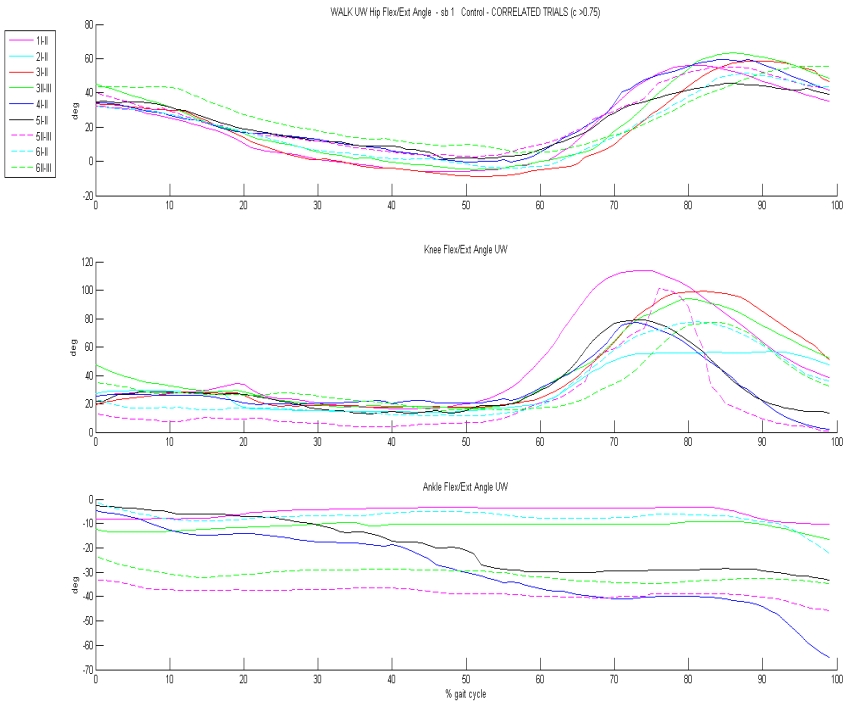

Figure 4.3: Subject 1: Gait Cycle Left Correlated Trials.

Left Gait Cycle Hip Correlation									
Trials									
1. (I-II)	1	0,283	0,910	0,938	0,985	0,967	0,983	0,909	0,751
2. (I-II)	0,283	1	0,561	0,513	0,299	0,492	0,377	0,566	0,785
3. (I-II)	0,910	0,561	1	0,992	0,935	0,966	0,957	0,996	0,939
3. (II-III)	0,939	0,513	0,992	1	0,958	0,976	0,978	0,990	0,908
4. (I-II)	0,985	0,299	0,935	0,958	1	0,971	0,989	0,938	0,781
5. (I-II)	0,967	0,492	0,966	0,976	0,971	1	0,981	0,968	0,881
5. (II-III)	0,984	0,377	0,957	0,978	0,989	0,981	1	0,955	0,822
6. (I-II)	0,909	0,566	0,996	0,990	0,938	0,968	0,955	1	0,940
6. (II-III)	0,751	0,785	0,939	0,908	0,781	0,881	0,822	0,940	1

Table 4.8: Subject 1: Left Gait Cycle Hip Correlation Coefficients.

Left Gait Cycle Knee Correlation									
Trials									
1. (I-II)	1	0,824	0,840	0,860	0,868	0,925	0,872	0,902	0,670
2. (I-II)	0,840	1	0,951	0,964	0,527	0,640	0,599	0,938	0,852
3. (I-II)	0,840	0,951	1	0,978	0,582	0,650	0,664	0,986	0,931
3. (II-III)	0,859	0,964	0,978	1	0,624	0,699	0,695	0,980	0,926
4. (I-II)	0,868	0,527	0,582	0,624	1	0,968	0,930	0,679	0,457
5. (I-II)	0,925	0,639	0,650	0,699	0,968	1	0,935	0,738	0,503
5. (II-III)	0,872	0,599	0,664	0,695	0,930	0,935	1	0,736	0,540
6. (I-II)	0,902	0,938	0,985	0,980	0,679	0,738	0,736	1	0,907
6. (II-III)	0,670	0,852	0,931	0,926	0,457	0,503	0,540	0,907	1

Table 4.9: Subject 1: Left Gait Cycle Knee Correlation Coefficients.

Left Gait Cycle Ankle Correlation									
Trials									
1. (I-II)	1	0,729	0,140	0,867	0,010	0,281	0,148	0,558	0,038
2. (I-II)	0,729	1	0,264	0,791	0,488	0,656	0,358	0,100	0,355
3. (I-II)	0,140	0,264	1	0,134	0,828	0,695	0,850	0,801	0,708
3. (II-III)	0,867	0,791	0,134	1	0,108	0,356	0,110	0,543	0,136
4. (I-II)	0,011	0,487	0,828	0,108	1	0,943	0,923	0,601	0,785
5. (I-II)	0,281	0,656	0,695	0,356	0,943	1	0,798	0,347	0,715
5. (II-III)	0,148	0,358	0,850	0,110	0,923	0,798	1	0,799	0,777
6. (I-II)	0,558	0,100	0,801	0,543	0,601	0,347	0,799	1	0,559
6. (II-III)	0,038	0,355	0,708	0,136	0,785	0,715	0,777	0,559	1

Table 4.10: Subject 1: Left Gait Cycle Ankle Correlation Coefficients.

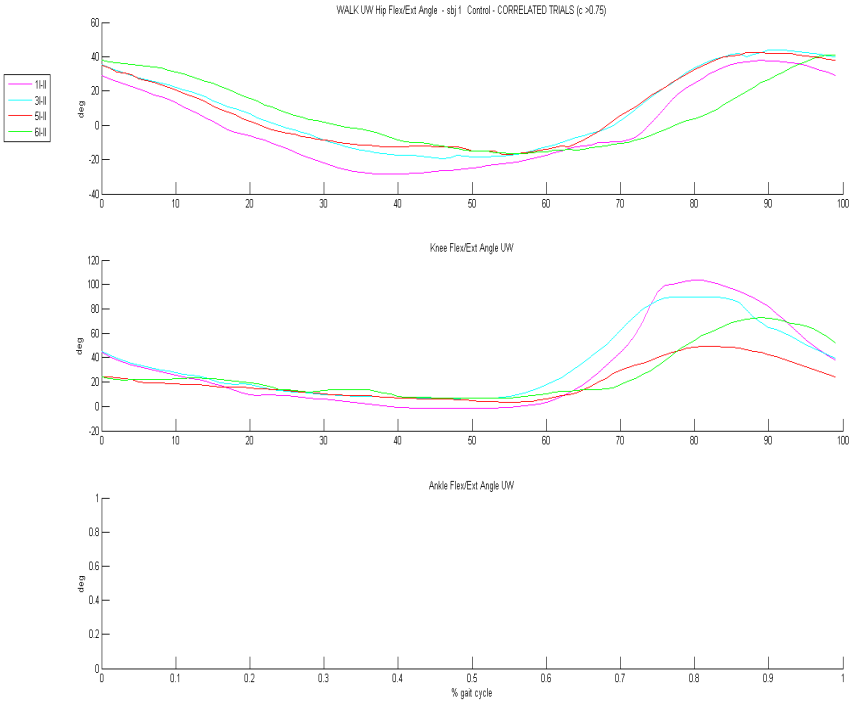

Figure 4.4: Subject 1: Gait Cycle Right Correlated Trials.

Right Gait Cycle Hip Correlation				
Trials				
1. (I-II)	1	0,990	0,985	0,787
3. (I-II)	0,990	1	0,993	0,815
5. (I-II)	0,985	0,993	1	0,793
6. (I-II)	0,787	0,815	0,793	1

Table 4.11: Subject 1: Right Gait Cycle Hip Correlation Coefficients.

Right Gait Cycle Knee Correlation				
Trials				
1. (I-II)	1	0,979	0,988	0,855
3. (I-II)	0,979	1	0,966	0,781
5. (I-II)	0,988	0,966	1	0,883
6. (I-II)	0,855	0,781	0,883	1

Table 4.12: Subject 1: Right Gait Cycle Knee Correlation Coefficients.

Right Gait Cycle Ankle Correlation				
Trials				
1. (I-II)	1	0,295	0,305	0,055
3. (I-II)	0,295	1	0,199	0,181
5. (I-II)	0,305	0,199	1	0,792
6. (I-II)	0,055	0,181	0,792	1

Table 4.13: Subject 1: Right Gait Cycle Ankle Correlation Coefficients.

4.1.2 Subject 2

Setup 1 (section 3.2.4) has been exploited to acquire the second control subject as well. Table 4.14 shows what has been achieved through data processing.

Trials	Left	Right
	Stance and Gait Cycles	
1.	I	-
2.	II	-
3.	II,III,gc(II-III)	-
4.	I,II,III,gc(I-II),gc(II-III)	II,gc(II-III)
5.	I,II,gc(I-II),gc(II-III)	gc(I-II)
6.	I,II,gc(I-II)	I

Table 4.14: Processed stance phases and gait cycles for each trials.

Stance Results

Hip, knee and ankle angles' patterns during stance phases which show high values (> 0.75) of correlation are reported in Fig. 4.5 for the left side, and in Fig. 4.6 for the right one. Correlation coefficients for each joint are indicated in Tab. 4.15-4.18.

Gait Cycles Results

Since only two of the acquired right gait cycles led to results, left and right outcomes for this subject are presented together without distinction (Fig. 4.7, Tab. 4.19, 4.20, 4.21).

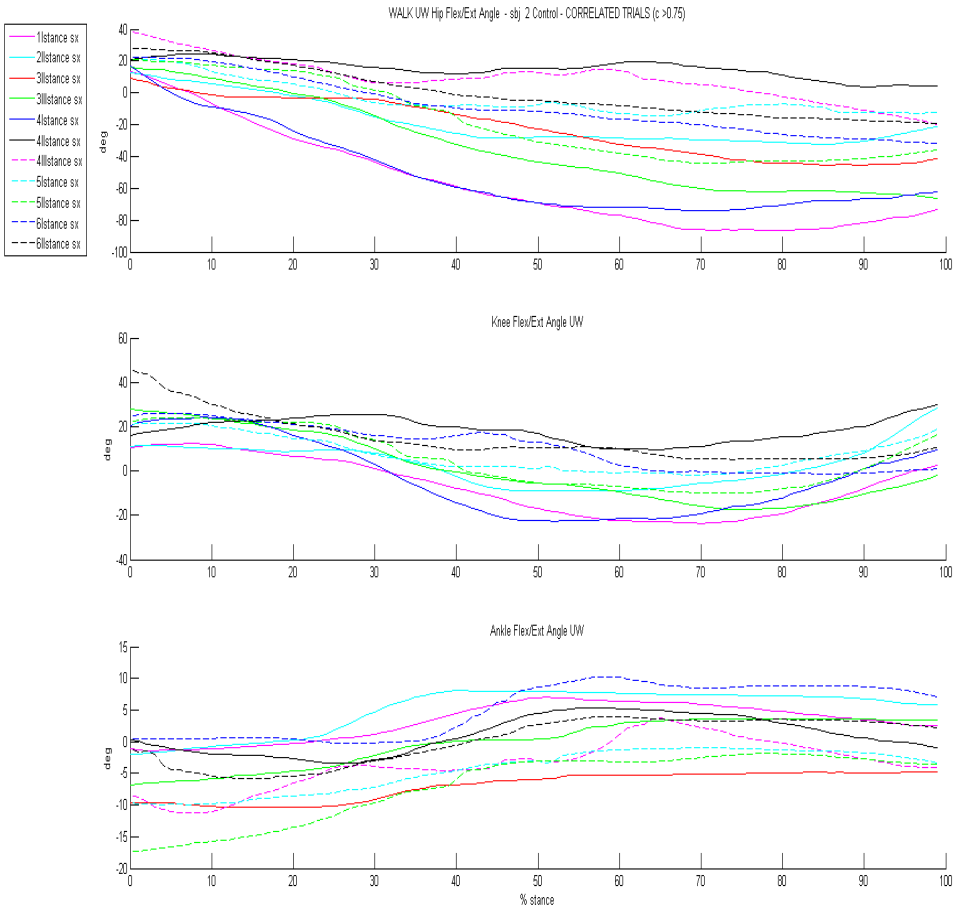

Figure 4.5: Subject 2: Left Correlated Trials.

Left Hip Correlation											
Trials											
1 (I st)	1	0,979	0,917	0,976	0,984	0,700	0,808	0,947	0,968	0,964	0,976
2 (II st)	0,979	1	0,850	0,945	0,989	0,702	0,760	0,948	0,945	0,936	0,951
3 (II st)	0,916	0,850	1	0,967	0,849	0,734	0,822	0,788	0,956	0,950	0,952
3 (III st)	0,976	0,945	0,967	1	0,944	0,760	0,835	0,898	0,990	0,987	0,994
4 (I st)	0,984	0,989	0,849	0,944	1	0,650	0,746	0,959	0,944	0,926	0,944
4 (II st)	0,700	0,702	0,734	0,760	0,650	1	0,922	0,693	0,683	0,841	0,811
4 (III st)	0,808	0,760	0,823	0,835	0,746	0,922	1	0,808	0,752	0,904	0,878
5 (I st)	0,947	0,948	0,788	0,898	0,959	0,693	0,808	1	0,873	0,910	0,917
5 (II st)	0,968	0,945	0,956	0,990	0,944	0,683	0,752	0,873	1	0,957	0,972
6 (I st)	0,964	0,936	0,950	0,987	0,926	0,841	0,904	0,910	0,957	1	0,997
6 (II st)	0,976	0,951	0,952	0,994	0,944	0,811	0,878	0,917	0,972	0,997	1

Table 4.15: Subject 2: Left Hip Correlation Coefficients.

Left Knee Correlation											
Trials											
1 (I st)	1	0,808	0,418	0,924	0,946	0,779	0,303	0,938	0,987	0,787	0,806
2 (II st)	0,808	1	0,201	0,556	0,851	0,827	0,539	0,854	0,785	0,289	0,455
3 (II st)	0,418	0,201	1	0,466	0,150	0,415	0,200	0,277	0,406	0,579	0,386
3 (III st)	0,924	0,556	0,466	1	0,846	0,551	0,172	0,833	0,946	0,932	0,921
4 (I st)	0,946	0,851	0,150	0,846	1	0,680	0,522	0,973	0,943	0,630	0,786
4 (II st)	0,779	0,827	0,415	0,551	0,679	1	0,075	0,666	0,740	0,437	0,287
4 (III st)	0,303	0,539	0,200	0,172	0,522	0,075	1	0,600	0,304	0,0828	0,375
5 (I st)	0,938	0,854	0,277	0,833	0,973	0,666	0,600	1	0,927	0,629	0,809
5 (II st)	0,987	0,785	0,406	0,946	0,943	0,740	0,304	0,927	1	0,798	0,826
6 (I st)	0,787	0,289	0,579	0,932	0,630	0,437	0,0828	0,629	0,798	1	0,841
6 (II st)	0,806	0,455	0,386	0,921	0,786	0,287	0,375	0,809	0,826	0,841	1

Table 4.16: Subject 2: Left Knee Correlation Coefficients.

Left Ankle Correlation											
Trials											
1 (I st)	1	0,933	0,861	0,838	0,166	0,892	0,844	0,910	0,917	0,840	0,869
2 (II st)	0,933	1	0,882	0,897	0,289	0,708	0,823	0,911	0,955	0,750	0,835
3 (II st)	0,861	0,882	1	0,970	0,616	0,789	0,797	0,974	0,957	0,929	0,975
3 (III st)	0,838	0,897	0,970	1	0,624	0,705	0,871	0,982	0,974	0,886	0,925
4 (I st)	0,166	0,289	0,616	0,624	1	0,141	0,290	0,522	0,499	0,570	0,547
4 (II st)	0,892	0,708	0,789	0,705	0,145	1	0,740	0,816	0,748	0,869	0,859
4 (III st)	0,844	0,823	0,797	0,871	0,290	0,740	1	0,897	0,865	0,770	0,814
5 (I st)	0,910	0,911	0,974	0,982	0,522	0,816	0,897	1	0,980	0,931	0,957
5 (II st)	0,917	0,955	0,957	0,974	0,499	0,748	0,865	0,980	1	0,883	0,920
6 (I st)	0,841	0,750	0,929	0,886	0,570	0,869	0,770	0,931	0,883	1	0,949
6 (II st)	0,869	0,835	0,975	0,925	0,547	0,859	0,814	0,957	0,920	0,950	1

Table 4.17: Subject 2: Left Ankle Correlation Coefficients.

Right Correlation						
	Hip		Knee		Ankle	
Trials						
4 (II st)	1	0.877	1	0.484	1	0.779
6 (I st)	0.877	1	0.484	1	0.779	1

Table 4.18: Subject 2: Hip, Knee and Ankle Right Correlation Coefficients.

Gait Cycle Hip Correlation								
Trials								
3. (II-III sx)	1	0,902	0,853	0,849	0,892	0,947	0,849	0,915
4. (I-II sx)	0,902	1	0,730	0,709	0,864	0,933	0,886	0,915
4. (II-III sx)	0,853	0,730	1	0,662	0,917	0,703	0,743	0,764
4. (II-III dx)	0,849	0,709	0,662	1	0,712	0,834	0,899	0,821
5. (I-II sx)	0,892	0,864	0,917	0,712	1	0,814	0,867	0,781
5. (II-III sx)	0,947	0,933	0,703	0,834	0,814	1	0,930	0,926
5. (I-II dx)	0,894	0,886	0,743	0,899	0,867	0,931	1	0,884
6. (I-II sx)	0,915	0,915	0,764	0,821	0,781	0,926	0,884	1

Table 4.19: Subject 2: Gait Cycle Hip Correlation Coefficients.

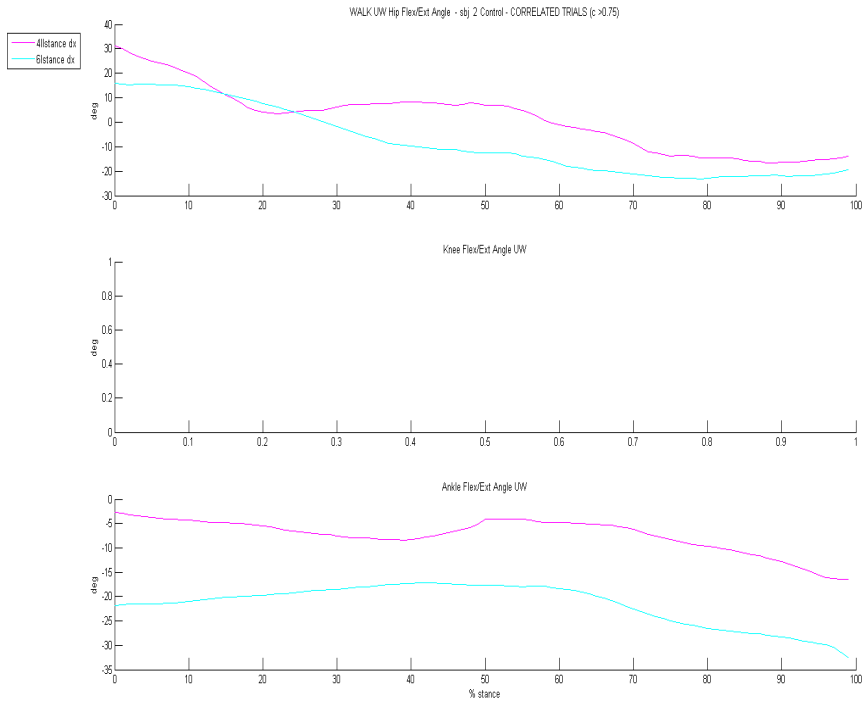

Figure 4.6: Subject 2: Right Correlated Trials

Gait Cycle Knee Correlation								
Trials								
3. (II-III sx)	1	0,749	0,964	0,904	0,961	0,890	0,929	0,823
4. (I-II sx)	0,749	1	0,806	0,713	0,858	0,936	0,821	0,737
4. (II-III sx)	0,964	0,806	1	0,825	0,960	0,908	0,942	0,885
4. (II-III dx)	0,904	0,713	0,825	1	0,915	0,859	0,894	0,606
5. (I-II sx)	0,961	0,858	0,960	0,915	1	0,948	0,976	0,817
5. (II-III sx)	0,890	0,936	0,908	0,859	0,948	1	0,910	0,807
5. (I-II dx)	0,929	0,821	0,942	0,893	0,976	0,910	1	0,797
6. (I-II sx)	0,823	0,737	0,885	0,606	0,817	0,807	0,797	1

Table 4.20: Subject 2: Gait Cycle Knee Correlation Coefficients.

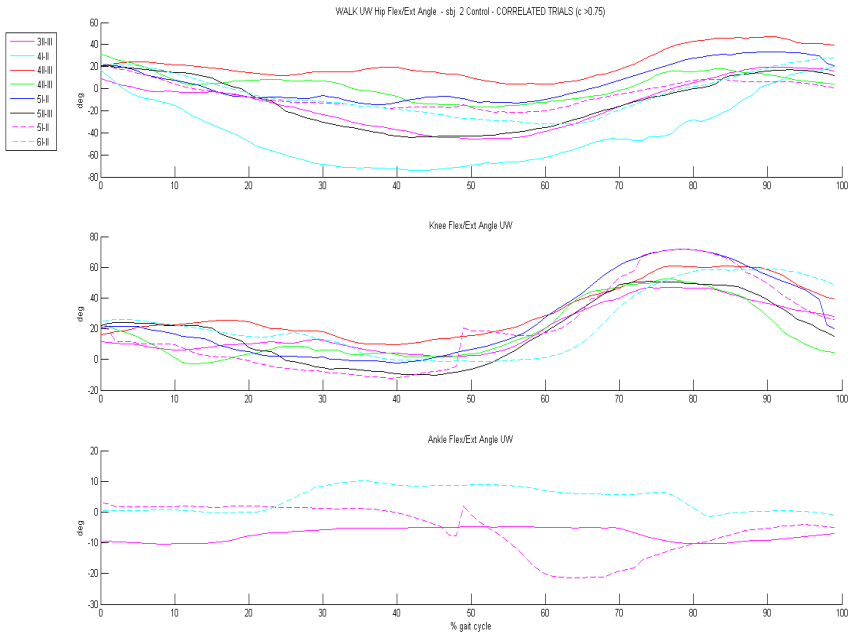

Figure 4.7: Subject 2: Gait Cycle Correlated Trials.

Gait Cycle Ankle Correlation								
Trials								
3. (II-III sx)	1	0,087	0,670	0,330	0,102	0,144	0,300	0,845
4. (I-II sx)	0,087	1	0,387	0,243	0,682	0,738	0,863	0,083
4. (II-III sx)	0,670	0,387	1	0,468	0	0,235	0,175	0,840
4. (II-III dx)	0,330	0,243	0,468	1	0,277	0,027	0,499	0,482
5. (I-II sx)	0,102	0,682	0	0,277	1	0,877	0,467	0,292
5. (II-III sx)	0,144	0,738	0,235	0,027	0,877	1	0,495	0,170
5. (I-II dx)	0,300	0,863	0,175	0,499	0,467	0,495	1	0,231
6. (I-II sx)	0,845	0,083	0,840	0,482	0,292	0,170	0,231	1

Table 4.21: Subject 2: Gait Cycle Ankle Correlation Coefficients.

4.1.3 Subject 3

Differently from the previous two subjects, this one has been acquired with Setup 2 (section 3.2.5). Less trials have been tested in this case: just 3 instead of 6, due to inconvenience with the swimming pool availability.

Trails	Left	Right
	Stance and Gait Cycles	
1.	I, gc(I-II)	-
2.	I,II,gc(I-II)	I, gc(I-II)
3.	II, gc(I-II)	I

Table 4.22: Processed stance phases and gait cycles for each trial.

Because of the limited number, left and right side's findings of both stance and gait cycles are grouped together.

Stance Results

Fig. 4.8 displays all the obtained correlated trials for this subject. Tables 4.23, 4.24 and 4.25 reported correlation coefficients for the three joints. The same results regarding the whole gait cycle are presented in the next paragraph (Fig. 4.9, Tab. 4.26-4.28).

Hip Correlation						
Trials						
1 (Ist sx)	1	0,952	0,987	0,981	0,930	0,965
2 (Ist sx)	0,952	1	0,918	0,967	0,833	0,943
2 (IIst sx)	0,987	0,918	1	0,958	0,966	0,965
2 (Ist dx)	0,982	0,967	0,958	1	0,896	0,969
3 (IIst sx)	0,930	0,833	0,966	0,896	1	0,955
3 (Ist dx)	0,965	0,943	0,965	0,969	0,955	1

Table 4.23: Subject 3: Hip Correlation Coefficients.

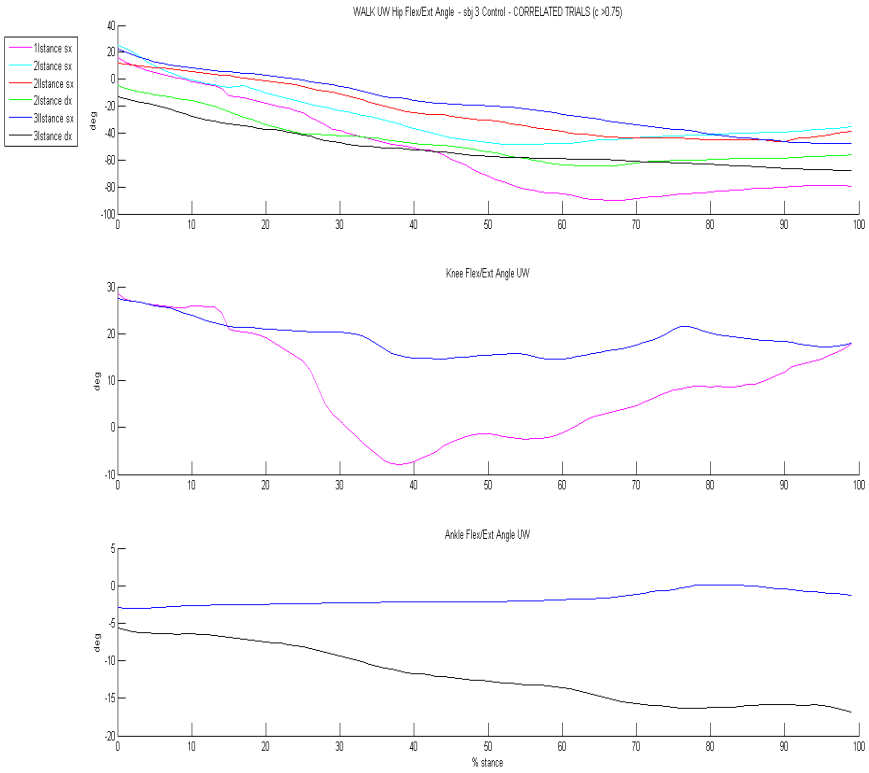

Figure 4.8: Subject 3: Correlated Trials.

Knee Correlation						
Trials						
1 (Ist sx)	1	0,505	0,508	0,612	0,850	0,589
2 (Ist sx)	0,505	1	0,317	0,435	0,387	0,588
2 (IIst sx)	0,508	0,317	1	0,664	0,248	0,440
2 (Ist dx)	0,612	0,435	0,664	1	0,488	0,803
3 (IIst sx)	0,850	0,387	0,248	0,488	1	0,631
3 (Ist dx)	0,589	0,588	0,440	0,803	0,632	1

Table 4.24: Subject 3: Knee Correlation Coefficients.

Gait Cycle Results

Ankle Correlation						
Trials						
1 (Ist sx)	1	0,222	0,147	0,601	0,352	0,194
2 (Ist sx)	0,222	1	0,605	0,353	0,539	0,631
2 (IIst sx)	0,147	0,605	1	0,615	0,697	0,920
2 (Ist dx)	0,601	0,353	0,615	1	0,889	0,851
3 (IIst sx)	0,352	0,539	0,697	0,889	1	0,877
3 (Ist dx)	0,194	0,631	0,920	0,851	0,877	1

Table 4.25: Subject 3: Ankle Correlation Coefficients.

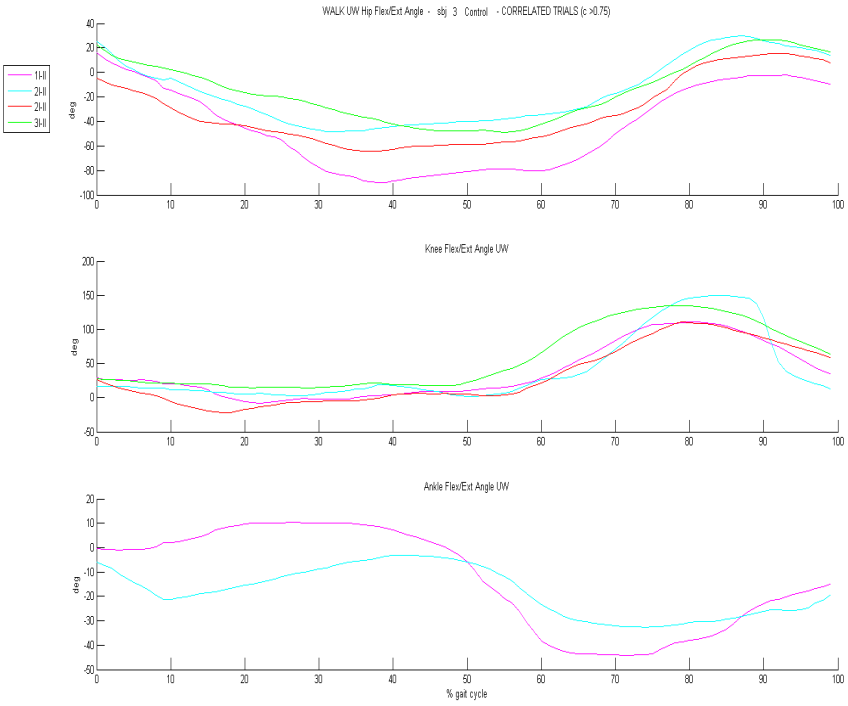

Figure 4.9: Subject 3: Correlated Gait Cycles.

Gait Cycle Hip Correlation				
Trials		Gait Cycles		
1 (I-II sx)	1	0,938	0,913	0,966
2 (I-II sx)	0,938	1	0,983	0,932
2 (I-II dx)	0,913	0,983	1	0,939
3 (I-II sx)	0,966	0,932	0,939	1

Table 4.26: Subject 3: Gait Cycle Hip Correlation Coefficients.

Gait Cycle Knee Correlation				
Trials		Gait Cycles		
1 (I-II sx)	1	0,930	0,969	0,969
2 (I-II sx)	0,930	1	0,899	0,882
2 (I-II dx)	0,969	0,899	1	0,955
3 (I-II sx)	0,969	0,882	0,954	1

Table 4.27: Subject 3: Gait Cycle Knee Correlation Coefficients.

Gait Cycle Ankle Correlation				
Trials				
1 (I-II sx)	1	0,833	0,665	0,287
2 (I-II sx)	0,833	1	0,421	0,317
2 (I-II dx)	0,664	0,422	1	0,208
3 (I-II sx)	0,287	0,317	0,208	1

Table 4.28: Subject 3: Gait Cycle Ankle Correlation Coefficients.

4.2 UW vs OW Gait Analysis

This section is dedicated to a comparison between the under-water and the normal dry condition of walking.

The total mean, which takes into account both sides, with its standard deviation, has been calculated for each control, obtaining UW bands representative of that subject. A comparison between these UW subject-specific bands and the mention OW bands is proposed (Subject 1: Fig. 4.10, 4.11, Subject 2: 4.12, 4.13, Subject 3: 4.14, 4.15).

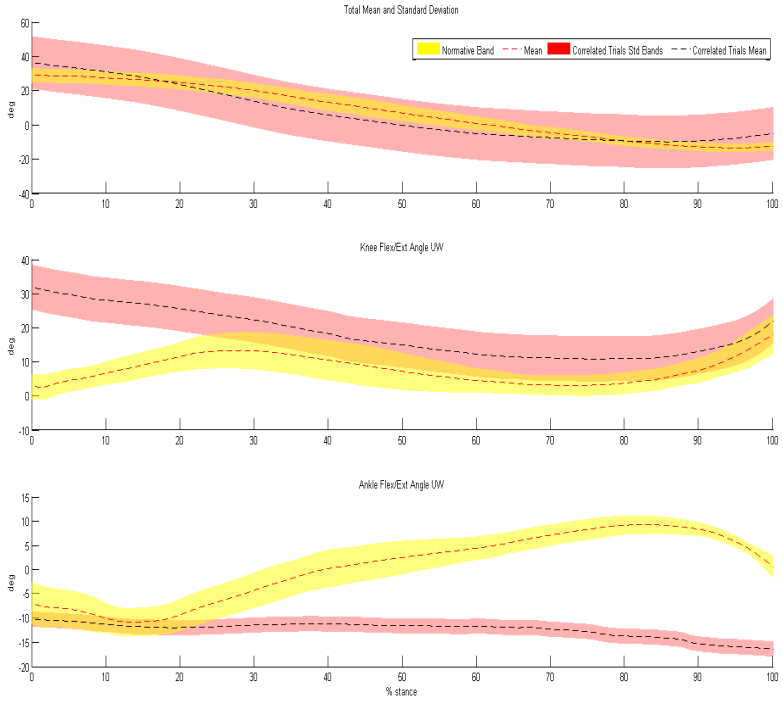

Figure 4.10: Subject 1: Global Mean (± 1 SD) vs Normative OW Bands.

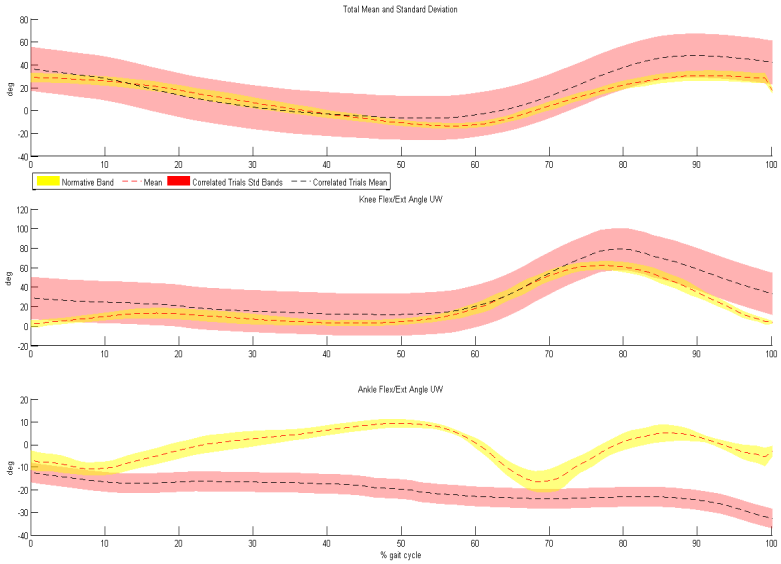

Figure 4.11: Subject 1: Global GC Mean (± 1 SD) vs Normative OW Bands.

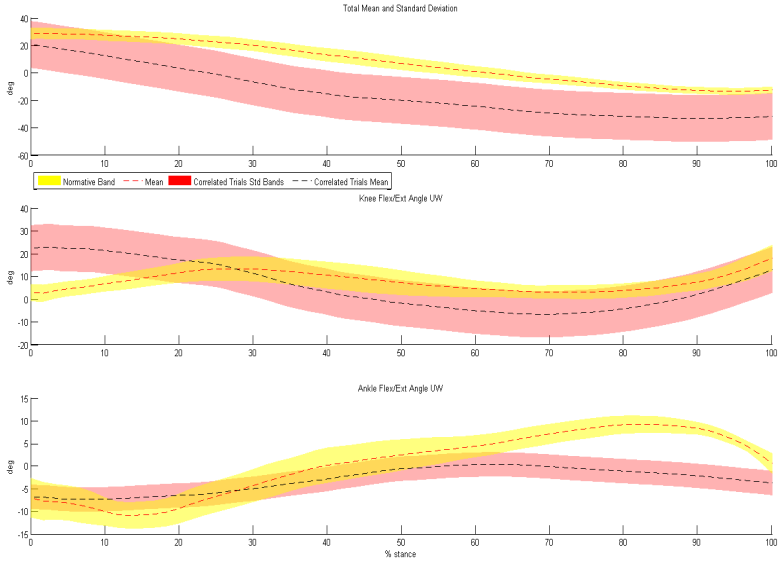

Figure 4.12: Subject 2: Global Mean (± 1 SD) vs Normative OW Bands.

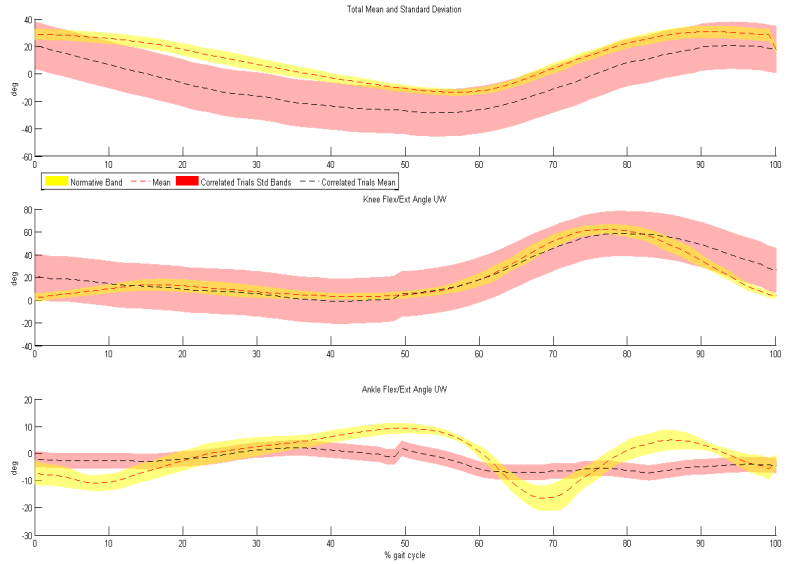

Figure 4.13: Subject 2: Global GC Mean (± 1 SD) vs Normative OW Bands.

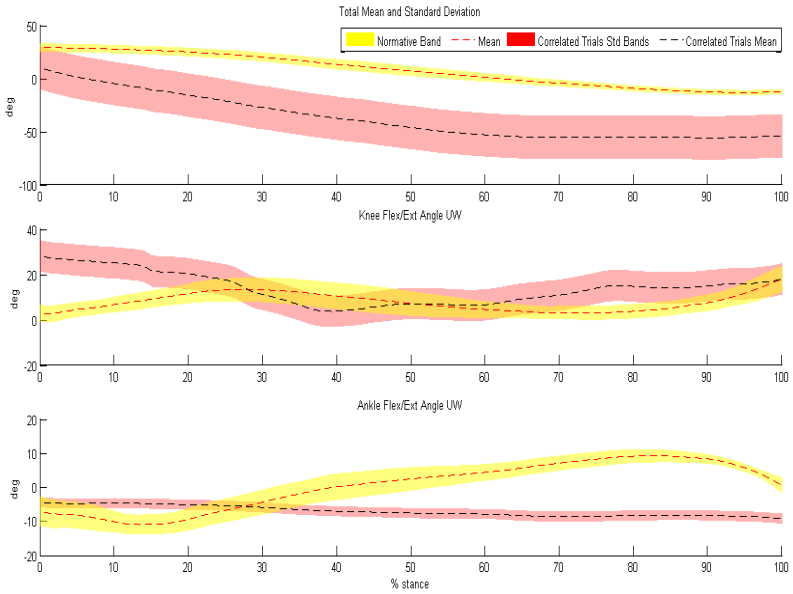

Figure 4.14: Subject 3: Correlated Trials Mean (± 1 SD).

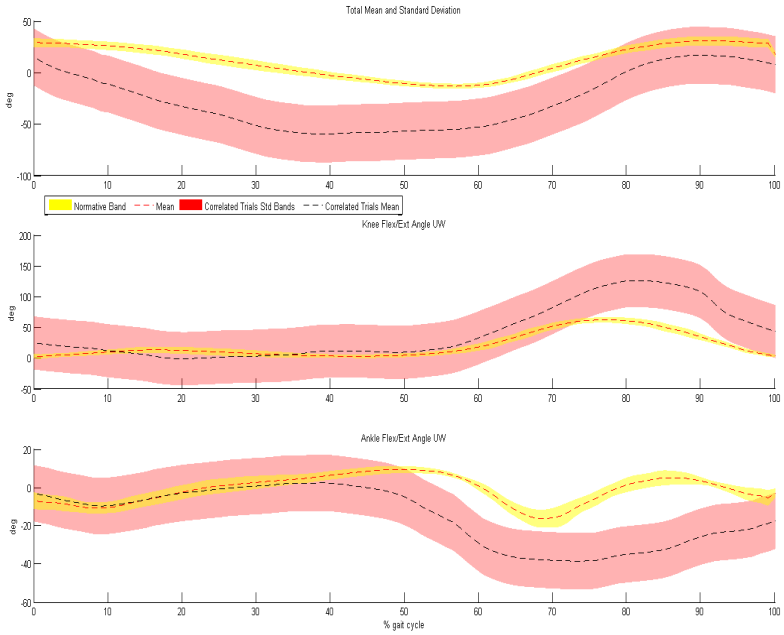

Figure 4.15: Subject 3: Correlated GC Mean (± 1 SD)vs Normative OW Bands.

UW Bands from control subjects

The same UW bands have been evaluated taking into account all control subjects correlated trials at once, as explained in section 3.3.2 (*Statistical Analysis*). Fig. 4.16 reported all controls correlated trials for the stance phase, and Fig. 4.18 for the whole gait cycle, used to compute the respective mean patterns. Resulting UW Bands from control subjects over the Normative OW Bands [109] are displayed in Fig. 4.17 and Fig. 4.19.

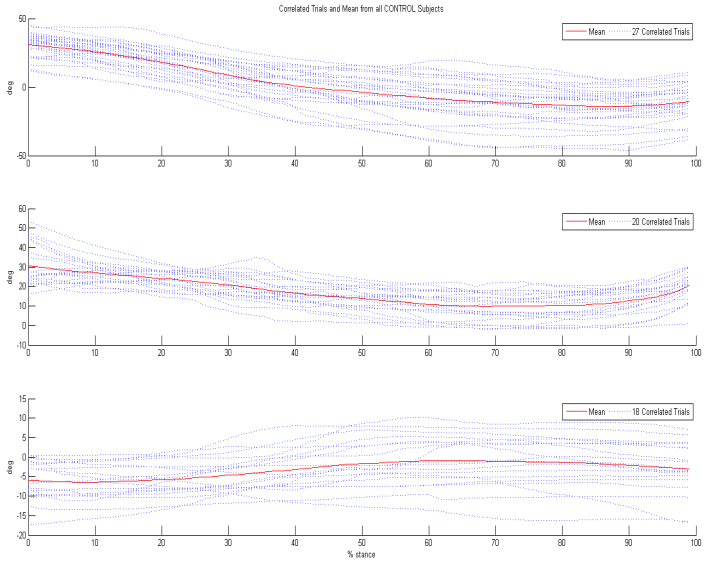

Figure 4.16: All Controls (sbj 1, sbj 2 and 3) Correlated Trials and Mean.

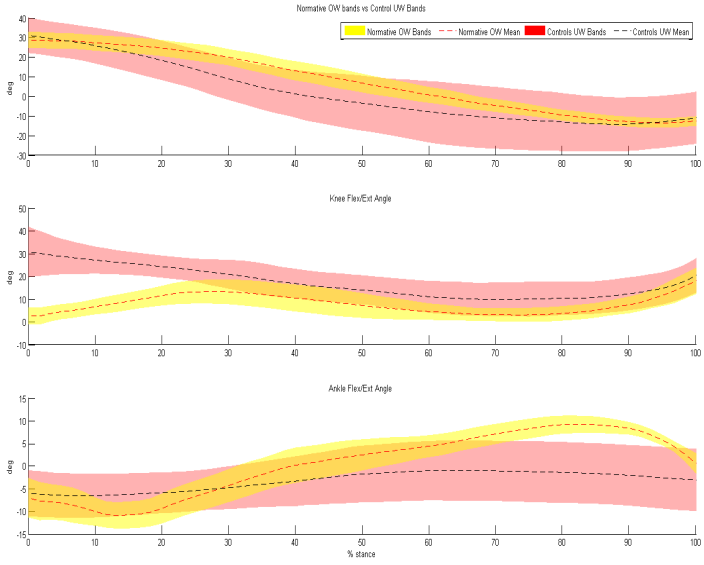

Figure 4.17: Normative OW vs Control UW bands.

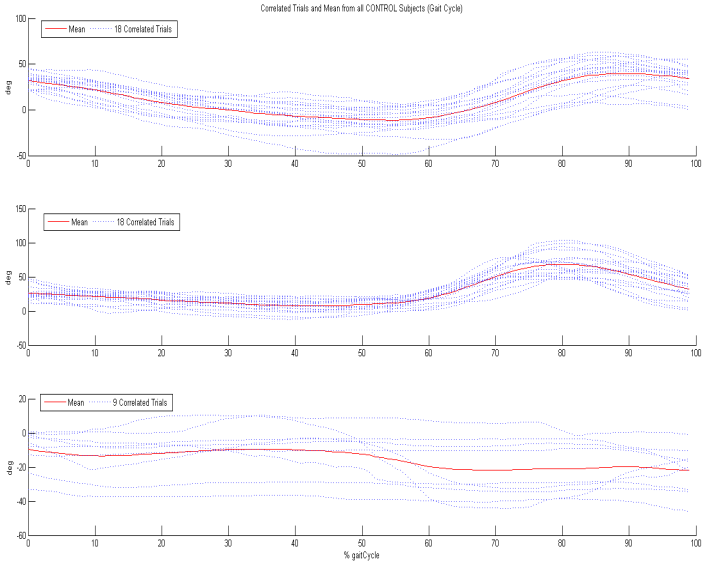

Figure 4.18: All Controls Correlated Gait Cycle and Mean.

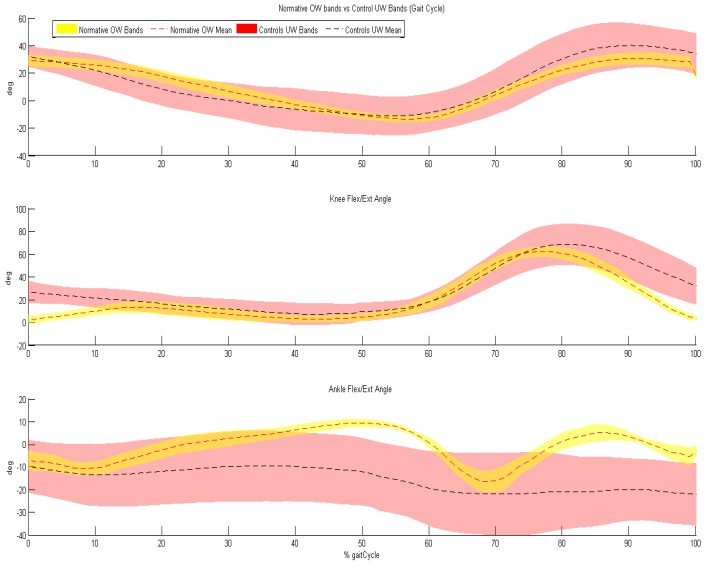

Figure 4.19: Normative OW vs Control UW bands.

4.3 Pathologic Subject

An ACL-injured subject has been investigated. The available stance phases and gait cycles extracted from the recorded videos are listed in the following table (Tab. 4.29).

Trials	Left	Right
	Stance	
1.	I, gc(I-II)	I
2.	I,II	I
3.	I,gc(I-II)	II
4.	I,II,gc(I-II)	I,gc(I-II)
5.	I,gc(I-II)	I
6.	I,gc(I-II)	I,II,gc(I-II)

Table 4.29: Processed stance phases and gait cycles for each trial.

Results are reported as for control subjects in section 4.1 (Fig. 4.20-4.22, Tab. 4.30-4.38).

Stance Results

Left Hip Correlation								
Trials								
1 (I st)	1	0,908	0,987	0,839	0,987	0,992	0,891	0,553
2 (I st)	0,908	1	0,877	0,950	0,941	0,934	0,993	0,844
2 (II st)	0,987	0,877	1	0,784	0,971	0,972	0,853	0,490
3 (I st)	0,839	0,950	0,784	1	0,902	0,850	0,950	0,848
4 (I st)	0,987	0,941	0,971	0,902	1	0,977	0,925	0,628
4 (II st)	0,992	0,934	0,972	0,850	0,977	1	0,920	0,619
5 (I st)	0,891	0,993	0,853	0,949	0,925	0,920	1	0,853
6 (I st)	0,553	0,844	0,490	0,848	0,628	0,619	0,853	1

Table 4.30: Pathologic subject: Left Hip Correlation Coefficients.

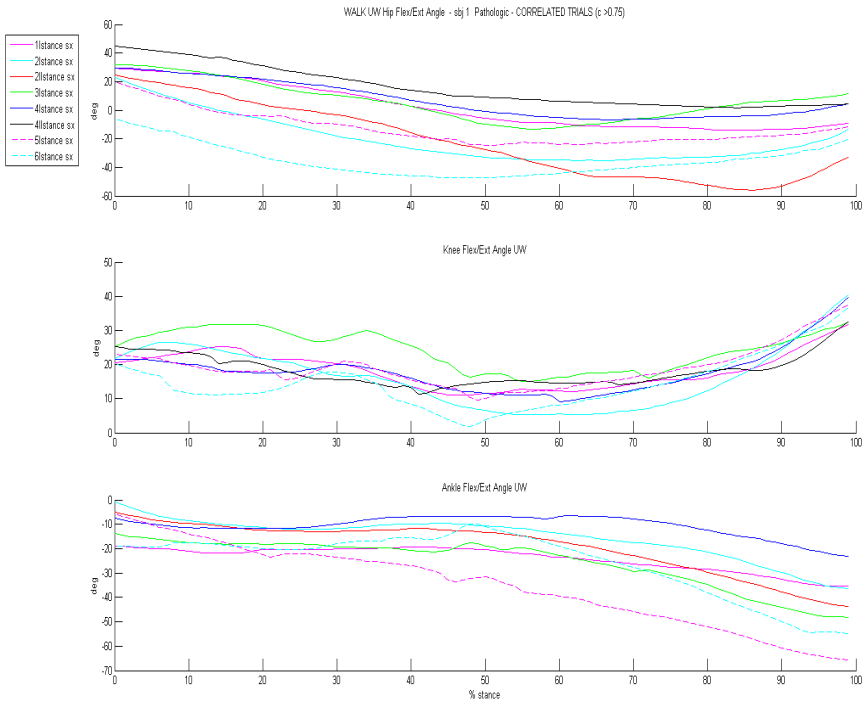

Figure 4.20: Pathologic subject: Left Correlated Trials.

Left Knee Correlation								
Trials								
1 (I st)	1	0,961	0,478	0,865	0,876	0,865	0,813	0,746
2 (I st)	0,961	1	0,540	0,888	0,924	0,876	0,840	0,740
2 (II st)	0,478	0,540	1	0,187	0,762	0,588	0,831	0,790
3 (I st)	0,865	0,888	0,187	1	0,727	0,641	0,607	0,507
4 (I st)	0,876	0,924	0,762	0,727	1	0,815	0,959	0,897
4 (II st)	0,865	0,876	0,588	0,641	0,815	1	0,785	0,696
5 (I st)	0,813	0,840	0,831	0,607	0,959	0,785	1	0,964
6 (I st)	0,746	0,740	0,790	0,507	0,897	0,696	0,964	1

Table 4.31: Pathologic subject: Left knee Correlation Coefficients.

Left Ankle Correlation								
Trials								
1 (I st)	1	0,971	0,985	0,980	0,793	0,151	0,910	0,965
2 (I st)	0,971	1	0,989	0,980	0,809	0,085	0,928	0,943
2 (II st)	0,985	0,989	1	0,993	0,770	0,048	0,948	0,955
3 (I st)	0,980	0,980	0,993	1	0,779	0,069	0,930	0,965
4 (I st)	0,793	0,809	0,770	0,779	1	0,599	0,547	0,872
4 (II st)	0,151	0,085	0,048	0,069	0,599	1	0,252	0,292
5 (I st)	0,910	0,928	0,948	0,930	0,547	0,252	1	0,821
6 (I st)	0,965	0,943	0,956	0,965	0,872	0,292	0,821	1

Table 4.32: Pathologic subject: Left Ankle Correlation Coefficients.

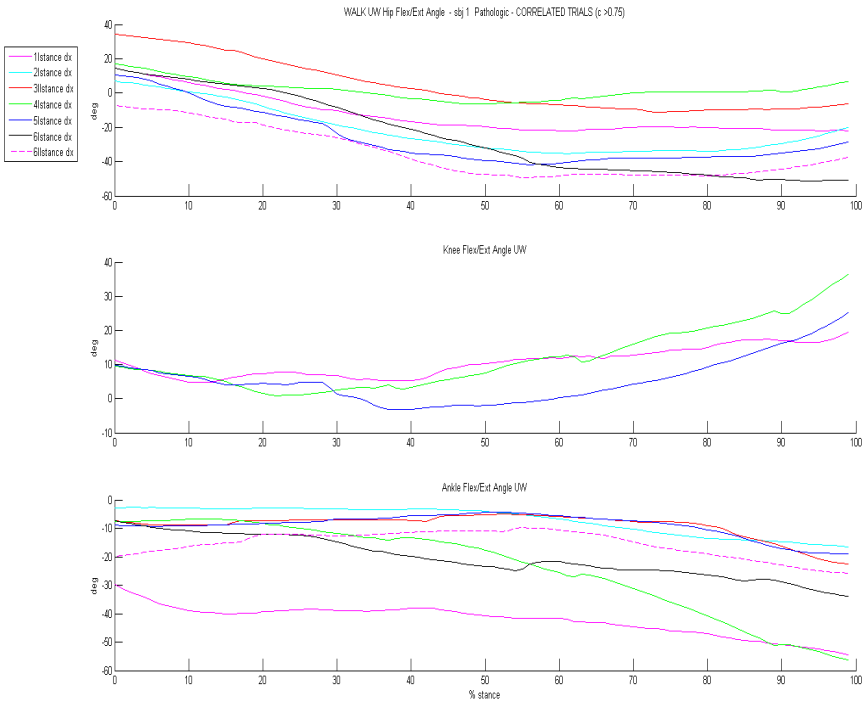

Figure 4.21: Pathologic subject: Right Correlated Trials.

Right Hip Correlation							
Trials							
1 (I st)	1	0,972	0,979	0,835	0,982	0,930	0,965
2 (I st)	0,972	1	0,970	0,866	0,989	0,907	0,988
3 (II st)	0,979	0,970	1	0,752	0,959	0,976	0,979
4 (I st)	0,835	0,866	0,752	1	0,900	0,624	0,830
5 (I st)	0,982	0,989	0,959	0,900	1	0,888	0,975
6 (I st)	0,930	0,907	0,976	0,624	0,888	1	0,940
6 (II st)	0,965	0,988	0,979	0,830	0,975	0,940	1

Table 4.33: Pathologic subject: Right Hip Correlation Coefficients.

Right Knee Correlation							
Trials							
1 (I st)	1	0,216	0,742	0,931	0,672	0,386	0,175
2 (I st)	0,216	1	0,653	0,405	0,799	0,674	0,685
3 (II st)	0,742	0,653	1	0,885	0,941	0,711	0,710
4 (I st)	0,931	0,405	0,885	1	0,800	0,529	0,365
5 (I st)	0,672	0,799	0,941	0,800	1	0,720	0,762
6 (I st)	0,386	0,674	0,711	0,529	0,720	1	0,656
6 (II st)	0,175	0,685	0,710	0,365	0,762	0,656	1

Table 4.34: Pathologic subject: Right Knee Correlation Coefficients.

Right Ankle Correlation							
Trials							
1 (I st)	1	0,945	0,751	0,953	0,730	0,884	0,642
2 (I st)	0,945	1	0,729	0,984	0,742	0,858	0,737
3 (II st)	0,751	0,729	1	0,733	0,969	0,531	0,892
4 (I st)	0,952	0,984	0,733	1	0,722	0,914	0,688
5 (I st)	0,730	0,742	0,969	0,722	1	0,453	0,943
6 (I st)	0,884	0,858	0,531	0,914	0,453	1	0,399
6 (II st)	0,642	0,737	0,892	0,688	0,944	0,399	1

Table 4.35: Pathologic subject: Right Ankle Correlation Coefficients.

Gait Cycle Results

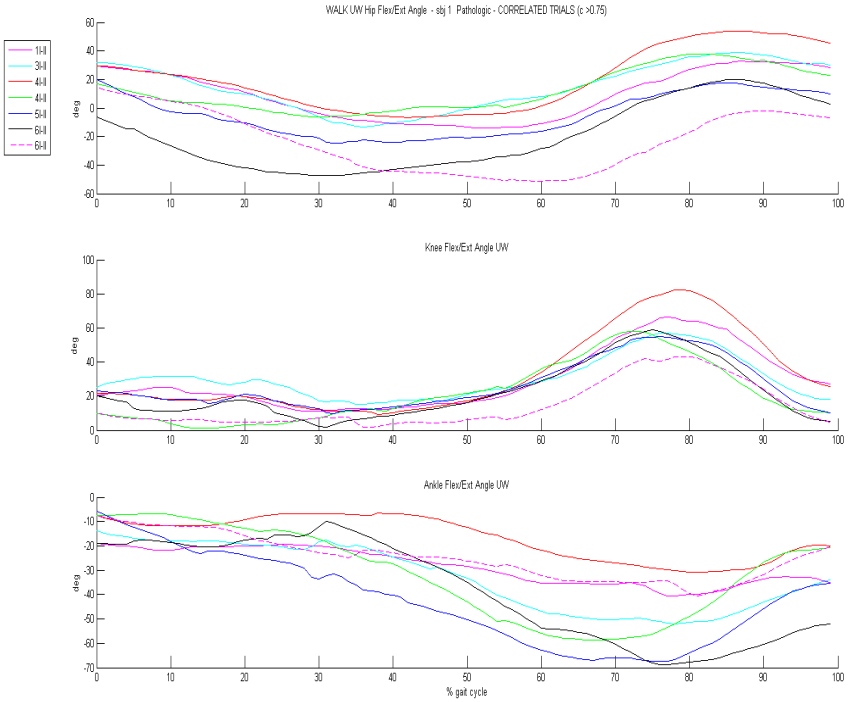

Figure 4.22: Pathologic subject: Gait Cycle Correlated Trials.

Gait Cycle Hip Correlation							
Trials							
1. (I-II sx)	1	0,905	0,930	0,732	0,935	0,777	0,889
3. (I-II sx)	0,905	1	0,947	0,885	0,976	0,914	0,668
4. (I-II sx)	0,930	0,947	1	0,917	0,964	0,934	0,666
4. (I-II dx)	0,732	0,885	0,917	1	0,895	0,986	0,350
5. (I-II sx)	0,935	0,976	0,964	0,895	1	0,925	0,705
6. (I-II sx)	0,777	0,914	0,934	0,986	0,925	1	0,423
6. (I-II dx)	0,889	0,668	0,666	0,350	0,705	0,423	1

Table 4.36: Pathologic subject: Gait Cycle Hip Correlation Coefficients.

Gait Cycle Knee Correlation							
Trials							
1. (I-II sx)	1	0,935	0,991	0,802	0,940	0,911	0,973
3. (I-II sx)	0,935	1	0,929	0,738	0,946	0,921	0,925
4. (I-II sx)	0,991	0,929	1	0,846	0,961	0,936	0,986
4. (I-II dx)	0,802	0,738	0,846	1	0,900	0,922	0,842
5. (I-II sx)	0,940	0,946	0,961	0,900	1	0,989	0,954
6. (I-II sx)	0,911	0,921	0,936	0,922	0,990	1	0,925
6. (I-II dx)	0,973	0,925	0,986	0,842	0,954	0,925	1

Table 4.37: Pathologic subject: Gait Cycle Knee Correlation Coefficients.

Gait Cycle Ankle Correlation							
Trials							
1. (I-II sx)	1	0,978	0,929	0,828	0,884	0,976	0,893
3. (I-II sx)	0,978	1	0,922	0,887	0,929	0,965	0,929
4. (I-II sx)	0,929	0,922	1	0,676	0,743	0,971	0,796
4. (I-II dx)	0,828	0,887	0,676	1	0,971	0,756	0,876
5. (I-II sx)	0,884	0,929	0,743	0,971	1	0,815	0,951
6. (I-II sx)	0,976	0,965	0,971	0,756	0,815	1	0,842
6. (I-II dx)	0,893	0,929	0,796	0,876	0,951	0,842	1

Table 4.38: Pathologic subject: Gait Cycle Ankle Correlation Coefficients.

4.4 Pathologic vs Controls

A comparison between pathologic and normal condition is proposed. It is divided into two parts: the first overlaps pathologic findings with standard bands of normal gait patterns out of water [109], while the second aims at showing up differences among an ACL-injured subject and an healthy one in the same under-water condition. The UW bands obtained from the three control subjects investigated in this study are used as reference (see section **??**).

4.4.1 Pathologic vs OW Standard Bands

Correlated stance mean of each limb and the overall mean are represented together with Normative OW Bands respectively on Fig. 4.23 and 4.25, while Fig. 4.25 displays the same but for the whole strides.

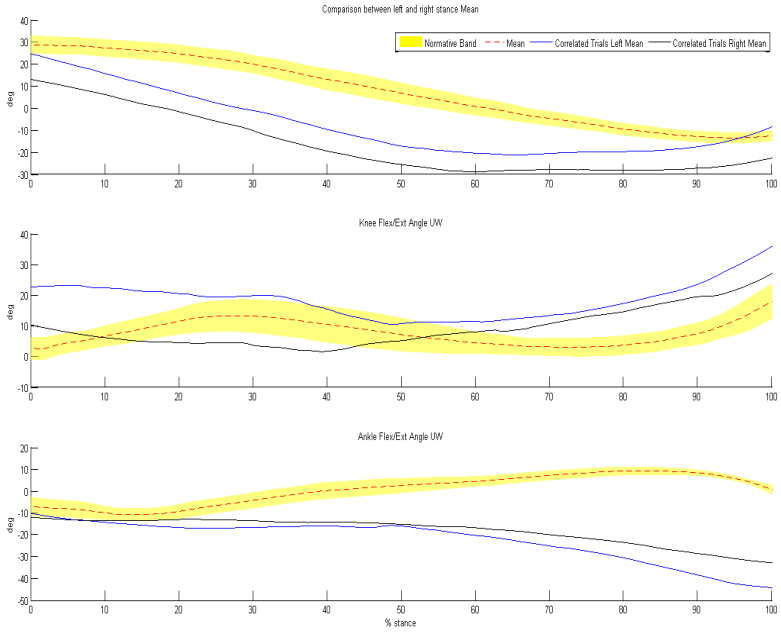

Figure 4.23: Pathologic Left and Right Correlated Trials Means vs OW Bands.

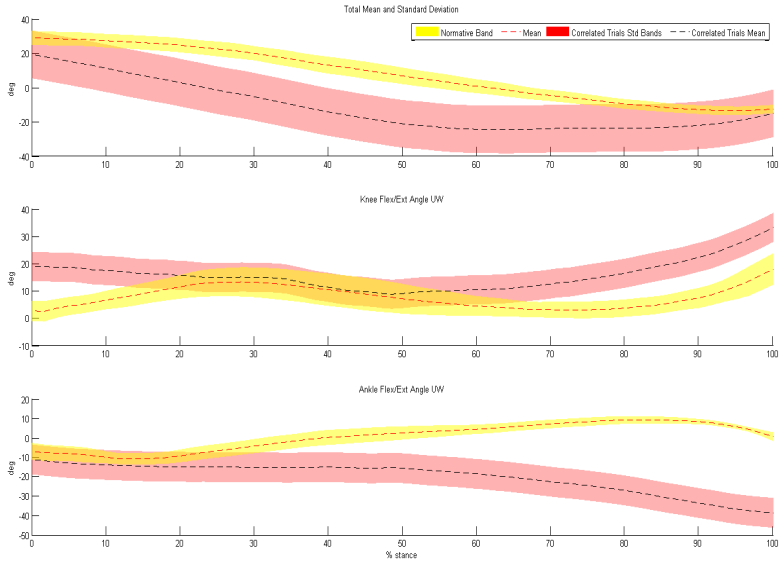

Figure 4.24: Pathologic Global Mean (± 1 SD) vs OW Bands.

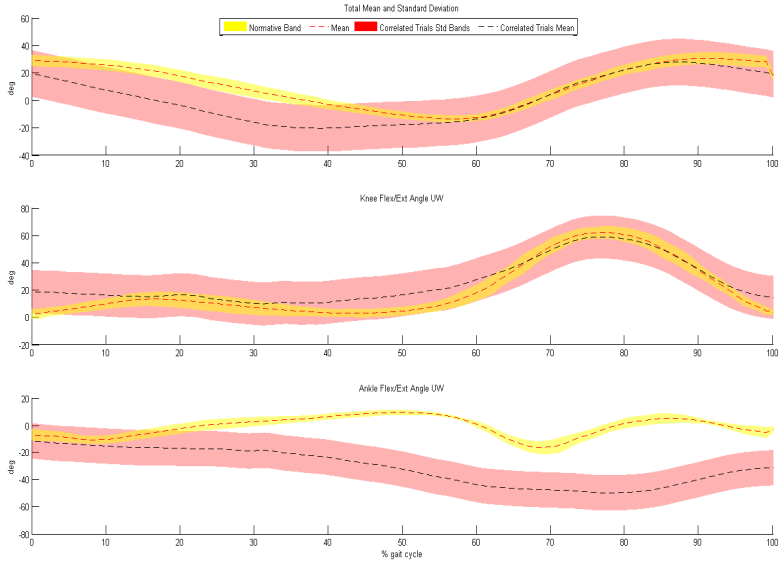

Figure 4.25: Pathologic GC Global Mean (± 1 SD) vs OW Bands.

4.4.2 Pathologic vs UW Control Bands

UW bands from control subjects are an aid in evaluating differences among healthy and injured subjects walking underwater. Prior to the total mean of pathologic patterns (Fig. 4.28), left and right correlated stance are compared to the UW bands from control as well (Fig. 4.26 and 4.28).

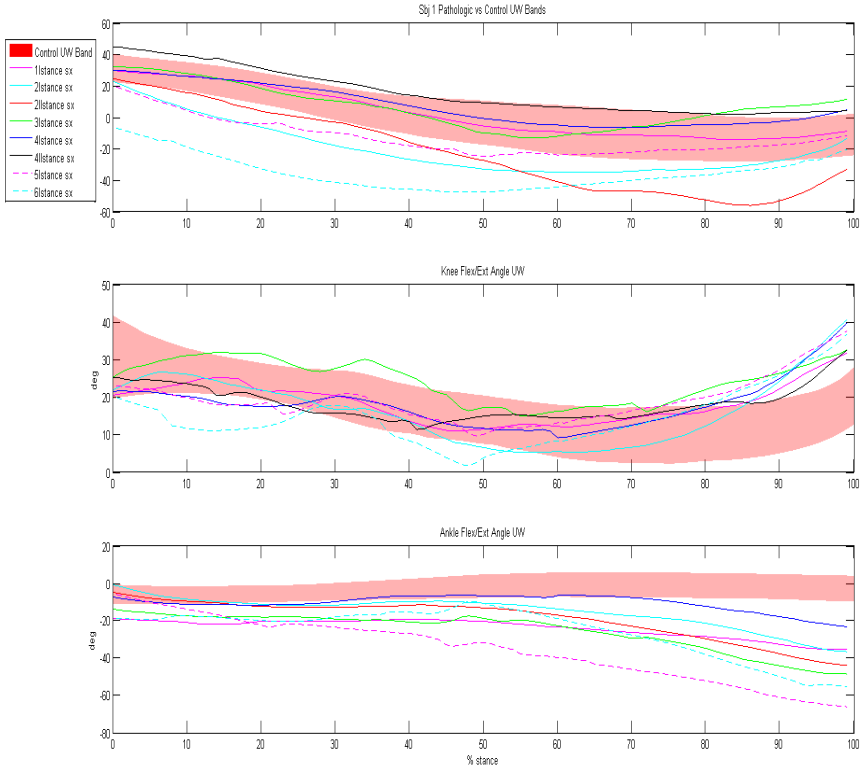

Figure 4.26: Pathologic Left Correlated Trials vs Control UW Bands.

Finally, correlated whole gait cycles and their mean versus the UW bands are shown in Fig. 4.29 and 4.30.

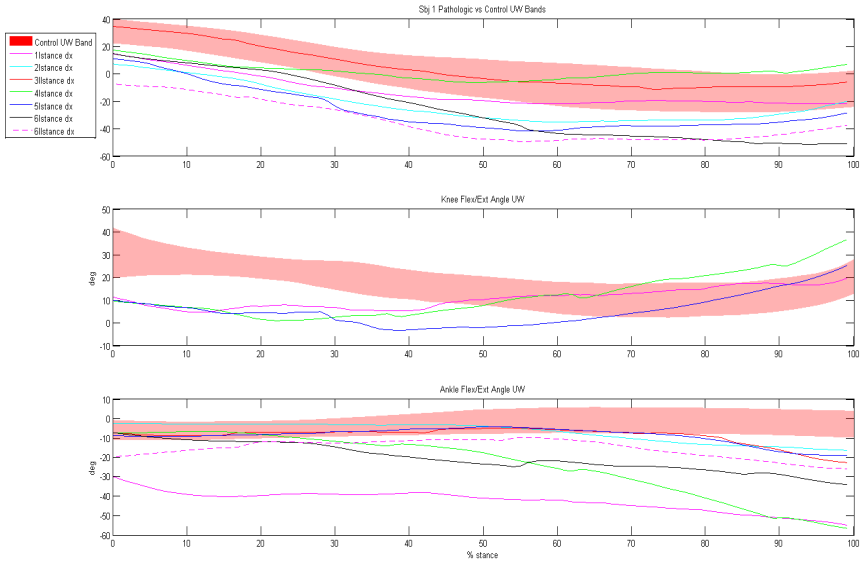

Figure 4.27: Pathologic Right Correlated Trials vs Control UW Bands.

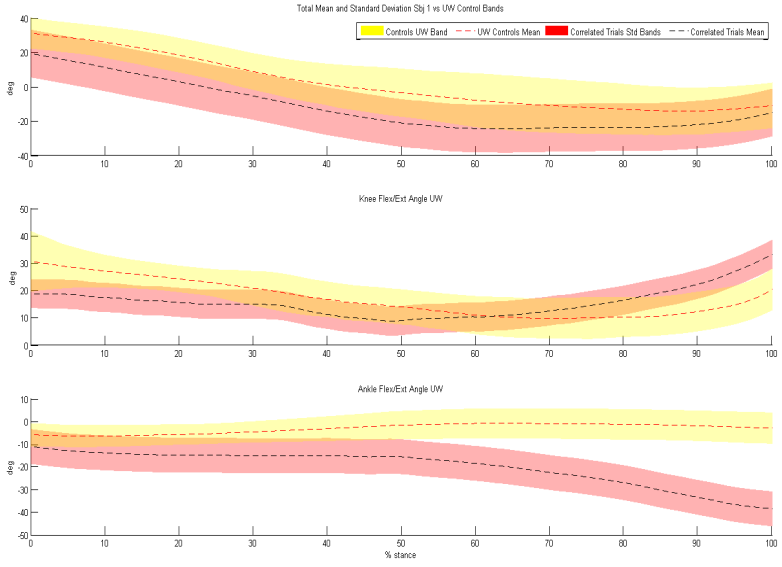

Figure 4.28: Pathologic Global Mean ($\pm$ 1 SD) vs Control UW Bands.

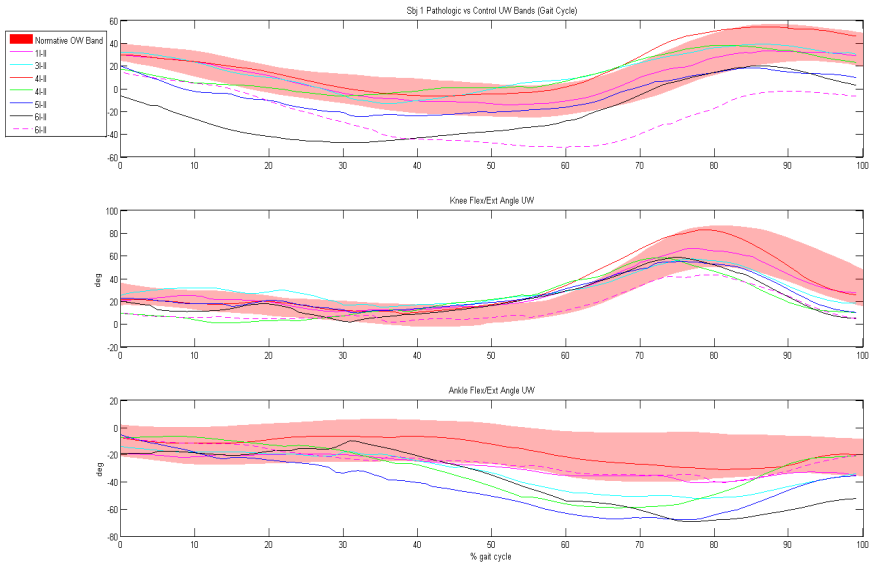

Figure 4.29: Pathologic GC Correlated Trials vs Control UW Bands.

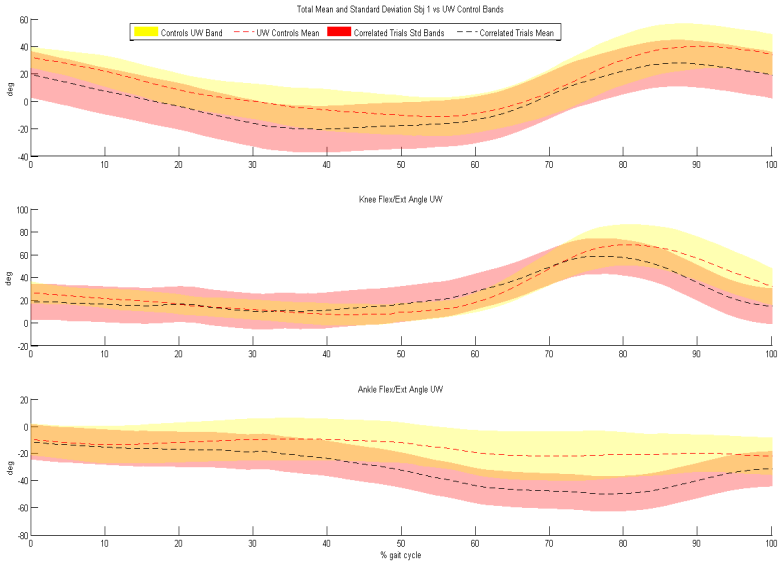

Figure 4.30: Pathologic Global GC Mean ($\pm$ 1 SD) vs Controls UW Bands.

Chapter 5

Conclusions

A fundamental need for modern biomechanical and clinical application is the ability to accurately capture normal and pathologic human movement without the artifacts associated with standard marker-based motion capture techniques. Moreover, the latter can not be employed in water environment, where the attachment of skin surface markers is not physically possible. A markerless approach, based only on synchronized video sequences, has been proposed as a potential solution.

In the present thesis, an automatic markerless motion capture system has been investigated and its accuracy in UW 3D lower limbs joint kinematics reconstruction has been tested.

Three healthy males and an ACL-injured subject who underwent surgical reconstruction of the ligament, were recruited. Six walking trials at a self-selected speed have been acquired with 6 subaqueous video cameras, in a swimming pool, with water at a shoulder level. Two setups have been experimented to investigate the critical aspects in the definition of camera's position. Lower limbs joint angles with the markerless technique have been extracted. Correlation was used to aid in selecting which of each subject's representative walking trials were to be included in the computation of the mean; thus the correlation coefficient was calculated for each subject's kinematic parameter. Walking trials with a correlation coefficient less than 0.75 (75%) were excluded from the statistical analysis.

It should be mentioned that correlation is a shape index, which relates curves

on the basis of shape similarities, considering each time instant. That's the reason why some trials are reported as correlated even if they differ from the others for a significant offset. Examples can be found among the correlated trials obtained for control subject 1 (Fig. 4.1, section 4.1.1): ankle angle of *5IIstance sx* starts at -35°and remains settled between the range -30°/-40°, while the standard trend usually varies from 10°to -10°. In Fig. 4.2 (section 4.1.1), the only two ankle correlated trials differ of about -15°, but their patterns are very similar.

Considering the gait cycles of the same subject displayed in Fig. 4.3 (section 4.1.1), the unusual knee trend of the stride indicated as *5II-III* may be due to an unsuccessful tracking during swing. An excessive knee flexion following the stance phase is evident for gait cycle *1I-II*. While for this subject it is just an isolated case and may be attributed to some inconvenience in the processing steps, for control subject 3 this prominent flexion of the knee joint is a recurrent pattern. Moreover, several trials with extremely high hip extension have been obtained for the same subject (Fig. 4.8 and 4.9, section 4.1.3). However, by visual inspection of the original videos,it has been verified that subject 3 really walked with a pronounced knee flexion and hip extension. Thus, such findings can be considered consistent with the acquired data.

By considering the data of subject 2, it can be noticed excessive extension angles just for the hip joint: *1Istance sx* (Fig. 4.5, section 4.1.2) reaches about -100°, while *4Istance sx* and *3IIstance sx*, as well as gait cycle *4I-II* (Fig. 4.7), exceed -60°. These critical values arise some doubts about their feasibility and make critical their acceptability.

Regarding the ankle joint, presence of less correlated trials is evident; for instance, in Fig. 4.7, an unexpected shift in correspondence of the 50% of stride can be found. It may be due to a problem in the matching step.

The outcomes for each subject have been summarized representing the corresponding correlated trials mean and its standard deviation. The resulting subject-specific representative bands have been compared with Normative OW Bands [109], to assess differences between walking on land and in water. In this context, a common finding among all the three recruited control subjects has been found: all of them walked in water with

a 20°greater knee flexion angle during the early contact phase and at the end of the whole gait cycle (Fig. 4.10-4.15, section 4.2). Since this variation from standard patterns out of water occurs for all controls, it may be expected that it represents a characteristic strictly related to an underwater walking gesture. This is in contrast with what is stated in literature [9], where it is reported that the knee joint in water presents a reduced flexion during the first 15% of the stride (known as the weight acceptance phase during walking) compared to land, and as a result, the knee is more extended in water than on land during the support phase (see section 2.2).
Knee flexion results greater also during all swing phase for subjects 1 and 3, while subject 2 presents values comparable with OW range.
With regard to the hip joint, the global mean reflects the excessive extension previously reported for subjects 2 and 3 during the stance phase, while findings for the swing phase are in disagreement: subject 1 shows a greater flexion preceding heel contact, while for the other two controls a smaller mean value at the end of stride cycle has been obtain.
Ankle mean and standard deviation have been computed considering the correlated trials, without including those characterized by non-physiologic offset. Thus, their number can not be considered enough to extrapolated more general considerations about the single subjects. Such number increases taking into account all control subjects correlated trials at once, at the expense of an higher critical standard deviation.
Hip and knee trends representing the UW bands obtained from all the three controls subjects point out what just discussed for each of them (Fig. 4.17 and 4.19). A significant difference comparing these UW bands with those out of water proposed by Sawacha et al. [109] stands in the greater standard deviations. This higher variability may be partially due to markerless approach technical drawbacks. Nevertheless, it is highly recommended to extend this study to a larger sample of subjects before taking into account inter-subject variations.

According to this study, the main differences between an underwater walking and a walking in dry condition are:

- about 20°greater values of knee flexion angle in correspondence of early contact phase and just before, at the end of the gait cycle;
- a slightly higher knee flexion during swing phase;
- a pronounced extension of hip joint during the stance phase;
- an higher value of hip flexion during swing phase.

Only the first and the third points are confirmed in the pathologic case, while hip and knee flexion mean in the mid swing well overlaps the corresponding OW mean.

Pathologic patterns have been compared to the obtained UW bands as well, to examine walking modifications caused by the ACL injury in the same underwater condition. Less knee flexion in the early phase of contact and at the end of the gait cycle characterized the pathologic trend when compared with the controls one. A more accentuated hip extension for the whole gait cycle is also evident in Fig. 4.30 (section 4.4).
According to the literature, it is known that significant changes in locomotion patterns of ACL-injured patients mainly affect tibial rotation and abduction, even though joint movement in the sagittal plane is the most investigated. It has been reported that ACL-D knees are significantly less extended than ACL-I knees during a large portion of midstance (30-44% of gait cycle) [47]. However, this is not appreciable looking at findings illustrated in section 4.4. This discrepancy may be explained considering that the literature regarding kinetics alterations of locomotion patterns following ACL injury is related to an out of water condition. No underwater gait analysis of ACL-injured patients has been performed until now.

The results obtained indicate that markerless motion capture has the potential to achieve a level of accuracy that facilitates the study of the biomechanics of normal and pathological human movement. However, some limitations have to be considered and improvements are still necessary.
Factors affecting the accuracy of a markerless motion capture system can be classified into errors due to limitations of the technical equipment and

errors due to the shape and/or size of the object or body under examination [93]. The appropriate configuration of the set of cameras is known to be a primary aspect for the adoption of a markerless technique [95]. Thus, in this study, two setups have been experimented to investigate the critical aspects in the definition of camera's position. No significant differences came out: the processing modules, including background subtraction, visual hull creation and iterative closest point method, yielded to comparable results.
However, common drawbacks have been found handling underwater data with a markerless approach. Background subtraction step is the most sensitive to the unusual aquatic environment. The presence of water causes continuous variation of the scene and makes necessary the adoption of an adaptive background model. The main problem within underwater images is represented by reflexes, which are identified as part of the foreground object and, consequently, extracted from the background. The moving subject shadow on the pool pavement is in same cases recognized as a foreground element too. To avoid its detection, more strict parameters can be imposed, at the expense of a loss in feet details. The consequence is a higher uncertainty in feet reconstruction, which explains the less correlation and less reliability of ankle joint angular patterns. The number of ankle angles correlated trials is evidently minor if compared with hip and knee joints, and the correlated patterns are often not able to follow smaller variations, as it is possible with a marker-based technique and in dry condition (see the comparison between UW and OW results about the flex/ext ankle angle values proposed in section 4.2).
Presence of other subjects or external moving objects inside the cameras' views during the acquisition can deeply influenced the outcomes of the background subtraction and should be carefully considered as well. Since very easily moving elements may be extracted as foreground together with the actual subject, they are highly undesirable and must be avoid.
Moreover, it has been noticed that particular features of the swimming pool such as, for example, color lines on the pool pavement, can be identified as background even if the subject in a specific frame covered them.
Therefore, special attention must been taken in planning an appropriate experimental setup.

In addition, it has been reported that the accuracy of markerless methods based on visual hulls does not rely only on cameras setting, but it is highly dependent on the number of cameras used [95]: according to *Mundermann et al.*, "Setups with less than 8 cameras yielded largely inaccurate visual hull constructions and great fluctuations for different poses and positions across a viewing volume, while setups with 16 and more cameras provided good volume estimations and consistent results". Thus, a partial solution to the technical experimental inconveniences may be the adoption of a larger number of cameras. It must be considered, however, that in UW environments electronic equipments should be reduced due to safety issues.

A next critical step is the matching process. Since the subjects walked with the head out of water, the reconstructed visual hulls appear without heads, while the model has been still automatically generated including all body parts. This causes the tracking algorithm to fit the head with points in the visual hull that belong to the body, mainly altering barycenter position, which have to be adjusted manually after few iterations.

This study supports the evidence that appropriate technical equipment and approaches for accurate markerless motion capture is critical. Even if additional evaluations of the system are still needed, the results demonstrate the feasibility of calculating meaningful joint kinematics from subjects walking without any markers attached to the limb. The markerless framework introduced in this work should be taken as just a basis and a starting point for developing a broader application of markerless motion capture. Each of the modules should be independently considered and improved as newer methods become available, thus making markerless tracking a feasible and practical alternative to marker based systems.
A Markerless approach offers the promise of expanding the applicability of human motion capture, since the implementation of this new technology will allow for simple, time-efficient, and potentially more meaningful assessments of gait in research and clinical practice.

Future Developments

Future developments should concentrate on enhancing the background subtraction step, as well as the matching process. An interesting improvement to test could be a modification in the model kinematic chain. It may be adapted to this underwater gait analysis specific application, eliminating the head, which is not present in the reconstructed visual hulls. The recruitment of a larger number of subjects, both healthy and pathologic, either to establish more reliable Normal Underwater Bands, or to be able to assess more general differences in the strategy of walking among the two groups, should be considered as well.

Bibliography

[1] J. Aggarwal and Q. Cai. Human motion analysis: a review. *Computer Vision and Image Understanding*, 73(3):295–304, 1999.

[2] T. Alkjaer, E.B. Simonsen, U. Jorgensen, and P. Dyhre-Poulsen. Evaluation of the walking pattern of two types of patients with anterior cruciate ligament deficiency: copers and non-copers. *European Journal of Applied Physiology*, 89:301–308, 2003.

[3] T.P. Andraicchi, P.L. Briant, S.L. Bevill, and S. Koo. Rotational changes at the knee after acl injury cause cartilage thinning. *Clinical Orthopaedics and Related Research*, 442:39–44, 2006.

[4] T.P. Andriacchi. Dynamics of pathological motion: Applied to the anterior cruciate deficient knee. *Journal of Biomechanics*, 23(1):99–105, 1992.

[5] T.P. Andriacchi and C.O. Dyrby. Interactions between kinematics and loading during walking for the normal and acl deficient knee. *Journal of Biomechanics*, 38:293–298, 2005.

[6] H. Asano, T. Muneta, H. Ikeda, K. Yagishita, Y. Kurihara, and I. Sekiya. Arthroscopic evaluation of the articular cartilage after anterior cruciate ligament reconstruction: a short-term prospective study of 105 patients. *Arthroscopy - The Journal of Arthroscopic and Related Surgery*, 20:474–481, 2004.

[7] R. Baker. The history of gait analysis before the advent of modern computers. *Gait and Posture*, 26:331–342, 2007.

[8] A.M. Barela and M. Duarte. Biomechanical characteristics of elderly individuals walking on land and in water. *J Electromyogr Kinesiol.*, 18(3):446–54, Jun 2008.

[9] A.M. Barela, S.F. Stolf, and M. Duarte. Biomechanical characteristics of aldults walking in shallow water and on land. *J Electromyogr Kinesiol.*, 16(3):250–6, Jun 2006.

[10] M. Berchuck, Bach B.R. Andriacchi, T.P. and, and B. Reide. Gait adaptations by patients who have a deficient anterior cruciate ligament. *JBJS*, 72A:871–7, 1990.

[11] P.J. Besl and N.D. McKay. A method for registration of 3-d shapes. *IEEE Transaction on Pattern Analysis and Machine Intelligence*, 14:239–256, 1992.

[12] A. Bharatkumar, K. Daigle, M. Pandy, Q. Cai, and J. Aggarwal. Lower limb kinematics of human walking with the medial axis transformation. *IEEE Workshop on Non-Rigid Motion*, pages 70–76, 1994.

[13] A. Biscarini and G. Cerulli. Modelling of the knee joint load in rehabilitative knee extension exercises under water. *J Biomech*, 40(2):345–55, 2007.

[14] A. Blake and M. Isard. Active contours: The application of techniques from graphics, vision, control theory and statistics to visual tracking of shape in motion. *Secaucus*, 1998.

[15] A. Bottino and A. Laurentini. A silhouette based technique for the reconstruction of human movement. *Computer Vision and Image Understanding*, 83:79–95, 2001.

[16] B. Brady, J. Redfern, G. Macdougal, and J. Williams. The addition of aquatic therapy to rehabilitation following surgical rotator cuff repair: a feasibility study. *Pysiotherapy Research International*, 13(3):153–161, 2008.

[17] S. Brandsson, J. Karlsson, L. Sward, J. Kartus, B.I. Eriksson, and J. Karrholm. Kinematics and laxity of the knee joint after anterior cruciate ligament reconstruction - pre- and post-operative radiostereometric studies. *American Journal of Sports Medicine*, 30:361–367, 2002.

[18] J. Bray. Markerless based human motion capture: a survey. Master's thesis, Department Systems Engineering Brunel University, 2001.

[19] C. Bregler and J. Malik. Tracking people with twists and exponential maps. *Proceedings of 1998 IEEE Computer Society Conference on Computer Vision and Pattern Recognition*, 1998.

[20] C.A. Bush-Joseph, D.E. Hurwitz, R.R. Patel, Y. Bahrani, R. Garretson, and Jr.B.R. Bach. Dynamic function after anterior cruciate ligament reconstruction with autologous patellar tendon. *American Journal of Sports Medicine*, 29:36–41, 2001.

[21] D.L. Butler, F.R. Noyes, and E.S. Grood. Ligamentous restrains to anterior-posterior drawer in the human knee: a biomechanical study. *J Bone Joint Surg*, 62 A:259–70, 1980.

[22] J.A. Campbell, L.J. D'Acquisto, and D.M. D'Acquisto. Metabolic and cardiovascular response to shallow water exercise in young and older women. *Med. Sci. Sports Exerc.*, 35:675–681, 2003.

[23] A. Cappello, A. Cappozzo, and P.E. Prampero. *Bioingegneria della Postura e del Movimento*, chapter Misura del movimento e della postura: sistemi a marcatori passivi e metodi stereofotogrammetrici, pages 79–101. Pàtron, 2003.

[24] E. Ceseracciu. A multi-approach method for accurate markerless capture and analysis of human motion. Master's thesis, University of Padua, 2007.

[25] E. Ceseracciu. *New frontiers of markerless motion capture: application to swim biomechanics and gait analysis.* PhD thesis, University of Padua, 2011.

[26] A.M.W. Chaudhari, P.L. Briant, S.L. Bevill, S. KOO, and T.P. Andriacchi. Knee kinematics, cartilage morphology, and osteoarthritis after acl injury. *Medicine and Science in Sports and Exercise*, 40:215–222, 2008.

[27] J. Cheng and J.M.F. Moura. Capture and representation of human walking in live video sequences. *IEEE Trans. on Multimedia*, 1:144–156, 1999.

[28] C. Cheung, S.S.and Kamath. Robust techniques for background subtraction in urban traffic video. *Visual Communications and Image Processing*, 5308:881–892, 2004.

[29] Kanade T. Cheung G., Baker S. Shape-from-silhouette of articulated objects and its use for human body kinematics estimation and motion capture. *IEEE Conference on Computer Vision and Pattern Recognition*, 2003.

[30] L. Chiari, U. Della Croce, A. Leardini, and A. Capozzo. *Human movement analysis using stereophotogrammetry - part 3: soft tissue artifact assessment and compensation.*, volume 21. 2005.

[31] L. Chiari, U. Della Croce, A. Leardini, and A. Capozzo. Human movement analysis using stereophotogrammetry - part 4: assessment of anatomical landmark misplacement and its effects on joint kinematics. *Gait and Posture*, 2005.

[32] L. Chiari, U. Della Croce, and A. Leardini, A.and Capozzo. *Human movement analysis using stereophotogrammetry - part 2: Instrumental errors*, volume 21. 2005.

[33] C.W. Chu, O.C. Jenkins, and M.J. Mataric. Markerless kinematic model and motion capture from volume sequences. *Proceedings of 2003 IEEE Computer Society Conference on Computer Vision and Pattern Recognition*, pages II–475–II–482, 2003.

[34] S. Corazza. *Identification of Human Kinematics throught Markerless Motion Capture.* PhD thesis, Università degli Studi di Padova, 2004.

[35] S. Corazza, E. Gambaretto, L. Mundermann, and T.P. Andriacchi. Automatic generation of a subject-specific model for accurate markerless motion capture and biomechanical applications. *IEEE transactions on bio-medical engineering*, 57:806–12, Apr. 2010.

[36] S. Corazza, L. Mundermann, and T.P. Andriacchi. Model-free markerless motion capture through visual hull and laplacian eigenmaps. *Summer Bioengineering Conference ASME*, 2005.

[37] S. Corazza, L. Mundermann, A.M. Chaudhari, C. Cobelli, and T.P. Andriacchi. A markerless motion capture system to study musculoskeletal biomechanics: Visual hull and simulated annealing approach. *Annals of Biomedical Engineering*, 34(6):1019–1029, 2006.

[38] D.M. Daniel, M.L. Stone, B.E. Dobson, D.C. Fithian, D.J. Rossman, and K.R. Kaufman. Fate of the acl-injured patient - a prospective outcome study. *American Journal of Sport Medicine*, 22:632–644, 1994.

[39] J. Deutscher, A. Blake, and I. Reid. Articulated body motion capture by annealed particle filtering. *Computer Vision and Pattern Recognition*, 2000.

[40] P. Devita, T. Hortobagyi, and J. Barrier. Gait adaptation before and after anterior cruciate ligament reconstruction surgery. *Med Sci Sports Exerc*, 29:853–9, 1997.

[41] M. Donati. *3-D reconstruction of the human skeleton during motion.* PhD thesis, University of Bologna, 2006.

[42] B.W. Evans, K.J. Cureton, and J.W. Purvis. Metabolic and circulatory responses to walking and jogging in water. *Res. Q. Exerc. Sport.*, 49:442–449, 1978.

[43] R. Ferber, L.R. Osternig, M.H. Woollacott, N.J. Wasielewski, and J.H. Lee. Gait mechanics in chronic acl deficiency and subsequent repair. *Clinics Biomechanics*, 17:274–285, 2002.

[44] K.G. Fitzgerald. Open versus closed kinetic chain exercise: Issue in rehabilitation after anterior cruciate ligament reconstruction surgery. *Physical Therapy*, 77(12), December 1997.

[45] N. Friedman and S. Russell. Image segmentation in video sequences: A probabilistic approach. *The Thirteenth Conference on Uncertainty in Artificial Intelligence (UAI)*, Aug. 1-3 1997.

[46] E. Gambaretto. Markerless motion capture for motion analysis. Master's thesis, Politecnico di Milano, 2006.

[47] B. Gao and Z. Naiquan. Alterations in three-dimensional joint kinematics of anterior cruciate ligament-deficient and -reconstructed knees during walking. *Clinical Biomechanics*, 25:222–229, 2010.

[48] D.M. Gavrila. The visual analysis of human movement: A survey. *Computer Vision and Image Understanding*, 73:82–92, 1999.

[49] A.D. Georgoulis, A. Papadonikolakis, C.D. Papageorgiou, A. Mitsou, and N. Stergiou. Three-dimensional tibiofemoral kinematics of the anterior cruciate ligament-deficient and recostructed knee during walking. *American Journal of Sports Medicine*, 31:75–79, 2003.

[50] P.E. Gill and W. Murray. Algorithms for the solution of the nonlinear least-squares problem. *SIAM Journal on Numerical Analysis*, 15:977–992, 1978.

[51] A. Gokeler, T. Schmalz, E. Knopf, J. Freiwald, and S. Blumentritt. The relationship between isokinetic quadriceps strength and laxity on gait analysis parameters in anterior cruciate ligament reconstructed knees. *Knee Surgery, Sports Traumatology, Arthroscopy*, 11:372–378, 2003.

[52] D. Gravila and L. Davis. 3-d model-based tracking of human in action: a multi-view approach. *Conference on Computer Vision Pattern Recognition*, 1996.

[53] W. Grimson, C. Stauffer, R. Romano, and L. Lee. Using adaptative tracking to classify and monitor activities in a site. *Computer Vision and Pattern Recognition*, June 1998. Santa Barbara, CA.

[54] E.S. Grood, W.J. Suntay, F.R. Noyes, and D.L. Butler. Biomechanics of the knee-extension exercise. *J Bone Joint Surg*, 66 A:725–34, 1984.

[55] R.A. Harrison, M. Hilman, and S. Bulstrode. Loading of the lower limb when walking partially immersed: Implications for clinical practice. *Physioteraphy.*, 78:164, 1992.

[56] *http* : *//www.biokineticspt.com/blog/uncategorized/aquatictherapy*. Aquatic therapy heals injuries while boosting performance. Biokinetic Sports Physical Therapy.

[57] *http* : *//www.clinicalgaitanalysis.com/history/enlightenment.html*. Clinical gait analysis, history of the study of locomotion.

[58] *http* : *//www.cmp.ucr.edu/collections/*. Animal locomotion plates, ucr/california museum of photography.

[59] *http* : //www.health-res.com/Traumatic-Synovitis-of Knee-Joint/.

[60] W.I Hurd and L. Snyder-Mackler. Knee instability after acute acl rupture affects movement patterns during the mid-stance phase of gait. *Journal of Orthopaedic Research*, 25:1369–1377, 2007.

[61] J.J. Irrgang and C.D. Harner. Recent advances in anterior cruciate ligament rehabilitation: Clinical factors that influence the program. *Journal of Sports Rehabilitation.*, 6:111, 1997.

[62] J. Jackman. *Bluescreen Compositing*. Focal Press, 2007.

[63] G. Johansson. Perception of biological motion and a model for its analysis. *Perception Psychophysics*, pages 14(2): 201–211, 1973.

[64] T. Jung. The influence of applying additional weight to the affected leg on gait patterns during aquatic treadmill walking in people poststroke. *Arch Phys Med Rehabil*, 91:129–36, January 2010.

[65] P. Kaewtrakulpong and R. Bowden. An improved adaptative background mixture model for real-time tracking with shadow detection. *Proc. 2nd European Workshop on Advanced Video Based Surveillance Systems*, pages 1–5, 2001.

[66] I.A. Kakadiaris and D. Metaxes. 3d human body model acquisition from multiple views. *Intl. Jl. Computer Vision*, 30:191–218, 1998.

[67] I.A. Kakadiaris and D. Metaxes. Model-based estimation of human motion. *IEEE Trans. Patt. Anal. Mach. Intell.*, 22:1453–1460, 2000.

[68] R. Kehl, M. Bray, and L.V. Gool. Full body tracking from multiple views using stochastic sampling. *IEEE Computer Society Conference on Computer Vision and Pattern Recognition*, pages 129–136, 2005.

[69] Z. Knoll, R.M. Kiss, and L. Kocsis. Gait adaptation in acl deficient patients before and after anterior cruciate ligament reconstruction surgery. *Journal of Electromyography and Kinesiology*, 14:287–294, 2004a.

[70] J. Kvist. Sagittal plane translation during level walking in poor-functioning and well-functioning patients with anterior cruciate ligament deficiency. *American Journal of Sports Medicine*, 32:1250–1255, 2004.

[71] Y.H. Kwon. A camera calibration algorithm for the underwater motion analysis. *Scientific Proceedings of the XVII International Symposium on Biomechanics in Sports*, pages 257–260, 1999.

[72] Y.H. Kwon. Object plane deformation due to refraction in 2-dimensional underwater motion analysis. *Journal of Applied Biomechanics*, 15:396–403, 1999.

[73] A. Laurentini. The visual hull concept for silhouette-based image understanding. *IEEE Transaction on Pattern Analysis and Machine Intelligence*, 16:150–162, 1994.

[74] J.M. Lavest and G. Rives. Dry camera calibration for underwater applications. *Machine Vision and Applications*, 13:245–253, Mar. 2003.

[75] L.S. Lohmander, A. Ostenberg, M. Englund, and H. Roos. High prevalence of knee osteoarthritis, pain and functional limitations in female soccer players twelve years after anterior cruciate ligament injury. *Arthritis and Rheumatism*, 50:3145–3152, 2004.

[76] H.J. Marans, R.W. Jackson, N.D. Glossop, and M.C. Young. Anterior cruciate ligament insufficiency: a dynamic three-dimensional motion analysis. *Am J Sports Med*, 17:325–32, 1989.

[77] K.L. Markolf, D.M. Byrchfield, M.M. Shapiro, M.F. Shepard, G.A. Finerman, and J.L. Slauterbeck. Combined knee loading states that generate high anterior cruciate ligament forces. *J Orthop Res*, 13:930–5, 1995.

[78] K. Masumoto, T. Shono, S. Takasugi, N. Hotta, and K. Fujishima. Muscle activation, cardiorespiratory response, and rating of perceived exertion in older subjects while walking in water and on dry land. *J. Electromyogr. Kinesiol.*, 2007.

[79] K. Masumoto, T. Shono, S. Takasugi, N. Hotta, K. Fujishima, and Y. Iwamoto. Age-related differences in muscle activity, stride frequency and heart rate response during walking in water. *J. Electromyogr. Kinesiol.*, 17:596–604, 2007.

[80] K. Masumoto, S. Takasugi, N. Hotta, K. Fujishima, and Y. Iwamoto. Electromyographic analysis of walking in water in healthy humans. *J Physiol Anthropol Appl Human.*, 23(4):119–27, Jul 2004.

[81] K. Masumoto, S. Takasugi, N. Hotta, K. Fujishima, and Y. Iwamoto. Muscle activity and heart rate response during backward walking in water and on dry land. *Eur. J. Appl. Physiol.*, 94:54–61, 2005.

[82] K. Masumoto, S. Takasugi, N. Hotta, K. Fujishima, and Y. Iwamoto. A comparison of muscle activity and heart response during backward

and forward walking on an underwater treadmill. *Gait Posture.*, 25:222–228, 2007.

[83] V. Maynard, A.M.O. Bakheit, J. Oldham, and J. Freeman. Intra-rater and inter-rater reliabitity of gait measurements with coda mpx30 motion analysis system. *Gait and Posture*, 17:59–67, 2003.

[84] V. Medved. *Measurement of human locomotion.* Boca Raton, 2001.

[85] A. Menache. *Understanding Motion Capture for Computer Animation and Video Games.* Morgan Kaufmann, 1999.

[86] S. Menato. Confronto tra tecnologia markerless e marker-based nell'analisi del cammino tramite acquisizione simultanea. Master's thesis, University of Padua, 2010.

[87] I. Miki, M.M. Trivedi, E. Hunter, and P.C. Cosman. Human body model acquisition and motion capture using voxel data. *AMD0 '02: Proceedings of the Second International Workshop on Articulated Motion and Deformable Objects*, pages 104–118, 2002.

[88] T. Miyoshi, T. Shirota, S. Yamamoto, K. Nakazawa, and M. Akai. Effect of the walking speed to the lower limb joint angular displacements, joint moments and ground reaction forces during walking in water. *Disabil. Rehabil.*, 26:724–732, 2004.

[89] T. Miyoshi, T. Shiroto, S.I. Yamamoto, K. Nakazawa, and M. Akai. Lower limb joint moment during walking in water. *Disabil Rehabil*, 25(21):1219–23, 2003.

[90] T. Miyoshi, T. Shiroto, S.I. Yamamoto, K. Nakazawa, and M. Akai. Functional roles of lower limb joint moments while walking in water. *Clin Biomech*, 20(2):194–201, 2005.

[91] T.B. Moeslund and E. Granum. A survey of computer vision-based human motion capture. *Computer Vision and Image Understanding*, 81:231–268, 2001.

[92] B.L Momberg, L. Quinette, and L. Crous. Accelerated hydrotherapy and land-based rehabilitation in soccer players after anterior cruciate ligament reconstruction: a series of three single subject case studies. *SAJSM*, 20(4), 2008.

[93] L. Mundermann, S. Corazza, and T.P. Andriacchi. The evolution methods for the capture of human movement leading to markerless motion capture for biomechanical application. *Journal of Neuroengineering and Rehabilitation*, 3, 2006.

[94] L. Mundermann, S. Corazza, and T.P. Andriacchi. Accurately measuring human movement using articulated icp with soft-joint constraints and a repository of articulated models. *IEEE Conference on computer vision and pattern recognition.*, 2007.

[95] L. Mundermann, S. Corazza, A.M. Chaudhari, E.J. Alexander, and T.P. Andriacchi. Most favorable camera configuration for a shape-from-silhouette markerless motion capture system for biomechanical analysis. *SPIE-ISandT Electronic Imaging*, 2005.

[96] E. Muybridge. The science of the horse's motions. *Scientific American*, pages 39–241, 1878.

[97] E. Muybridge. The human figure in motion, 1907.

[98] W. Nebelung and H. Wuschech. Thirty-five years of follow-up of anterior cruciate ligament-deficient knees in high-level athletes. *Arthroscopy*, 21:696–702, 2005.

[99] F.R. Noyes, P.A. Mooar, D.S. Matthews, and D.L. Butler. The symptomatic anterior cruciate deficient knee. part i: the long-term functional disability in athletically active individuals. *Journal of Bone and Joint Surgery American*, 65:154–162, 1983.

[100] R. Papannagari, T.J. Gill, L.E. Defrate, J.M. Moses, A.J. Petruska, and G.A. Li. In vivo kinematics of the knee after anterior cruciate ligament recosntruction - a clinical and functional evaluation. *American Journal of Sports Medicine*, 34, 2006.

[101] L.E. Paulos, F.C. Payne, and T.D. Rosenberg. *Rehabilitation after anterior cruciate ligament surgery.*, chapter The Anterior Cruciate Deficient Knee, pages 291–314.

[102] F.J. Perales. Human motion analysis and synthesis using computer vision and graphics techniques. state of art and applications. Master's thesis, Department of Computer Science Universitat de les Illes Balears(UIB), 2001.

[103] M. Piccardi. Background subtraction techniques: a review. *IEEE International Conference on Systems, Man and Cybernetics*, 4:30099–3104, 2004.

[104] T. Poyhonen, H. Kyrolainen, K.L. Keskinen, A. Hautala, J. Savolainen, and E. Malkia. Electromyographic and kinematic analysis of therapeutic knee exercise under water. *Clinic Biomech*, 16:496–504, 2001.

[105] T. Poyhonen, H. Kyrolainen, K.L. Keskinen, A. Hautala, J. Savolainen, and E. Malkia. Neuromuscular function during therapeutic knee exercises under water and on dry land. *Arch Phys Med Rehabil*, 82(10):1446–52, 2001.

[106] J. Prins and D. Cutner. Aquatic therapy in the rehabilitation of athletic injuries. *Clinics in Sport Medicine*, 18(2), April 1999.

[107] C. Ridder, O. Munkelt, and H. Kirchner. Adaptative background estimation and foreground detection using kalman-filtering. *Proceeding of International Conference on recent Advances in Mechatronics, ICRAM95*, pages 193–195, 1995.

[108] J.E. Riviera. Open versus closed kinetic chain rehabilitation of the lower extremity: A functional and biomechanical analysis. *Journal of Sports Rehabilitation*, (3:14), 1994.

[109] Z. Sawacha, G. Guarnieri, G. Cristoferi, and A. Guiotto. Diabetic gait and posture abnormalities: A biomechanical investigation through

three dimensional gait analysis. *Clinical Biomechanics*, 24(9):722–728, November 2009.

[110] K.D. Shelbourne and P. Nitz. Accelerated rehabilitation after anterior cruciate ligament reconstruction. *Am J Sports Med*, 18(3):292–9, 1990.

[111] L. Sigal, A.O. Balan, and M.J. Black. Humaneva: Synchronized video and motion capture dataset and baseline algorithm for evaluation of articulated human motion. *International Journal of Computer Vision*, 87:4–27, Aug 2009.

[112] L.E. Silva, V. Valim, and A.P. Pessanha. Hydrotherapy versus conventional land-based exercise for the management of patients with osteoarthritis of the knee: A randomized clinical trial. *Physical Therapy.*, 88(1), January 2008.

[113] J. Starck and A. Hilton. Spherical matching for temporal correspondence of non-rigid surfaces. *Computer Vision*, 2:1387–1394, 2005.

[114] C. Stauffer and W. Grimson. Adaptive background mixture models for real time tracking. *Computer Vision and Pattern Recognition.*, 1999.

[115] A. Sundaresan and R. Chellappa. Multiple-camera tracking of articulated human motion using motion and shape. *Asian Conference on Computer Vision*, 2006.

[116] A. Sundaresan, A. RoyChowdhury, and R. Chellappa. Multiple view tracking of human motion modelled by kinematic chains. *International Conference on Image Processing*, 2004.

[117] J.M. Thein and L.T. Brody. Aquatic-based rehabilitation and training for the elite athlete. *J Orthop Sports Phys Ther*, 27(1):32–41, 1998.

[118] J.M. Thein and T.L. Brody. Aquatic-based rehabilitation and training for the shoulder. *Journal of Athletic Training*, 35(3), September 2000.

[119] Wolf-S.L. Tovin, B.J., B.H. Greenfield, J. Crouse, and B. A. Woodfin. Comparison of the effects of exercise in water and on land on

the rehabilitation of patients with intra-articular anterior cruciate ligament reconstructions. *Physical Therapy*, 74(8), August 1994.

[120] A. Valtonen, T. Poyhonen, S. Sipila, and A. Heinonen. Effects of aquatic resistance training on mobility limitation and lower-limb impairments after knee replacement. *Arch Phys Med Rehabil*, 91, June 2010.

[121] L. Wang, W. Hu, and T. Tan. Recent developments in human motion analysis. *Pattern Recognition*, 36(3):585–601, 2003.

[122] G. Wexler, D.E. Hurwitz, C.A. Bush-Joseph, T.P. Andriacchi, and B.R. Bach. Functional gait adaptation in patients with anterior cruciate ligament deficiency over time. *Clin Orthop*, 348:166–75, 1998.

[123] J.T. Woolfenden. Aquatic physical therapy approaches for the extremities. *Orthopedic Physical Therapy Clinics of North America: Aquatic Therapy.*, page 209, 1994.

[124] L-Q Zhang, R.G. Shiavi, T.J. Limbird, and J.M. Minorik. Six degrees-of-freedom kinematics of acl deficient knees during locomotion-compensatory mechanism. *Gait and Posture*, 17:34–42, 2003.

[125] Z. Zhang and O.M. Way. Flexible camera calibration by viewing a plane from unknown orientations. *Proceedings of the Seventh IEEE International Conference on Computer Vision*, 1:666–673, 1999.

Ringraziamenti

Al termine di questo percorso di studi che ha segnato e riempito questi ultimi sei anni della mia vita, desidero esprime innanittuto il mio grazie più caro a tutte le persone e gli amici *che ho incontrato strada facendo, e che, in un modo o in un altro, chi prima, chi dopo, ne hanno fatto parte.*

Dai compagni con cui ho condiviso la singola esperienza, a chi era con me ogni giorno a seguire lezioni e preparare esami, con cui ho affrontato, una dopo l'altra, difficoltà comuni e raccolto piccole soddisfazioni, con cui ho faticato e penato, ma anche chiacchierato, riso, scherzato, nelle varie pause, così come anche al di fuori.
Avete davvero reso i miei anni universitari, per quanto impegnativi, un autentico piacere.

Allo stesso modo, ringrazio tutti gli amici esterni al mondo universitario: gli amici di sempre, *e* tutte le mie compagne di squadra, *dalle "veterane" con cui ho scoperto e iniziato ad amare il calcio a 5, che più di tutte hanno dovuto inizialmente sopportare la mia assenza nelle uscite di svago per motivi di studio; alle amiche con cui ho avuto la fortuna di provare le emozioni più belle e guadagnare insieme le soddisfazioni più grandi; a quelle che hanno dovuto giocare anche per me quando ho preso e, proprio sul più bello, sono partita, abbandonandovi, per l'Erasmus; fino ad arrivare ai nuovi, forti e preziosi, legami nati quest'anno.*

Non vi è alcun dubbio, amici miei tutti, che senza ciascuno di voi, questi anni di studio, di vita e di crescita, non sarebbero stati lo stesso per me.

Esprimo poi la mia sincera gratitudine alla Prof.ssa Zimi Sawacha, per aver guidato costantemente il mio lavoro, non mancando nel comprendere e rispettare le mie esigenze.

Ringrazio veramente con sentito affetto tutto il Laboratorio di Analisi del Movimento *dell'*Università di Padova.
Desidero ricordare in particolare: l'impeccabile e insostituibile tecnico Martina Negretto; l'Ing. Annamaria Guiotto, "direttrice dei lavori tuttofare", sempre pronta ad aiutare ed elargire consigli; la mia compagna di scrivania, nonchè di viaggio, Dott.ssa Fabiola Spolaor, che si è divertita a prendermi in giro all'infinito, ma che tra caffè, chiacchierate e strigliate mi è sempre stata vicina; e la Dott.ssa Elena Ceseracciu, che con i suoi orari bizzarri all'inizio mi ha fatto tribolare.

Grazie per avermi accolto tra voi e fatto sentire immediatamente a mio agio, per aver reso le mie lunghe giornate di lavoro decisamente più piacevoli, serene e sopportabili, per avermi tanto incoraggiata e sostenuta nei momenti di sconforto, e per avermi regalato più di qualche sorriso. La vostra compagnia sarà senz'altro uno dei ricordi migliori che custodirò di questi mesi di tesi.

Ad Elena riservo un grazie particolare, per avermi insegnato con pazienza tutto quello che mi è servito e mi ha permesso di realizzare questo lavoro, e per avermi, nel contempo, gratuitamente trasmesso anche parte della sua esperienza con importanti consigli.

Infine, non posso non rivolgere un grazie, che non sarà mai abbastanza, ai miei genitori, che pur non condividendo tante mie idee e scelte, non mi hanno mai fatto mancare il loro amore e il loro supporto, i loro insegnamenti e consigli, e mi hanno permesso di raggiungere questo traguardo.